CAMILA ASSIS TAVARES

PROBING INTERACTIONS BETWEEN VANADIUM COMPLEXES AND POTENTIAL TARGETS FOR ALZHEIMER'S TREATMENT: PARAMETERIZATION OF A NEW AMBER FORCE FIELD AND BIOLOGICAL APPLICATIONS

LAVRAS-MG
2023

CAMILA ASSIS TAVARES

PROBING INTERACTIONS BETWEEN VANADIUM COMPLEXES AND POTENTIAL TARGETS FOR ALZHEIMER'S TREATMENT:
PARAMETERIZATION OF A NEW AMBER FORCE FIELD AND BIOLOGICAL APPLICATIONS

A thesis submitted to Federal University of Lavras, as partial fulfillment of the requirements of Graduate Program in Agrochemistry, Chemistry/Biochemistry field of study, for the degree of Doctor of Philosophy.

Advisor
Prof. Dra. Elaine Fontes Ferreira da Cunha
Co-Advisor
Prof. Dr. Teodorico de Castro Ramalho

LAVRAS-MG
2023

Ficha catalográfica elaborada pelo Sistema de Geração de Ficha Catalográfica da Biblioteca Universitária da UFLA, com dados informados pelo(a) próprio(a) autor(a).

Tavares, Camila Assis.
Probing interactions between vanadium complexes and potential targets for Alzheimer's treatment: parameterization of a new AMBER force field and biological applications / Camila Assis Tavares. - 2023.
166 p.

Orientador(a): Elaine Fontes Ferreira da Cunha.
Coorientador(a): Teodorico de Castro Ramalho.
Tese (doutorado) - Universidade Federal de Lavras, 2023.
Bibliografia.

1. Complexos de Vanádio. 2. Campo de Força AMBER. 3. Dinâmica Molecular. I. da Cunha, Elaine Fontes Ferreira. II. Ramalho, Teodorico de Castro. III. Título.

CAMILA ASSIS TAVARES

PROBING INTERACTIONS BETWEEN VANADIUM COMPLEXES AND POTENTIAL TARGETS FOR ALZHEIMER'S TREATMENT: PARAMETERIZATION OF A NEW AMBER FORCE FIELD AND BIOLOGICAL APPLICATIONS

SONDANDO INTERAÇÕES ENTRE COMPLEXOS DE VANÁDIO E ALVOS EM POTENCIAL PARA O TRATAMENTO DE ALZHEIMER: PARAMETRIZAÇÃO DE UM NOVO CAMPO DE FORÇA AMBER E APLICAÇÕES BIOLÓGICAS

A thesis submitted to Federal University of Lavras, as partial fulfillment of the requirements of Graduate Program in Agrochemistry, Chemistry/Biochemistry field of study, for the degree of Doctor of Philosophy.

APPROVED on February 24th, 2023.

Prof. Drª. Adélia Justina Aguiar Aquino	TTU
Prof. Drª. Ana Paula de Lima Batista	UFSCar
Prof. Drª. Melissa Soares Caetano	UFOP
Prof. Dr. Sylvio Roberto Accioly Canuto	USP

Elaine F. F. da Cunha

Advisor
Prof. Dra. Elaine Fontes Ferreira da Cunha

Co-Advisor
Prof. Dr. Teodorico de Castro Ramalho

LAVRAS-MG
2023

To all self-doubting souls.

ACKNOWLEDGEMENTS

I would like to express my gratitude to my parents, Maria Aparecida and Juscelino, for being present and helping me pave my way through this long journey, always supporting my decisions, and to my sister Luciana and my brother Junior, who have always stood right by my side, giving me strength to keep going.

My profound appreciation to my niece Ana Júlia and my nephew Renato Augusto, who I have learned a lot from. Thank you two for being understandable on your own tiny little ways.

Thanks should also go to my aunt Neila for making herself present and a safe place in days of chaos.

A special thanks to my friends, Adenir, Andrilene, Balakrishnan, Carlos, Denner, Elizandra, Flávia, Gabriela, Karen, Marlene, Mary, Mayra, Monique, and Venan, for all the moments you showed me that "normalcy is an imbecile and sterile illusion".

I am beyond thankful to my therapist, Graciela Antônia dos Santos, for being the best professional I have ever deserved. I appreciate these 2 years of awkward silences and random trivia, besides the intense work.

I am also grateful for all the artists I deeply cherish and somehow have helped me in this journey. Art is what makes me whole.

The completion of this Ph.D. would not have been possible without the cooperation of my lab partner Taináh, who was always ready to help me overcome all the technical obstacles we have encountered throughout the research.

My sincere acknowledgments to Professors Elaine F. F. da Cunha and Teodorico Castro Ramalho, for their guidance and patience. I certainly learned a lot from both of you.

I am deeply indebted to the members of my thesis committee for the unparalleled knowledge shared, and the generosity with their time. Undoubtedly, their suggestions will be of great value.

I hereby express my gratitude to the Federal University of Lavras - UFLA, the Brazilian National Council for Scientific and Technological Development - CNPQ, the Coordination for the Improvement of Higher Education Personnel - CAPES, and The Foundation for Research of the State of Minas Gerais – FAPEMIG for the opportunity to develop this research.

I'd like to recognize all the faculty members who have acted as role models for my professional growth.

I want to give my deepest appreciation to all people who fought against 4 years of a dystopian government. May this dark period never be repeated in the history of Brazil.

And finally, I would like to thank everyone who contributed in some way in yet another stage of my life.

“Nothing in life is to be feared, it is only to be understood.”

(Marie Curie)

RESUMO

A doença de Alzheimer (DA) afeta uma grande parte da população mundial, com impactos sociais e econômicos. Uma das hipóteses etiológicas propõe que existe uma ligação entre DA e diabetes mellitus tipo 2 (DMT2), embora o mecanismo ainda não tenha sido desvendado. Estudos mostram que complexos de vanádio, como o BMOV e o $VO(metf)_2 \cdot H_2O$, são agentes potenciais contra este distúrbio neurodegenerativo. Dessa forma, as simulações de Dinâmica Molecular (DM) são vantajosas para obter informações sobre a estrutura e interação destes complexos com os alvos biológicos envolvidos no processo, nesse caso, AMPK e PTP1B. Entretanto, as DMs dependem da escolha de bons campos de forças. Portanto, o presente trabalho visa desenvolver parâmetros de campo de força AMBER para BMOV e $VO(metf)_2 \cdot H_2O$, uma vez que a literatura carece de tais informações sobre complexos metálicos. A partir de cálculos quanto-mecânicos, foram encontradas estruturas com mínimos de energia global, empregando o nível de teoria B3LYP/def2-TZVP mais ECP para o átomo de vanádio. As cargas RESP e os cálculos da matriz de Hessiana foram realizados usando os mesmos funcional e função de base. Os valores das constantes de força foram obtidos através da diagonalização da matriz de Hessiana e os parâmetros de Lennard-Jones foram atribuídos com base no GAFF, para todos os átomos, exceto vanádio. A fim de validar os campos de força desenvolvidos, foram realizadas simulações de DM no vácuo e em temperatura ambiente. Depois disso, foram realizados cálculos de DMs a fim de adquirir informações sobre as interações relevantes entre os complexos de vanádio e as proteínas associadas a estas duas condições. Os novos modelos desenvolvidos e relatados por este trabalho se mostraram eficientes para descrever as moléculas sob estudo, quando comparadas aos dados experimentais e as referências quânticas. Além disso, grandes insights sobre o comportamento dos sistemas, tais como resíduos relevantes que interagem com BMOV e $VO(metf)_2 \cdot H_2O$ são relatados. Espera-se que este trabalho possa ajudar a motivar trabalhos futuros envolvendo complexos de vanádio para o tratamento DA.

Palavras-chave: Complexos de Vanádio. Campo de Força AMBER. Dinâmica Molecular. Docking Molecular. Doença de Alzheimer.

ABSTRACT

Alzheimer's disease (AD) affects a large part of the world population, with social and economic impacts. One of the etiological hypotheses proposes that there is a link between AD and type 2 diabetes mellitus (T2DM), even though the mechanism is yet to be unraveled. Studies show that vanadium complexes, such as the BMOV and $VO(metf)_2 \cdot H_2O$, are potential agents against this neurodegenerative disorder. Thus, Molecular Dynamics (MD) simulations are advantageous for obtaining information about the structures and interactions of these complexes with the biological targets involved in the process, namely AMPK and PTP1B. However, DMs are dependent on the choice of a good force field. Therefore, the present work aims to develop AMBER force field parameters for BMOV and $VO(metf)_2 \cdot H_2O$, since the literature lacks such information on metal complexes. From quantum-mechanical calculations, the global minimum energy structures were found, with theory level B3LYP/def2-TZVP plus ECP for the vanadium atom. RESP charges and Hessian matrix calculations were performed using the same functional and basis set. The values of force constants were obtained by diagonalizing the Hessian matrix and the Lennard-Jones parameters were assigned based on GAFF, for all atoms except vanadium. In order to validate the developed force fields, MD simulations in vacuum and room temperature were carried out. After that, MDs were performed in order to acquire information about relevant interactions between vanadium complexes and the proteins associated to AD. The new models developed and reported by this work showed to be efficient to describe the molecules under study, when compared to experimental data and to quantum references. Furthermore, great insights about the behavior of the systems, such as relevant residues that interact with BMOV and $VO(metf)_2 \cdot H_2O$ are reported. It is expected that this work may assist to motivate future work involving vanadium complexes for the treatment AD.

Keywords: Vanadium Complexes. AMBER Force Field. Molecular Dynamics. Molecular Docking. Alzheimer’s Disease.

LIST OF ABBREVIATIONS

AD	Alzheimer's Disease
AMPK	5′ AMP-activated Protein Kinase
APP	Amyloid Precursor Protein
ATP	Adenosine Triphosphate
Aβ	Beta-amiloyd
BDNF	Brain-derived Neurotrophic Factor
BLA	Bond Length Alternation
BMOV	Bis(maltolato)oxovanadium (IV)
DFT	Density Functional Theory
ECP	Effective Core Potential
FF	Force Field
GAFF	General AMBER Force Field
GMQE	Global Model Quality Estimate
HBond	Hydrogen Bond
MD	Molecular Dynamics
MM	Molecular Mechanics
NVT	Constant temperature, constant volume
PDB	Protein Data Bank
PES	Potential Energy Surface
PTP1B	Tyrosine-protein Phosphatase Non-receptor Type 1
QM	Quantum Mechanics
RCSB	Research Collaboratory for Structural Bioinformatics
RESP	Restrained Electrostatic Potential
RMSD	Root Mean Square Deviation
RMSF	Root Mean Square Fluctuation
T2DM	Type 2 Diabetes Mellitus
TIP3P	Transferable Intermolecular Potential with 3 Points
UFF	Universal Force Field

UN	United Nations
VC	Vanadium Complex
VMD	Virtual Molecular Dynamics
WHO	World Health Organization
ZORA	Zero Order Regular Approximated Hamiltonian

TABLE OF CONTENT

CHAPTER ONE – OUTLINE AND SCOPE

1. INTRODUCTION

Alzheimer's Disease is a neurodegenerative disorder that is known for loss of cognitive functions and memory. Its symptoms may include difficulties on solving problems, completing ordinary tasks, keeping track of time, in addition to the inability to retrieve the name of relatives, mood swings and withdrawal from social interaction, affecting elderly people in its majority (VOLICER, 2020).

Due to its complexity, the etiology of AD is still uncertain. However, some hypotheses have been proposed regarding the factors that may influence on its development. Interestingly, one of the hypothesis associates AD to type 2 diabetes mellitus (T2DM) due to AD being considered a metabolic disorder (PAUDEL; PARK; JUNG; YOKOZAWA *et al.*, 2020).

Although, AD does not have a cure, one of the most promising strategies that have been investigated is the drug repurposing, where compounds with antidiabetic effects are considered good candidates for the treatment of this neurodegenerative disease (AKTER; LANZA; MARTIN; MYRONYUK *et al.*, 2011).

Different metal complexes have been investigated based on their potential application in AD. Among those complexes are platinum, ruthenium, iridium, rhodium, cobalt, and vanadium complexes. Due to similarities regarding the mechanism between AD and T2DM, it has been shown that vanadium complexes have the potential to improve cognitive functions, relieving some symptoms (LIU; QU; WANG, 2018).

Complexes as bis(maltolato)oxovanadium (IV) (BMOV) and bis(N',N'-dimethylbiguanidato)-oxovanadium (IV) ($VO(metf)_2 \cdot H_2O$) were reported as potential insulin-mimetic agents, among other remarkable effects, and are described as possible agents against this disease (SALO-AHEN; ALANKO; BHADANE; BONVIN *et al.*, 2021; WOO; YUEN; THOMPSON; MCNEILL *et al.*, 1999).

It is essential to have more information provided about those complexes in order to assist upcoming studies on drug development(LIU; QU; WANG, 2018). For this reason, theoretical studies should be conducted to investigate structural and thermodynamics properties along with the interaction between vanadium complexes and the biological target of interest. Besides that, parameterization set for metal-centered molecules is considered to be necessary as well, since there is a scarcity of such information on literature (PEREIRA; PRANDI; RAMALHO, 2021).

Computational Chemistry allows the acquisition of information about structural properties of molecules, contributing significantly to the understanding of chemical

behavior(COSTA, 2014). One of the traditional methods used to obtain this type of information is classical Molecular Dynamics (MD).

In light of the foregoing, the work intends to obtain AMBER force field parameters for BMOV and $VO(metf)_2 \cdot H_2O$, since these molecules might affect the progress of AD, in addition to pointed out relevant interactions between those two complexes and proteins associated to AD, AMPK and PTP1B. Thus, it is believed that the work may contribute to further parameterization studies of metal complex force field, enabling the investigation of compounds with potential effect for the treatment of AD.

2. RESEARCH OBJECTIVES

2.1.General Objectives

This work aims at developing AMBER force field parameters for vanadium complexes based on obtaining minimum energy through quantum-mechanical calculations, followed by validation of the acquired results based on Molecular Dynamics, as well as investigating their interaction with the biological targets associated to type 2 Diabetes Mellitus and Alzheimer's disease.

2.2.Specific Objectives

Thus, the specific objectives of this work are:

a. To choose vanadium complexes that have possible application in the treatment of Alzheimer's disease;
b. To develop accurate AMBER force field parameters for the selected complexes;
c. To analyze the efficiency of the method used through validation process, and;
d. To conduct docking and MD studies between vanadium complexes and proteins associated to AD.

3. LITERATURE REVIEW

3.1.Alzheimer’s Disease: the most common form of dementia

According to World Health Organization, dementia is a syndrome that deteriorates the cognitive function and has affected around 50 million people worldwide (WHO, 2022). Even though improvements in nutrition, health care and lifestyle have been made to reduce the risk of developing such condition, it is predicted that 152 million people worldwide will be affected by this disease (LIVINGSTON; HUNTLEY; SOMMERLAD; AMES *et al.*, 2020).

It is also suggested that although life expectancy and quality of life are associated with each other, it is not always attainable to achieve these two goals simultaneously. In some cases, even if the person reaches an advanced age, there is still the possibility of developing neurodegenerative diseases, for instance (BORTOLUZZI; MASCARELO; DELLANI; ALVES *et al.*, 2021).

The term "dementia" is a general term for several neurodegenerative diseases, such as Alzheimer’s disease (AD), which contributes to 60-70% of dementia cases. It is important to stress that besides having physical and psychological impacts for the disease patient and their family, AD has a great economic impact on health systems (PAUDEL; PARK; JUNG; YOKOZAWA *et al.*, 2020).

AD is a complex neurodegenerative disorder, that directly affects brain function, leading to the death of nervous system cells. It was discovered in 1906 by Alois Alzheimer, a German psychiatrist and neuropathologist, that found anomalies identified as amyloid plaques and neurofibrillary tangles in dead neurons in the brain of a 51-year-old woman that showed a loss of short-term memory as one of her symptoms (VOLICER, 2020).

AD is considered being a progressive chronic disorder and its three stages have been characterized by Cumming and Benson in 1992. Fundamentally, in the first stage, memory impairment is the most significant indicator. Later on, communication and cognitive abilities are compromised. Lastly, in the third stage, all cognitive functions collapse (BONDI; EDMONDS; SALMON, 2017; HONIG; MAYEUX, 2001).

Those stages are commonly showed as difficulties in solving problems, completing ordinary tasks, keeping track of time, in addition to the inability to retrieve the name of relatives, mood swings and withdrawal from social interaction (FALCO; CUKIERMAN; HAUSER-DAVIS; REY, 2016).

The most relevant abnormalities that occur in the brain are neurovascular degeneration, neuronal and synaptic loss, and the presence of senile plaques composed of aggregates of β-amyloid filaments. Patients affected by this disease tend to die between 6 to 12 years after the onset of the condition (FALCO; CUKIERMAN; HAUSER-DAVIS; REY, 2016).

All the changes that occur due to this disease are reflected in the morphology of the brain. There is a disconnection between brain areas and a decrease in brain volume, which leads to brain atrophy, as can be seen in Figure 1 (SMITH, 2019).

Figure 1 – Brain of a person with Alzheimer's Disease (left), and brain of a healthy person (right).

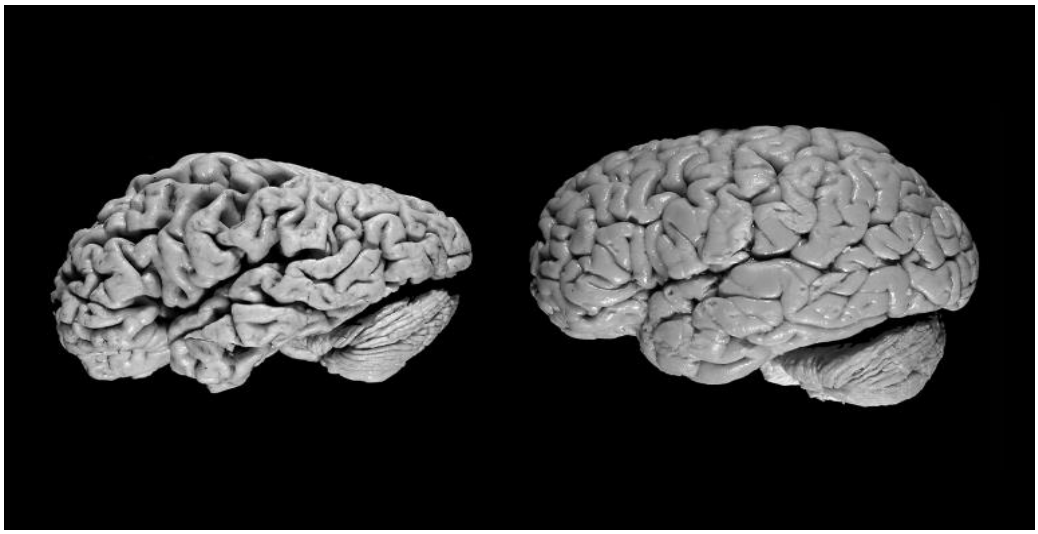

Source: Smith (2019).

Although its etiology is not well-defined, some hypotheses have been proposed concerning the set of causes of AD. Among them, the amyloid hypothesis, also known as amyloid cascade hypothesis, is the mainstream premise that has been under study over 25 years (PAUDEL; PARK; JUNG; YOKOZAWA *et al.*, 2020).

The natural process occurs as follows: β- and γ-secretase are responsible for the cleavage of amyloid precursor protein (APP) producing the Aβ peptide. Later, Aβ is processed by various secretases and proteases and then is degraded or removed. Meanwhile, if Aβ is not removed, two amino acids are generated, the sequences with 40 amino acids (Aβ1-40) and 42 amino acids (Aβ1-42), that may aggregate in brain cell, leading to apoptosis of the cell (FALCO; CUKIERMAN; HAUSER-DAVIS; REY, 2016), i. e., neurodegeneration is caused by aggregation of oligomeric or fibrillar Aβ peptide, that are generated by the proteolytic cleavage of amyloid precursor protein (APP) (KAMETANI; HASEGAWA, 2018).

Although this hypothesis has been vastly explored and seems to be a solid approach for the therapeutics of AD, some challenges still need to be overcome. Limitations such as developed drugs that might act on targets that are not present *in vivo*, reproducibility of experiments, and weak bonds between drugs and Aβ monomers are among the reasons that justify the difficulties on searching for Alzheimer's treatment through the amyloid hypothesis (DOIG; DEL CASTILLO-FRIAS; BERTHOUMIEU; TARUS *et al.*, 2017).

In the meantime, the type 3 diabetes hypothesis has been under investigation as well. This hypothesis considers AD as a metabolic condition that is linked to Type 2 Diabetes Mellitus (T2DM), through the insulin signaling of the brain (KANG; WANG; QIAO; ZHANG *et al.*, 2022). It has been proposed that the progression of T2DM can lead to cognitive decline and cognitive abnormalities.

3.2.Potential targets: AMPK and PTP1B

As mentioned in the last section, both T2DM and AD has a pathological link, however, it is yet not clear how mechanistically this may occur. It is proposed that metabolic changes in the organism may increase a chance to develop AD due disturbance in the transport of glucose to the brain and in the metabolism of such carbohydrate (SUN; MA; SUN; WANG *et al.*, 2020).

Studies have shown that proteins such as AMPK and PTP1B are involved in the insulin signaling and can be modulated in order to maintain the glycemic control. Consequently, it is possible to infer that these biological systems are promising targets regarding the treatment of AD (CHEN; HUANG; LIU; HUANG *et al.*, 2021; VIEIRA; LYRA E SILVA; FERREIRA; DE FELICE, 2017).

5′ AMP-activated protein kinase (AMPK) (Figure 2) is a metabolic enzyme that can increase glucose transport and regulate free fatty acids in T2DM.11 In the glucose metabolism in the brain, AMPK can act by increasing the glucose uptake in different stages (MURALEEDHARAN; DASGUPTA, 2022). Moreover, AMPK is associated with AD as well, where the expression of Aβ and hyperphosphorylation of tau can be decreased (GE; ZHOU; CHEN; WU *et al.*, 2022).

Figure 2 – 3D structure of 5′ AMP-activated protein kinase (AMPK).

Source: From author.

AMPK is connected to a great variety of biological processes and its activation involves three mechanisms, namely direct activation, biding by an upstream kinase, leading to the phosphorylation at Thr172, and reducing the level of dephosphorylation at the same residue (CHEN; HUANG; LIU; HUANG *et al.*, 2021).

This heterotrimer is comprised of a catalytic α subunit, and regulatory β and γ subunits. The α subunit contains a kinase domain, an autoinhibitory domain (that acts negatively regulating kinase activity), and a globular domain. The domain in the β subunit allows the protein to identify cellular energy reserves in the form of glycogen and acts as a bridge between the other two subunits. Finally, the γ subunit provides binding sites for the regulatory nucleotides AMP and ATP (FOGARTY; HARDIE, 2010).

In turn, PTP1B (Figure 3), another promising biological target, known as protein tyrosine-protein phosphatase non-receptor type 1, also plays an important role in the insulin pathway, where it induces the insulin resistance. It is important to highlight that, PTP1B also modulates a regulator of synaptic plasticity, the brain-derived neurotrophic factor (BDNF) (VIEIRA; LYRA E SILVA; FERREIRA; DE FELICE, 2017).

Figure 3 – Structure of Tyrosine-protein phosphatase non-receptor type 1 (PTP1B).

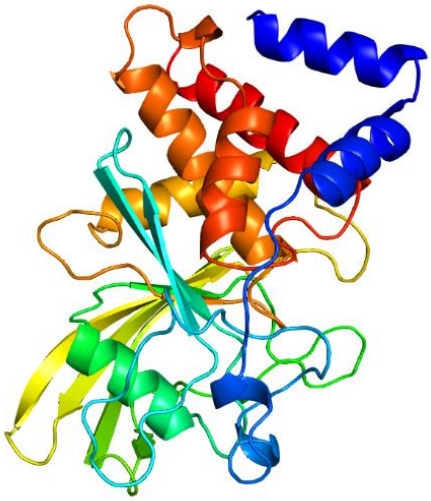

Source: From author.

Its structure consists of three domains, namely an N-terminal catalytic domain, a proline rich domain, and a C-terminal domain. In the first domain abovementioned, the modulation of the activity of PTP1B happens through phosphorylation. The proline rich domain modulates its interactions with other protein. Lastly, the C-terminal responsible for targeting the enzyme to the endoplasmic reticulum membrane (LIU; MATHIEU; BERTHELET; ZHANG *et al.*, 2022).

Besides the activity of PTP1B in the insulin signaling, it has been reported in the literature its activity as a regulator in several processes in the nervous system, for instance, restoration of hypothalamic insulin and leptin signaling, and modulation of BDNF, a regulator of synaptic plasticity (VIEIRA; LYRA E SILVA; FERREIRA; DE FELICE, 2017).

In light of these considerations, studies investigating these proteins may add to the therapies currently available for the treatment of this neurodegenerative disease, where different antidiabetic compounds are explored for the treatment of AD, showing improvement of neurological abilities (AKTER; LANZA; MARTIN; MYRONYUK *et al.*, 2011; STANCIU; BILD; ABABEI; RUSU *et al.*, 2020).

3.3.Current Therapies: managing the symptoms

Nowadays, the mainstream therapeutical approach for AD in clinical use are cholinesterase inhibitor such as tacrine, donezepil, galantine or the N-methyl-D-aspartate receptor memantine (STANCIU; BILD; ABABEI; RUSU *et al.*, 2020).

Promising approaches have been under investigation as well, for instance the disease-modifying therapeutics that aim to improve cognitive functions and decrease symptoms without affecting or modifying the disease. Chaperones can help with the progression of AD by inducing refolding of proteins, stabilizing their structure, and restoring their function. Natural extracts can also be potential agents in this quest due to their neuroprotective effect (BREIJYEH; KARAMAN, 2020).

Additionally, some ongoing trials have been reported regarding the efficiency and acceptability of antidiabetic compounds for the treatment of AD. Among those findings, different antidiabetic compounds showed improvement of cognitive ability, spatial memory, inhibition of β-sheet structures and brain Aβ levels (AKTER; LANZA; MARTIN; MYRONYUK *et al.*, 2011; RAIMUNDO; FERREIRA; MARTINS; MENEZES, 2020; STANCIU; BILD; ABABEI; RUSU *et al.*, 2020).

As mentioned, insulin mediated novel therapies are explored, since AD is considered a metabolic disease. In this case, hypoglycemic and anti-hypoglycemic agents show effects in this neurodegenerative disease in experimental and clinical studies, where the central effects are increasing, neurogenesis and synaptic plasticity, and reducing protein aggregation (BOCCARDI; MURASECCO; MECOCCI, 2019).

A strategy that has drawn attention to the drug design field is the use of metal complexes which potential application includes therapy and diagnosis, where complexes of copper, gallium, zirconium technetium, and iridium have shown positive results for AD diagnosis; platinum, ruthenium, rhodium, cobalt and vanadium based-compounds showed to be effective regarding Aβ aggregation (LIU; QU; WANG, 2018). Due to such favorable findings, repurposing metal-based antidiabetic drugs may be beneficial in prevent AD from progressing.

3.4.Vanadium Complexes in Medicine

Due to high specificity and selectivity, metallodrugs are considered to be great regulatory agents in several biological processes. An outstanding example is cisplatin, which has been used in cancer treatments. Additionally, vanadium complexes are between the most active metallodrugs candidates (KIOSEOGLOU; PETANIDIS; GABRIEL; SALIFOGLOU, 2015).

The first reports of the use of vanadium date back to the 18th century. However, vanadium started to draw attention from scientists after the discovery of its biological role on

inhibition of (Na,K)-ATPase, in 1970s (DEL CARPIO; HERNÁNDEZ; CIANGHEROTTI; COA *et al.*, 2018).

Vanadium complexes have a large spectrum of potential activity. Several studies have reported application in treatment of different conditions in addition to diabetes, such as leishmaniasis, Chagas' disease, influenza, Dengue fever, cancer and AD (DEL CARPIO; HERNÁNDEZ; CIANGHEROTTI; COA *et al.*, 2018; REHDER, 2012).

Among the beneficial vanadium effects, it must be mentioned insulin-enhancing, antihyperglycemic and antihyperlipidemic effects, in addition to antiviral, anti-inflammatory, and anticoagulation effects (SEMIZ, 2022).

Remarkable achievements were reached by two vanadium complexes (VC) particularly. The first one, bis(N',N'-dimethylbiguanidato)-oxovanadium(IV) (Figure 4), $VO(metf)_2 \cdot H_2O$, that showed better hypoglycemic properties than its independent ligand, metformin, a well-known drug used in the therapeutics of diabetes (RUSANOV; ZOU; BABAK, 2022).

Figure 4 – Chemical structure of $VO(metf)_2 \cdot H_2O$.

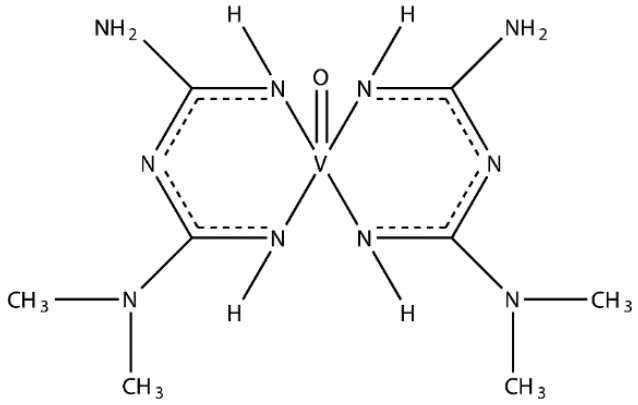

Source: From author.

Furthermore, $VO(metf)_2 \cdot H_2O$ showed efficient action when compared to another vanadium complex, BMOV, leading to lowering of blood-glucose. The antidiabetic effect of $VO(metf)_2 \cdot H_2O$ was almost as good as BMOV, considered a benchmark in diabetes treatment (WOO; YUEN; THOMPSON; MCNEILL *et al.*, 1999).

As just mentioned, the vanadium complex known as bis(maltolato)oxovanadium (IV) (Figure 5), BMOV, is successfully used as antidiabetic medicament, and it is considered a reference for this purpose. Its promising results includes enhancing insulin receptor *in vivo*, inhibiting PTP1B activity as a consequence (PETERS; DAVIS; HOWARD; POKROSS *et al.*, 2003).

Figure 5 – 2D structure of BMOV.

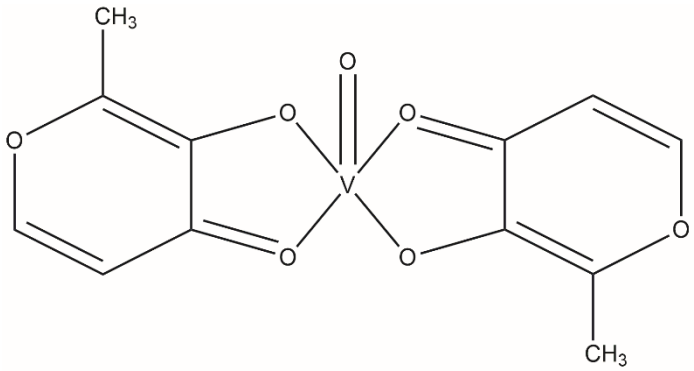

Source: From author.

Another work indicates BMOV as a partner in metabolic regulation, where it showed improved efficacy on glycemia in streptozotocin-diabetic rats, a more promising result than the vanadyl sulfate molecule (TREVIÑO; DIAZ, 2020).

Given such relevant effects and the link between diabetes and AD, both $VO(metf)_2 \cdot H_2O$ and BMOV may be beneficial in treating AD patients. Although experimental techniques, such as X-ray crystallography, are essential to precisely describe the structure of a complex, a theoretical approach may contribute significantly by seeking to understand the structural, and chemical behavior of such complex, making possible the study of this potential agent against the amyloid-related disease AD.

3.5.Theoretical Approach

Computational chemistry is a branch of Chemistry that has grown exponentially over the last 50 years (JENSEN, 2022). Since then, this resourceful field has been applied in different areas of research, assisting the acquiring of information regarding molecular properties (LESZCZYNSKI, 2012). Moreover, information that is difficult to obtain experimentally can be obtained by theoretical methods (JENSEN, 2022).

The better computational capacity coupled with the development of more accurate computational methods allows the prediction of the existence of molecular species under real conditions, in addition to properties such as molecular structure, vibrational and electronic spectra, intermolecular interactions, chemical reactivity, and mechanisms of chemical reactions (KIRCHMAIR; GÖLLER; LANG; KUNZE *et al.*, 2015; PLIEGO JR, 2006).

In the next sections, different methods relevant for this work will be addressed, namely molecular docking, molecular dynamics (MD), and quantum mechanics (QM) method, in order to provide a theoretical background for the studies conducted in the following chapters.

Molecular Docking

Molecular docking is a computational calculation method of great relevance in the elucidation of systems composed of biomolecules, of which the 3D structures have already been investigated (SHOICHET; MCGOVERN; WEI; IRWIN, 2002). The analysis of interactions and their respective energies are performed considering the orientations of a molecule inserted into the cavity of a biological receptor. Generally, the biological receptor, also known as protein, is associated with a signaling pathway that is considered key to the treatment of diseases, or even to the cure (MAGALHÃES; BARBOSA; DARDENNE, 2007).

In general, the energy involved in the process in which the docking of the ligand to the receptor occurs is an extremely important information for this method, where lower energy values are associated with an energetically more favorable conformation for the ligand (MAGALHÃES; BARBOSA; DARDENNE, 2007).

Briefly, the docking study can be divided into three stages. The first one is characterized by the choice of a promising ligand and biological target. The second step includes a search of possible conformations and their respective energy, and free energy surface of the ligand-receptor interaction. Lastly, a scoring function is used to select the best conformations and rank them according to their energies (TORRES; SODERO; JOFILY; SILVA-JR, 2019). This strategy is well-depicted in Figure 6.

Enthalpic and entropic effects govern the interaction between the receptor and the ligand can be estimated using Equation 1, according to the binding Gibbs free energy (ΔG_{lig}), of which:

$$\Delta G_{lig} = \Delta H - T\Delta S = RTlnK_i \quad , \tag{1}$$

where K_i is the dissociation constant, ΔH represents the enthalpy change, T is the temperature, ΔS, the entropy change, and R, the universal gas constant (BROOIJMANS; KUNTZ, 2003).

Figure 6 – Molecular docking strategy.

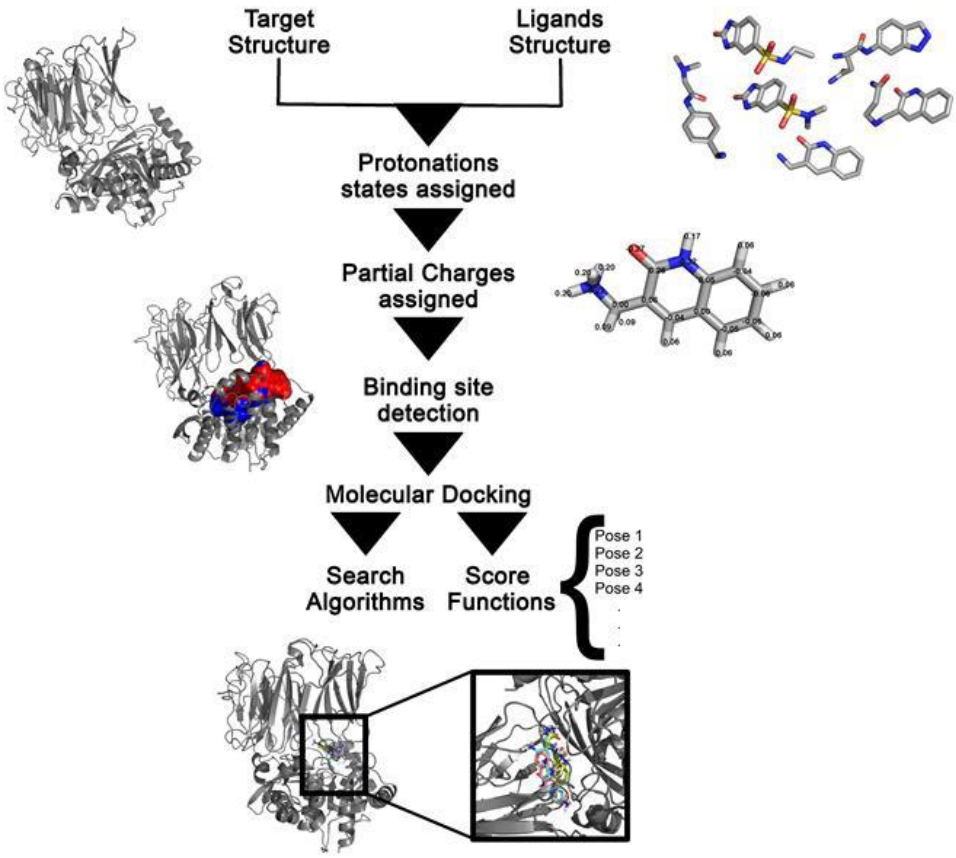

Source: Torres (2019)

In addition, it is possible to mathematically describe the docking performance function (docking scoring function), also known as a score as:

$$E_{score} = E_{inter} + E_{intra} \quad , \tag{2}$$

where E_{inter} represents the interaction energy of the ligand with the protein and E_{intra} represents the internal energy of the ligand(THOMSEN; CHRISTENSEN, 2006).

When not knowing the binding site location *a priori*, two approaches are possible: the use of algorithms to predict the most probable binding site available in the software, for instance the use of MolDock algorithm, that identifies potential binding sites through an integrated cavity detection algorithm, or a simulation called “blind docking”, that has a great computational cost due to scanning the entire protein for the search (TORRES; SODERO; JOFILY; SILVA-JR, 2019).

Complex docking studies play a huge role for the elucidation of receptor-ligand molecular recognition mechanisms, facilitating the efficient discovery and planning of new drugs (MENG; ZHANG; MEZEI; CUI, 2011).

Molecular Dynamics

Governed by the laws of classical mechanics, Molecular Mechanics (MM) is the simplest and fastest computational chemistry method that predicts the motions and energies of systems under different thermodynamic conditions. It can be used to study a diverse phenomenon of small molecules as well as large biological systems in their equilibrium states (ALAVI, 2020; KOSTAL, 2016).

Unlike the quantum mechanical approach, electrons are not dealt with explicitly. Moreover, the atoms are considered as a set of particles that are connected by harmonic or elastic forces with equilibrium distances equal to experimental or calculated bond lengths, in other words, quantum effects are not considered (KOSTAL, 2016; MARTÍNEZ; BORIN; SKAF, 2007).

Molecular dynamics (MD) is a computational technique within MM that allows the investigation of the evolution of configurations of a system over time and, from the positions obtained, it is possible to determine the macroscopic properties of the system (MARTÍNEZ; BORIN; SKAF, 2007).

In order to perform MD calculations, the Newton's equations of motion must be solved as so the positions and interactions between atoms can be found (ALAVI, 2020; MARTÍNEZ; BORIN; SKAF, 2007). In this case,

$$\vec{F} = m_i \vec{a}_i(t) \tag{3}$$

$$\vec{F} = -\frac{\partial V_{total}(\vec{r}_1, \vec{r}_2, \ldots, \vec{r}_n)}{\partial \vec{r}_n} \tag{4}$$

where $\vec{F}$ is the force acting on a particle i, m_i represents the atomic mass, a_i, the acceleration, and V_{total} is the total potential dependent on the position of the particle, represented by $\vec{r}_i$.

Equations (3) and (4) are solved simultaneously, providing a set of equations for each particle. For a complex system with a large number of particles, the Newtonian equations must be solved through numerical integration (PEREIRA, 2020).

Although, MD is considered being an effective theoretical method that provides accurate description of system, its results are highly dependent on a reliable parameterization of the force field (MARTÍNEZ; BORIN; SKAF, 2007).

Force fields are a set of parameters required to describe interactions in a molecular system and are described by potential energy functions of structural contributions, bond lengths,

bond angles, dihedral angles, and interactions between non-bonded atoms (MARTÍNEZ; BORIN; SKAF, 2007).

As mentioned above, the potential energy takes into account all the contributions of the forces acting on each atom by a total potential function (Equation 5):

$$V_{total} = V_{bonds} + V_{angles} + V_{dihedrals} + V_{Coulomb} + V_{Lennard-Jones} \quad (5)$$

where the bonded terms represented by V_{bonds}, V_{angles}, and $V_{dihedrals}$ describe the bond stretching, angular, and dihedral potential, respectively, as shown by Figure (7). It is important to highlight that these potentials are based on Hooke's law. In addition, the non-bonded terms are classified as electrostatic and van der Waals interactions, i. e., $V_{Coulomb}$ and $V_{Lennard\text{-}Jones}$(KOSTAL, 2016).

Figure 7 - Graphic representation of bonded terms for a force field: (a) bond stretching (b) angular deformation and (c) dihedral angle rotation.

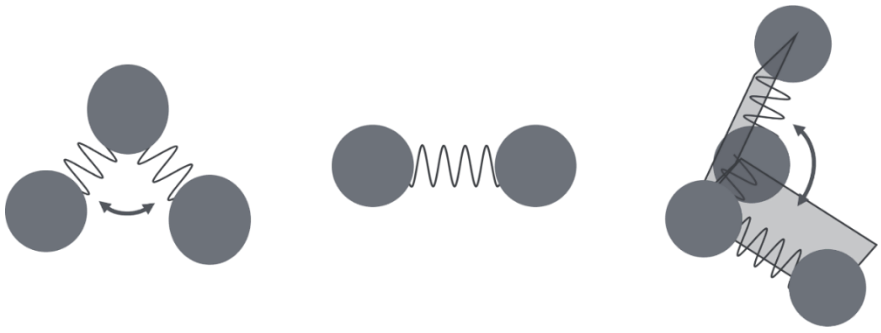

(a) (b) (c)

Source: From author.

Equation (6) can be written with further details as so the total potential energy is given by:

$$V_{total} = \sum_{bonds} K_b(b - b_0)^2 + \sum_{angles} K_\theta(\theta - \theta_0)^2 + \sum_{dihedrals} K_\phi\,[cos(n\phi\ -\ \delta) + 1]$$

$$+ \sum_{Coulomb} \left[\frac{q_i q_j}{4\pi\varepsilon_0 r_{ij}}\right] + \sum_{Lennard-Jones} 4\epsilon_{ij}\left[\frac{\sigma^{12}}{r_{ij}^{12}} - \frac{\sigma^6}{r_{ij}^6}\right] \quad (6)$$

where K_b, K_θ, and K_Φ are the force constants, b and θ correspond to bond length and angle respectively, b_0 and θ_0 are the equilibrium values, n is the periodicity, ϕ represents the dihedral angle, δ is the phase angle, r_{ij} is the distance between atoms i and j, ϵ is the depth of the potential

well, σ is the distance at which the Lennard-Jones Potential is zero, q_i and q_j are the partial atomic charges of each atom, and ε_0 corresponds to vacuum permittivity.

The attempt to model a chemical system described by the force field can be very challenging (MARTÍNEZ; BORIN; SKAF, 2007). The equilibrium values and the force constants for all bonds, angles and dihedrals are required to describe the interactions of a molecular system as demonstrated by Equations (5) and (6).

Such parameters can be obtained through automatic tools for different force fields, for example AMBER, CHARMM, and GROMOS, yet the parameter set could not transferable between force fields due to peculiarities of each interacting system and the choice of force fields is an essential step for the correct description of the system under study (MARTÍNEZ; BORIN; SKAF, 2007; PEREIRA, 2020; VANOMMESLAEGHE; GUVENCH, 2014).

The quality of a force field relies on how accurately the parameters can describe the molecules under study. Thus, combining the equation of potential energy with good parameterization will provide satisfactory results with plausible thermodynamic properties (JACOBS, 2017).

Conventionally, developing parameters for a force field consists of quantum-mechanical calculation taking as a reference for the development of the parameters, comparison of the structure with experimental data or the QM structure, and adapting the parameters until they are capable of reproducing the molecule accurately (VANOMMESLAEGHE; GUVENCH, 2014).

When dealing with complexes that have a metal center, the set of parameters are quite scarce in the literature, slowing the development of accurate models (LI; MERZ, 2017; WOLOHAN; YOO; WELCH; REICHERT, 2005). With that being said, the development of a new force field for metal-centered molecules are considered being thoroughly relevant, since metal compounds play an important role in several fields.

Quantum Mechanics and Density Functional Theory

The advent of quantum mechanics (QM) brought a closer-to-real perspective to investigations at the microscopic level. Its development took about three decades to consolidate and involved great names in science, such as Max Planck, Albert Einstein, Werner Karl Heinsenberg, Erin Schrödinger, and Paul Dirac (ALCÁCER, 2007).

Quantum mechanics methods have been widely used in different applications, particularly in the computer-aided drug design field. In this case, this method can provide results with high reliability (ZHOU; HUANG; CAFLISCH, 2010).

It can be said that the main goal of QM is solving the time-independent Schrödinger equation (Equation 7), allowing to describe the motion of quantum systems. Once solved for a specific system, any physical property can be determined for that system in question (LAPOINTE; WEAVER, 2007).

$$\left[-\frac{\hbar^2}{2m}\left(\frac{\partial^2}{\partial x^2}+\frac{\partial^2}{\partial y^2}+\frac{\partial^2}{\partial z^2}\right)+V(x,y,z)\right]\Psi(x,y,z)=i\hbar\frac{d}{dt}\Psi(x,y,z) \tag{7}$$

where $\hbar$ represents the Planck constant divided by 2π, m is the mass of the electron, V is associated with the potential energy, Ψ is the wave function, and i is an imaginary number (GRIFFITHS; FREITAS, 2011).

When dealing with large systems, QM methods are not advised, i.e., methods based on quantum mechanics are limited by systems with few molecules, due to due to the high computational demand (PEREIRA, 2016).

However, different approximations are needed to make it possible to study systems larger than the hydrogen atom, thus extending its application. Approximation methods were than proposed, Density Functional Theory (DFT) is routinely implemented in the study of molecular modeling (BICKELHAUPT; BAERENDS, 2000).

DFT was born in 1964 and was coined by two scientists, Hohenberg and Kohn. A year later, it was implemented in a paper by Kohn and Sham. This theory relies on two theorems and is a popular alternative to solve Schrödinger's equation, where instead of using the wave function, the parameter considered is the electronic density (DUARTE, 2001).

Briefly, the first theorem of DFT states that the electron density is sufficient to describe the system, i.e., when knowing the density, it is possible to determine the corresponding potential. The second theorem, in its turn, declares that the minimum energy of a system is related to the electronic density of that same system in its ground state. In other words, these two theorems allow to determine the ground state of a system using the electronic density instead of the wave function (DUARTE, 2001).

Mathematically, the ground state of a system is expressed by Equation 8 and is a functional of the density, where terms $T[\rho]$ and $V[\rho]$ are associated to kinetic and potential

energy. The potential energy includes nuclei-electron and Coulomb interactions. Lastly, $E_{xc}[\rho]$ takes into consideration the exchange correlation energy (PEREIRA, 2016).

$$E_0[\rho] = T[\rho] + V[\rho] + E_{XC}[\rho] \quad (8)$$

Finally, DFT is a very popular and widely employed theory that facilitates computational calculations, without fully calculating the Schrodinger equation, by providing quite remarkable results (CAPELLE, 2006).

REFERENCES

AKTER, K. *et al*. Diabetes mellitus and Alzheimer's disease: shared pathology and treatment? **British Journal of Clinical Pharmacology**, v. 71, p. 365-376, 2011.

ALAVI, S. Molecular Simulations: fundamentals and practice. Wienheim: Wiley-VCH, 2020.

ALCÁCER, L. **Introdução à química quântica computacional**. Lisboa: IST Press, 2007. 325 p.

BICKELHAUPT, F. M.; BAERENDS, E. J. Kohn-Sham density functional theory: predicting and understanding chemistry. **Reviews in Computational Chemistry**, p. 1-86, 2000.

BOCCARDI, V.; MURASECCO, I.; MECOCCI, P. Diabetes drugs in the fight against Alzheimer's disease. **Ageing Research Reviews,** v. 54, p. 100936, 2019.

BONDI, M. W.; EDMONDS, E. C.; SALMON, D. P. Alzheimer's Disease: Past, Present, and Future. **Journal of the International Neuropsychological Society,** v. 23, n. 9-10, p. 818-831, 2017.

BORTOLUZZI, E. C. et al. Expectativa de vida de idosos e doenças crônicas. **Brazilian Journal of Health Review,** v. 4, n. 1, p. 3057-3071, 2021.

BREIJYEH, Z.; KARAMAN, R. Comprehensive review on Alzheimer's disease: causes and treatment. **Molecules,** v. 25, n. 24, p. 5789, 2020.

BROOIJMANS, N.; KUNTZ, I. D. Molecular recognition and docking algorithms. **Annual Review of Biophysics and Biomolecular Structure,** v. 32, n. 1, p. 335-373, 2003.

CAPELLE, K. A bird's-eye view of density-functional theory. **Brazilian Journal of Physics,** v. 36, p. 1318-1343, 2006.

CHEN, M. et al. AMPK: A bridge between diabetes mellitus and Alzheimer's disease. **Behavioural Brain Research,** v. 400, p. 113043, 2021.

COSTA, M. A. S. **Investigação Teórica do Processo de Inclusão do Fluconazol com Ciclodextrinas e Calixarenos**. 2014. 26f. Monografia (Bacharelado em Química) - Departamento de Química, Universidade Federal de São João del-Rei, São João del-Rei, 2014.

DEL CARPIO, E. *et al*. Vanadium: History, chemistry, interactions with α-amino acids and potential therapeutic applications. **Coordination Chemistry -Reviews,** v. 372, p. 117-140, 2018.

DOIG, A. J. et al. Why Is Research on Amyloid-β Failing to Give New Drugs for Alzheimer's Disease? **ACS Chemical Neuroscience,** v. 8, n. 7, p. 1435-1437, 2017.

DUARTE, H. A. Índices de reatividade química a partir da teoria do funcional de densidade: formalismo e perspectivas. **Química Nova,** v. 24, p. 501-508, 2001.

FALCO, A. D. et al. Doença de Alzheimer: hipóteses etiológicas e perspectivas de tratamento. **Química Nova,** v. 39, n. 1, p. 63-80, 2016.

FOGARTY, S.; HARDIE, D. G. Development of protein kinase activators: AMPK as a target in metabolic disorders and cancer. **Biochimica et Biophysica Acta,** v. 1804, n. 3, p. 581-91, 2010.

GE, Y. *et al*. Role of AMPK mediated pathways in autophagy and aging. **Biochimie,** v. 195, p. 100-113, 2022.

GRIFFITHS, D. J. **Mecânica Quântica**. 2 ed. Ed. Pearson Prentice Hall. São Paulo, 2011.
HONIG, L.; MAYEUX, R. Natural history of Alzheimer's disease. **Aging Clinical and Experimental Research,** v. 13, n. 3, p. 171-182, 2001.

JACOBS, M. R. **Parametrização de campo de força derivado de cálculos mecânico-quânticos para o cristal líquido 4-ciano-4'-pentilbifenila**. 2017. 75 f. Dissertação (Mestrado em Química) – Instituto de Química, Universidade Federal do Rio Grande do Sul, Porto Alegre, 2017.

JENSEN, F. Computational chemistry: The exciting opportunities and the boring details. **Israel Journal of Chemistry,** v. 62, n. 1-2, p. e202100027, 2022.

KAMETANI, F.; HASEGAWA, M. Reconsideration of amyloid hypothesis and tau hypothesis in Alzheimer's disease. **Frontiers in neuroscience**, p. 25, 2018.

KANG, P. et al. Dissecting genetic links between Alzheimer's disease and type 2 diabetes mellitus in a systems biology way. **Frontiers in Genetics,** v. 13, p. 1019860, 2022.

KIOSEOGLOU, E. *et al*. The chemistry and biology of vanadium compounds in cancer therapeutics. **Coordination Chemistry Reviews,** v. 301, p. 87-105, 2015.

KIRCHMAIR, J. *et al*. Predicting drug metabolism: experiment and/or computation? **Nature Reviews Drug Discovery,** v. 14, n. 6, p. 387-404, 2015.

KOSTAL, J. Computational Chemistry in Predictive Toxicology: status quo et quo vadis? In: FISHBEIN J. C.; HEILMAN, J. M. **Advances in Molecular Toxicology**. Amsterdam: Elsevier, 2016. cap. 4, p. 139-186.

LAPOINTE, S. M.; WEAVER, D. F. A review of density functional theory quantum mechanics as applied to pharmaceutically relevant systems. **Current Computer-Aided Drug Design,** v. 3, n. 4, p. 290-296, 2007.

LESZCZYNSKI, J. *et al*. **Handbook of Computational Chemistry**. Nova York: Springer Science & Business Media, 2012.

LI, P.; MERZ, K. M. Metal Ion Modeling Using Classical Mechanics. **Chemical Reviews,** v. 117, n. 3, p. 1564-1686, 2017.

LIU, H.; QU, Y.; WANG, X. Amyloid b-targeted metal complexes for potential applications in Alzheimer's disease. **Future Medicinal Chemistry**, v. 10, n. 6, p. 679-701, 2018.7

LIU, R. et al. Human Protein Tyrosine Phosphatase 1B (PTP1B): From Structure to Clinical Inhibitor Perspectives. **International Journal of Molecular Sciences,** v. 23, n. 13, p. 7027, 2022.

LIVINGSTON, G. *et al*. Dementia prevention, intervention, and care: 2020 report of the Lancet Commission. **Lancet,** v. 396, n. 10248, p. 413-446, 2020.

MAGALHÃES, C. S.; BARBOSA, H. J. C.; DARDENNE, L. E. Métodos de Docking Receptor-Ligante para o Desenho Racional de Compostos Bioativos. In: MORGON, N H.; COUTINHO, K. (Ed). **Métodos de química teórica e modelagem molecular**. 539f. São Paulo: Livraria da Física, 2007.

MARTINEZ, L.; BORIN, I. A.; SKAF, M. S. Fundamentos de Simulação por Dinâmica Molecular. In: MORGON, Nelson H. **Métodos de Química Teórica e Modelagem Molecular**. São Paulo: Livraria da Física, 2007. cap. 12, p. 413-452.

MENG, X.-Y. et al. Molecular docking: a powerful approach for structure-based drug discovery. **Current Computer-aided Drug Design,** v. 7, n. 2, p. 146-157, 2011.

MURALEEDHARAN, R.; DASGUPTA, B. AMPK in the brain: its roles in glucose and neural metabolism. **FEBS J,** v. 289, n. 8, p. 2247-2262, 2022.

PAUDEL, P. *et al*. A systematic review on anti-Alzheimer's disease activity of prescription Kangen-karyu. **Drug Discoveries & Therapeutics**, v.14, n. 2, p. 61-66, 2020.

PEREIRA, A. F. **Development and biological application of a quantum mechanically derived force field: the case of a platinum (II) complex**. 2020. 102f. Tese (Mestrado em Agroquímica) - Departamento de Química, Universidade Federal de Lavras, Lavras, 2020.
PEREIRA, A. F.; PRANDI, I. G.; RAMALHO, T. C. Parameterization and validation of a new force field for Pt (II) complexes of 2-(4'-amino-2'-hydroxyphenyl) benzothiazole. **International Journal of Quantum Chemistry**, v. 121, n. 6, p. 1-10, 2021.

PEREIRA, R. A. **Estudo teórico de compostos de inclusão dos herbicidas 2,4-D e Dicamba em b-Ciclodextrina**. 2016. 102f. Tese (Doutorado em Química) - Departamento de Química, Universidade Federal de Lavras, Lavras, 2016.

PETERS, K. G. *et al*. Mechanism of insulin sensitization by BMOV (bis maltolato oxo vanadium); unliganded vanadium (VO4) as the active component. **Journal of Inorganic Biochemistry,** v. 96, n. 2, p. 321-330, 2003.

PLIEGO JR, J. R. Modelos contínuos do solvente: fundamentos. **Química Nova,** v. 29, p. 535-542, 2006.

RAIMUNDO, A. F. *et al*. Islet Amyloid Polypeptide: A Partner in Crime With Aβ in the Pathology of Alzheimer's Disease. **Frontiers in Molecular Neuroscience,** v. 13, p. 35, 2020.
REHDER, D. The potentiality of vanadium in medicinal applications. **Future Medicinal Chemistry,** v. 4, n. 14, p. 1823-1837, 2012.

RUSANOV, D. A.; ZOU, J.; BABAK, M. V. Biological Properties of Transition Metal Complexes with Metformin and Its Analogues. **Pharmaceuticals,** v. 15, n. 4, 2022.

SALO-AHEN, O. M. H. *et al*. Molecular Dynamics Simulations in Drug Discovery and Pharmaceutical Development. **Processes,** v. 9, n. 1, 2021.

SEMIZ, S. Vanadium as potential therapeutic agent for COVID-19: A focus on its antiviral, antiinflamatory, and antihyperglycemic effects. **Journal of Trace Elements in Medicine and Biology,** v. 69, p. 126887, 2022.

SHOICHET, B. K. *et al*. Lead discovery using molecular docking. **Current Opinion in Chemical Biology,** v. 6, n. 4, p. 439-446, 2002.

SMITH, D. Artificial intelligence can detect Alzheimer's disease in brain scans six years before a diagnosis. **University of California San Fransisco**, p. 01-02, 2019.

STANCIU, G. D. *et al*. Link between diabetes and Alzheimer's disease due to the shared amyloid aggregation and deposition involving both neurodegenerative changes and neurovascular damages. **Journal of Clinical Medicine**, v. 9, p. 1713-1738, 2020.

SUN, Y. et al. Metabolism: A Novel Shared Link between Diabetes Mellitus and Alzheimer's Disease. **Journal of Diabetes Research,** v. 2020, p. 4981814, 2020.

THOMSEN, R.; CHRISTENSEN, M. H. MolDock: a new technique for high-accuracy molecular docking. **Journal of Medicinal Chemistry,** v. 49, n. 11, p. 3315-3321, 2006.
TORRES, P. H. et al. Key topics in molecular docking for drug design. **International Journal of Molecular Sciences,** v. 20, n. 18, p. 4574, 2019.

TREVIÑO, S.; DIAZ, A. Vanadium and insulin: Partners in metabolic regulation. **Journal of Inorganic Biochemistry,** v. 208, p. 111094, 2020.

VANOMMESLAEGHE, K. et al. Molecular mechanics**. Current Pharmaceutical Design**, v. 20, p. 3281-3292, 2014.

VIEIRA, M. N. et al. Protein Tyrosine Phosphatase 1B (PTP1B): A Potential Target for Alzheimer's Therapy? **Frontiers in Aging Neuroscience,** v. 9, p. 7, 2017.

VOLICER, L. Physiological and pathological functions of beta-amyloid in the brain and Alzheimer's disease: a review. **Chinese Journal of Physiology**, v. 63, n. 3, p. 95-100, 2020.

WOLOHAN, P. et al. QSAR studies of copper azamacrocycles and thiosemicarbazones: MM3 parameter development and prediction of biological properties. **Journal of Medicinal Chemistry,** v. 48, n. 17, p. 5561-5569, 2005.

WOO, L. C. Y. *et al*. Vanadyl–biguanide complexes as potential synergistic insulin mimics. **Journal of Inorganic Biochemistry,** v. 76, n. 3, p. 251-257, 1999.

WORLD HEALTH ORGANIZATION. Dementia. 2021. Disponibiliza informações sobre a Demência. Disponível em: https://www.who.int/news-room/fact-sheets/detail/dementia. Acesso em: 15 dezembro 2022.

ZHOU, T.; HUANG, D.; CAFLISCH, A. Quantum mechanical methods for drug design. **Current Topics in Medicinal Chemistry,** v. 10, n. 1, p. 33-45, 2010.

CHAPTER TWO – FIRST PAPER

Molecular Dynamics-Assisted Interaction of Vanadium Complex-AMPK: from the force field development to biological application for Alzheimer's treatment

Article online on Journal of Physical Chemistry B
DOI: 10.1021/acs.jpcb.2c07147

Abstract

Large part of the world population is affected by Alzheimer's disease (AD) and diabetes mellitus type 2, which causes both social and economic impacts. These two conditions are associated to one protein, AMPK. Studies have shown that vanadium complexes, such as bis(N',N'-dimethylbiguanidato)-oxovanadium (IV), $VO(metf)_2 \cdot H_2O$, are potential agents against AD. A crucial step on drug design studies is obtaining information about the structure and interaction of these complexes with the biological targets involved in the process through Molecular Dynamics (MD) simulations. However, MDs depend on the choice of a good force field that could present reliable results. Moreover, general force fields are not efficient for describing the properties of metal complexes, and a $VO(metf)_2 \cdot H_2O$-specific force field does not yet exist, thus the proper development of a parameter set is necessary. Furthermore, this investigation is essential and relevant given the importance for both the scientific community and the population that is affected by this neurodegenerative disease. Therefore, the present work aims to develop and validate the AMBER force field parameters for $VO(metf)_2 \cdot H_2O$, since the literature lacks such information on metal complexes, and investigate through classical molecular dynamics the interactions made by the complex with the protein. The proposed force field proved to be effective for describing the vanadium complex (VC), supported by different analysis and validation. Moreover, it had a great performance when compared to general AMBER force field. Beyond that, MD findings provided an in-depth perspective about vanadium complex-protein interactions that should be taken into consideration in future studies.

Keywords: Vanadium Complex. AMBER Force Field. Molecular Dynamics. Docking. Alzheimer’s Disease.

1. Introduction

According to data published by World Health Organization (WHO) and United Nations (UN), life expectancy has increased in the last 20 years, reaching 72.28 years, worldwide.[1,2] Furthermore, records show that between years 1950 and 2020, life expectancy increased 25.3 years. Regarding elderly people, it increased, in average, 6.7 years during the same period.[1] However, such milestone is not achieved due to a reduction of years lived with disability but because of a decrease of mortality. In other words, the increasing on life expectancy does not necessarily improve the quality of life of a population. The health of the population plays an important role on such statistic indicator.[1]

One of the conditions that most affects health and is most prevalent among the elderly population is dementia. Based on data reported by WHO, it affects around 50 million people worldwide. Dementia is a general term for neurodegenerative diseases, with Alzheimer's Disease (AD) being the most commonly known, occurring in about 60-70 % of dementia cases.[2]

AD is a neurodegenerative disorder that is known for loss of cognitive functions and memory. Its symptoms may include difficulties on solving problems, completing ordinary tasks, and keeping track of time, in addition to the inability to retrieve the name of relatives, mood swings and withdrawal from social interaction. It affects elderly people in its majority, and it is related to aging of the cells from the nervous system. The aging process of the nervous system, in turn, is related to the programmed cell death, also known as apoptosis, triggered by beta-amyloid peptide.[3]

Due to its complexity, the etiology of AD is still uncertain. However, some hypotheses have been proposed regarding the factors that may influence on its development.[4,5] Despite directly targeting one of the most acceptable hypotheses to seems a safe approach,[6] it is known that some obstacles have not yet been overcome, leading to a failure in the search for agents associated with the therapy of this disease[7] or even, the discovery of new treatments may require novel approaches, which is quite challenging.[8]

One of them associates the development of AD to type 2 diabetes mellitus (T2DM) in which the link between those two conditions is the protein kinase AMPK, where the progression of T2DM can lead to cognitive impairment.[9] Furthermore, there is a possibility that T2DM may affect the development of AD through the insulin signaling in the brain.[10]

5' AMP-activated protein kinase (AMPK) is a metabolic enzyme that plays important roles in both AD and T2DM.[9] Studies have shown that such enzyme can increase the glucose

transport and regulate free fatty acids, in T2DM.[11] Moreover, in AD, AMPK can reduce Aβ expression and indirectly inhibit hyperphosphorylation of tau.[12] In this sense, AMPK may be an excellent biological target in studies where the prevention and treatment of AD are the main goal.

Some treatments are available in order to reduce the cognitive impairment even though the cure has not been discovered yet.[13] Approaches include targeting different pathways, for instance, exploring the possibility of the use of drugs that are already used in the treatment of T2DM as possible candidates for AD treatment.[14] Different metal complexes have been investigated based on their potential application in AD. Among those complexes are platinum, ruthenium, iridium, rhodium, cobalt, and vanadium complexes.[15]

A great example of a vanadium complex (VC) that has shown to be efficient in the treatment of T2DM and is considered a potential agent against AD is bis(N',N'-dimethylbiguanidato)-oxovanadium (IV), $VO(metf)_2 \cdot H_2O$ (Figure 1). Studies have indicated the good performance of $VO(metf)_2 \cdot H_2O$ in decreasing the level of insulin in rats, in other words, this VC led to a more promising antidiabetic response than its ligand metformin, known to be an efficient antidiabetic.[16] Furthermore, it has also been shown that such VC had its action compared to BMOV, a reference in the treatment of diabetes, where its efficiency was quite similar to the compound in question.[17] Thus, vanadium complexes, specially $VO(metf)_2 \cdot H_2O$, deserve all attention from the scientific community due to their potential effect against diseases.

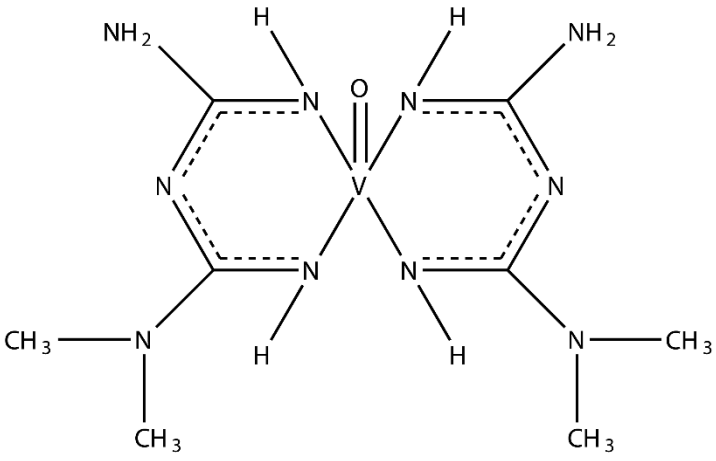

Figure 1. Structure of bis(N',N'-dimethylbiguanidato)-oxovanadium (IV), $VO(metf)_2 \cdot H_2O$.

To provide relevant and valuable information about interactions of such complexes in the biological environment, computational investigations may be of significant benefit.[18]

Classical Molecular Dynamics (MD) is one of the mostly used tools to assist in further drug design studies.[19] MD relies on a proper choice of force fields (FF) to describe systems, and regarding inorganic compounds, information such as parameters to describe the molecules are somewhat scarce and need to be developed.[20,21] Furthermore, general force fields may not accurately describe the molecule,[22] reinforcing the idea that developing a new force field for metal-centered molecules is essential. Interestingly, force fields for $VO(metf)_2 \cdot H_2O$ are yet to be described in the literature and will be approached in this work.

In the light of the foregoing, this work aims to obtain the AMBER force field parameters of the $VO(metf)_2 \cdot H_2O$, due to its potential action against AD. Thus, it is believed that the work may contribute to further parameterization studies of metal complex force field, enabling the investigation of compounds with potential effect for the treatment of AD. To accomplish this, the first step was to develop the force field for the vanadium complex. Then, an MD simulation in vacuum was performed in order to investigate the structural behavior of such complex and this new force field was validated by comparing with the data derived from DFT calculations. After that, the docking study with $VO(metf)_2 \cdot H_2O$ and the protein AMPK was performed, where the best lower energy pose that reproduced interactions already described by the literature was selected as a starting point for the study of the behavior of the system through MD simulation.

2. Computational Details

Structural Optimization

The initial structure of the vanadium complex under study was built using the software GaussView 5.0.8.[23] A relaxed potential energy surface (PES) scan of the two dihedrals (N8-C6-M0-C8 and N4-C2-N5-C4) (Figure 2) were conducted. Such conformational analysis was performed through DFT calculations, using B97-D functional and 6-311G++ basis function.[24] Since it is highly important to have a reference with a global minimum energy, and consequently, aiming for a system with an accurate structure, the optimization of the molecule with theory level B3LYP and basis set def2-TZVP plus LANL2DZ ECP for vanadium atom was obtained using Gaussian 09[25] as a starting point for the development of the force field. Evidence showed that hybrid B3LYP exchange correlation functional in combination with polarized valence triple-zeta basis set were adequate to describe a system containing vanadium, presenting results with good agreement when comparing to experimental data.[26] In addition, an

optimization through Molecular Mechanics method, using the AMBER force field was found through the software HyperChem 7.0[27] for further investigation and comparison.

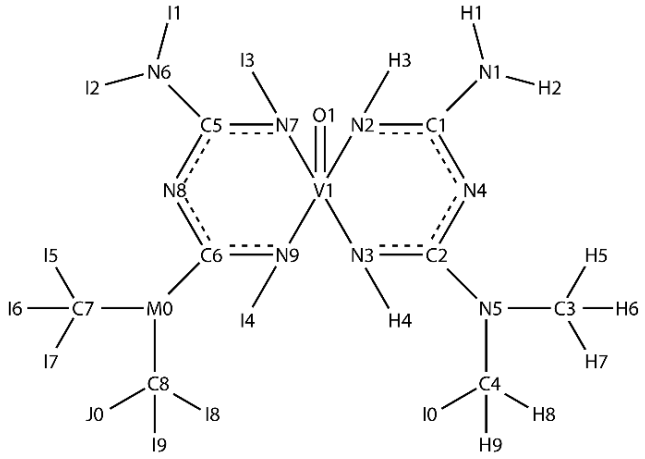

Figure 2. Atom types assigned to the VC. N and M, C, H and I, O, and V represent nitrogen, carbon, hydrogen, oxygen, and vanadium atoms respectively.

Although the metal atom present in the complex is relatively lighter than other metals and does not present prominent relativistic effects, a calculation using the software ORCA 4.0[28] was performed, adopting the B3LYP functional and def2-TZVP as a basis set with relativistic method ZORA.[29] Such investigation was carried out to analyze if the results provided by the quantum mechanical (QM) calculation (LANL2DZ ECP) are close to the ones provided by the relativistic ZORA method.

Development of the New Amber force field

To better describe the system under study and develop a set of parameters, an identification and labeling of the structure were performed. Although automatic tools are used to model systems of interest,[30] it is crucial to guarantee that the molecule to be described represents a structure as close to reality as possible. Using atom types in this set of parameters allows to distinguish the atoms in a better manner, considering structural and vibrational characteristics.[21]

Using the VMD 1.9.1 software,[31] the atom types were assigned utilizing two characters (one letter and one number) due to AMBER simulation package requirement, where C represent carbon atoms; N and M, nitrogen atoms; H and I, hydrogen atoms, O, oxygen atoms and V, vanadium atom, as shown Figure 2.

The parameterization was carried out adopting the structure with global minimum energy derived from the DFT calculations. Thus, the potential energy (V_{total}) of a molecule can be described as a summation of all terms that are involved in the system total energy, i.e., the total potential energy equals to the sum of bonded terms (bond, angles, and dihedrals) and non-bonded terms (Coulomb and Lennard-Jones), as stated by Equation 1:

$$V_{total} = \sum_{bonds} K_b(b - b_0)^2 + \sum_{angles} K_\theta(\theta - \theta_0)^2 + \sum_{dihedrals} K_\phi\,[cos(n\phi\ -\ \delta) + 1]$$

$$+ \sum_{Coulomb} \left[\frac{q_i q_j}{4\pi\varepsilon_0 r_{ij}}\right] + \sum_{Lennard-Jones} 4\epsilon_{ij}\left[\frac{\sigma^{12}}{r_{ij}^{12}} - \frac{\sigma^6}{r_{ij}^6}\right] \qquad (1)$$

where K_b, K_θ, and K_Φ are the force constants, b and θ correspond to bond length and angle respectively, b_0 and θ_0 are the equilibrium values, n is the periodicity, ϕ represents the dihedral angle, δ is the phase angle, r_{ij} is the distance between atoms i and j, ϵ is the depth of the potential well, σ is the distance at which the Lennard-Jones Potential is zero, q_i and q_j are the partial atomic charges of each atom, and ε_0 corresponds to vacuum permittivity.[32]

Further, from Equation 1, it can be seen that the AMBER force field is able to approximate the energy surface based on Newton's equations of motion, describing the forces acting on each atom due to the contributions of bonded and non-bonded atoms, emphasizing one of the two assumptions involved in common force fields, additivity, i.e., the overall energy associated to a system is the sum of different potentials with simple physical interpretations.[33] It is important to highlight that in this case, proper dihedrals were considered sufficient to describe the structure of CV, thus parameters for the improper dihedrals are absent.

The Hessian matrix calculation from the global minimum geometry was performed using the same functional and basis set as stated earlier in this chapter (B3LYP/def2-TZVP plus ECP for the vanadium atom). Based on the internal coordinate method, the force constants for the bonded terms were acquired through diagonalization of the Hessian matrix. It is noteworthy mentioning that since the obtained parameters highly depend on the internal coordinates originated from the QM calculation, different internal coordinates will result in different force constants.[34] The calculation of the Restrained Electrostatic Potential (RESP) atomic charges was carried out to obtain the Coulomb interaction parameters. Lastly, the Lennard-Jones parameters for all atoms, except vanadium, were assigned based on General AMBER Force

Field (GAFF) values. The non-bonded Lennard-Jones parameters ϵ and σ for vanadium atom were attributed according to values found in the literature.[35]

Once all the information needed about the parameters of VC was acquired, an MD simulation in vacuum was performed, at room temperature (T=300 K) and total simulation time of 20 ns, using AMBER11 simulation package.[36] Finally, a comparison between the structural data set and a quantum reference was made, considering only the last 10 ns of the simulation to ensure that the equilibration of the molecule was reached.

Docking Studies

The 3D structure of the protein AMPK was obtained from RCSB Protein Data Bank (PDB ID: 6C9G).[37] Due to absence of some residues of amino acids and aiming a more realistic structure to avoid inaccurate representations, a preparation of the protein was conducted. For this, the platform SWISS-Model was used to generate a homology model of the 3D structure based on templates available on the server.[38] After that, an alignment of the model obtained by the last step was performed through LovoAlign server.[39] The list of the equivalence of the residues in the original PDB file and the homology model generated by this step can be found in Table S1.1 in the Support Information (SI).

BIOVIA Discovery Studio Visualizer v. 21[40] was used to prepare the protein structure, where hydrogens atoms were added, and charges were calculated. Molegro Virtual Docker 2011 was used for the docking studies.[41] Based on the information reported by literature,[42] the antidiabetic drug known as metformin interacts with residues from AMPK-α1, namely Asp-217, Asp-218, and Asp-219. Such residues are equivalent to residues Asp-215, Asp-216, and Asp-217 in the homology model. Considering that the vanadium complex under study has two metformin as ligands, the previous information was considered to be a great insight about the docking site. Regarding the parameters used for the investigation, the flexible residues were included within a radius of 8 Å and the binding site radius was set as 7 Å. The score algorithm used was MolDock Score [GRID] with grid resolution of 0.30 Å and the search algorithm used was MolDock Optmizer.[43]

Molecular dynamics simulation

Simulations were conducted using the AMBER20 package and Amber ff99SB-ILDN force field[44] for the protein and were divided in four steps, namely minimization, heating, equilibration and production. The first step was performed by minimizing the energy of the

system with 2000 cycles of steepest descent method with a system restriction of 500.0 kcal/mol followed by 8000 cycles of conjugate gradient method. Next, the temperature of the system was increased gradually from 0 to 300 K in 5 steps of 50 ps each using the NVT ensemble and equilibrated at the same temperature, where the restriction was systematically decreased. Finally, for the production step, the simulation was performed with explicit solvent, using the TIP3P model, during 800 ns, without any restraint and in the presence of counterions, to maintain the neutrality of the simulated systems.[44] The final system included the AMPK protein, around 84,853 water molecules, and one Cl^- ion, leading to a simulated system that contains 270,496 atoms.

3. Results and Discussion

Conformational Search and Structural analysis

$VO(metf)_2 \cdot H_2O$ was previously optimized through Molecular Mechanics to avoid possible convergence errors, where UFF (Universe force field) was used for this calculation. The optimization was carried out using the Gaussian software. Then, the molecule in question was subjected to the scan calculation, in which the dihedrals N8-C6-M0-C8 and N4-C2-N5-C4 had their torsion angles varied, with increments of 30°. For this DFT calculation, B97-D functional and 6-311G++ basis function was used. As a result, the conformation with energy of -1,181,845.70 kcal/mol was chosen as the most stable and the one that better described the structural properties of the vanadium complex in a more realistic way.

Next, DFT calculations from different software, B3LYP/def2-TZVP LANL2DZ ECP (Gaussian) and B3LYP/def2-TZVP ZORA (ORCA) were performed, besides the optimization of the molecule using AMBER force field available on HyperChem. The results obtained by forementioned step were compared in order to evaluate the performance of the level of theory chosen to describe the system in question.

The structural validation included a total of 41 bonds and 72 bond angles and will be promptly addressed. The obtained results are available in Tables 1 and 2, where selected bond lengths and angles are shown in angstroms and degrees, respectively. The full information is available in SI (Tables S2.1 and S2.3).

Table 1. Selected bond lengths in Angstroms (Å) of different methods and levels of theory.

	AMBER *(HyperChem)*	**B3LYP/def2-TVZP LANL2DZ ECP** *(Gaussian 09)*	**B3LYP/def2-TVZP ZORA** *(ORCA)*
N2-V1	1.839	2.037	2.042
N3-V1	1.843	2.055	2.051
V1-O1	1.880	1.579	1.595
N7-V1	1.848	2.046	2.043
N9-V1	1.846	2.045	2.050

According to the gathered information, optimization using AMBER force field available on HyperChem did not present results with good agreement when compared with data obtained by a quite robust method (B3LYP/def2-TZVP ZORA), which re-emphasizes the need for more accurate AMBER force field parameters to describe the system under discussion.

Table 2. Selected bond angles in degrees (°) of different methods and levels of theory.

	AMBER *(HyperChem)*	**B3LYP/def2-TVZP LANL2DZ ECP** *(Gaussian 09)*	**B3LYP/def2-TVZP ZORA** *(ORCA)*
N2-V1-O1	117.754	110.114	108.146
N3-V1-O1	115.619	106.161	107.364
N2-V1-N7	80.736	87.063	86.898
N3-V1-N9	77.617	86.725	87.060
N3-V1-N7	130.033	147.690	144.919
N2-V1-N9	128.385	139.820	144.056
N2-V1-N3	84.467	82.159	82.377
V1-N3-C2	123.096	130.690	130.317
C5-N7-V1	118.600	128.866	128.800

It is possible to notice that the AMBER force field available on HyperChem fails to describe the structure of the complex when compared to relativistic method ZORA in which the mean of relative error for bond lengths and bond angles do not present reliable values. Such information can be retrieved in Table S2.5, in the SI.

The comparison between the relativistic method ZORA and the DFT calculation performed on Gaussian was carried out in order to investigate whether the minimized geometry obtained with ECP would present a geometry close to the one provided by the relativistic ZORA method, since no experimental data for the vanadium complex was available.

From Tables 1 and 2, it is possible to evaluate the calculations performed in Gaussian and ORCA, suggesting that the B3LYP/def2-TVZP LANL2DZ ECP level of theory used in this work to obtain the lowest energy geometry of the vanadium complex is as effective as the relativistic ZORA method. It is relevant to point out that when considering the effective core potential (ECP), any substantial increase in computational cost was not experienced. Moreover, the level of theory chosen for the optimization of the VC under study showed good performance on describing the structure of the system.

Validation of the New Force Field

In this step of validation, a comparison of bond lengths and bond angles was made among the values obtained from the quantum reference and the simulations using the new force field and GAFF, being possible to assess the deviations that the force field under study has in contrast with the reference and the general AMBER force field available on HyperChem. Furthermore, this investigation was performed considering the last 10 ns of the MD simulations.

According to Table 3, a good agreement between the values of bond lengths of the new force field and values derived from the DFT calculation was found. The complete comparison, including all bonds, can be found in SI, Table S3.1. It is noticeable that the new force field had a better performance regarding describing the bonds of the system under study. The mean of relative error (Table S3.5) obtained by the force field developed in this work showed smaller value (0.671%) when compared to the mean of relative error from GAFF (1.345%), which suggests that the general force field could not describe the bonds as efficient as the new force field.

Table 3. Selected bond lengths in Angstroms (Å) obtained by different calculations for validation purposes.

	B3LYP/def2-TVZP+LANL2DZ ECP *(Gaussian 09)*	**MD with GAFF** *(average)*	**MD with New FF** *(average)*
N2-V1	2.037	2.012	2.046
N3-V1	2.055	2.072	2.037

V1-O1	1.579	1.569	1.570
N7-V1	2.046	1.999	2.050
N9-V1	2.045	2.050	2.037

The good results obtained by the new force field is more pronounced when analyzing the bond angles, where the same pattern can be observed (Table 4). The new force field showed values closer to the reference (5.407%), with smaller mean of relative error (Table S3.5) when comparing to the values obtained by the GAFF simulation (7.345%). Once again, the new parameter set showed better performance than the general and widely used GAFF.

Table 4. Comparison of selected bond angles (º) obtained by different calculations for validation purposes.

	B3LYP/def2-TVZP+LANL2DZ ECP *(Gaussian 09)*	**MD with GAFF** *(average)*	**MD with New FF** *(average)*
N2-V1-O1	110.114	113.600	106.256
N3-V1-O1	106.161	48.671	98.213
N2-V1-N7	87.063	47.201	60.949
N3-V1-N9	86.725	53.313	128.946
N3-V1-N7	147.690	73.493	127.501
N2-V1-N9	139.820	100.064	130.776
N2-V1-N3	82.159	66.947	74.303
V1-N3-C2	130.690	131.880	131.775
C5-N7-V1	128.866	124.994	126.351

The results obtained by this analysis reinforce the importance of developing parameters for $VO(metf)_2 \cdot H_2O$ in order to describe the structure of the system with more accuracy.

New Amber Force Field Performance

The evolution of MD simulation in vacuum was monitored by a time-dependent calculation of the root mean square deviation (RMSD). It should be noted that the structure derived from DFT calculations was taken as a reference for such analysis. It is important to mention that the total time of simulation was 20 ns, however for the analysis, only the last 10 ns were considered in order to assure that the complex reached equilibrium. Based on Figure 3,

it is possible to observe that during the last 10 ns, the structure under study had an amplitude of oscillation of 0.5 Å, with average of RMSD equal to 0.839 Å ± 0.002 Å. Moreover, RMSD analysis demonstrates that the equilibrium condition was achieved, in other words, the complex attained a stable conformation. It is important to note that the simulation was carried out in vacuum, i.e., in the absence of molecules that could restrict the flexibility of the molecule.

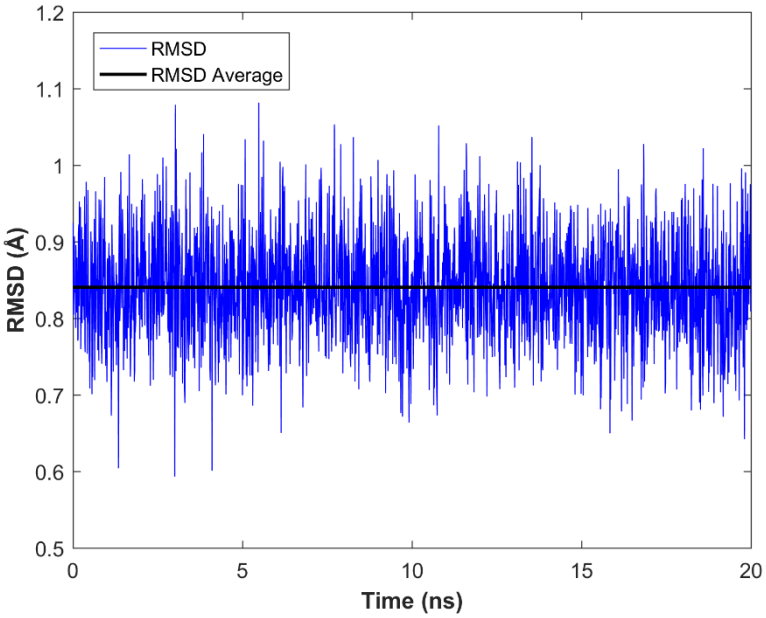

Figure 3. RMSD vs. time graph calculated for vanadium (IV) complex in vacuum.

In addition to the analysis of the VC in vacuum, an MD simulation in aqueous solution (Figure S4.2), using the TIP3P model for water molecules was carried out as well. Once again, the complex achieved a stable conformation, where the RMSD analysis shows equilibrium condition of the molecule under study. Moreover, VC presented amplitude of oscillation of 0.701 Å with average of RMSD equal to 0.337 Å ± 0.003 Å.

Bond Length Alternation

The geometric analysis of bond length alternation (BLA) was performed as well. The calculation of BLA is mathematically described by Equation 2:

$$BLA = \frac{1}{N_s}\sum l_S - \frac{1}{N_D}\sum l_D \qquad (2)$$

where N_S is the number of conjugated single bonds, N_D is the number of conjugated double bonds, l_S and l_D are the length of single and double bonds respectively.

A system is considered ideally conjugated when the average of the difference between single and double bond lengths is equal to zero. The average BLA values of the geometry were extracted from the last 10 ns of MD simulation for the new force field and GAFF. Figure 4 shows the BLA models computed from quantum reference (0.010 Å) in addition to the MD simulation using the new force field (0.009 Å) and GAFF (0.006 Å) parameters. According to the graph, the value obtained for the new force field showed very good agreement between the DFT approach, accurately describing the complex and proving the quality of the developed parameter set.

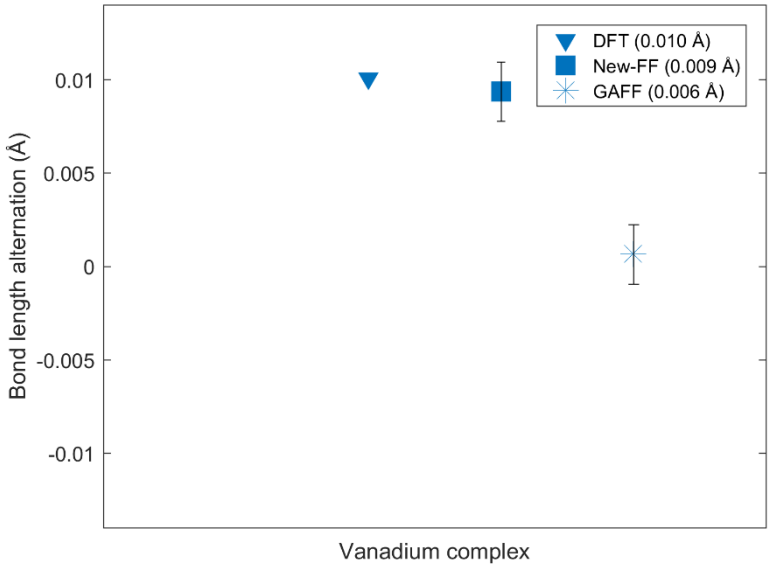

Figure 4. BLA analysis comprised of mean values of bond lengths from different models based on DFT, GAFF and New Force Field.

Protein Preparation

For the protein structure homology modelling, 123 residues were inserted to the structure whilst four residues were removed. A complete table with all residues from the model and the original structure is available in S1.1, where it is possible to see all equivalents residues. Moreover, the structure used as a template (SMTL ID: 5ezv.1) showed parameters closer to 1, i.e., parameters considered to be more than adequate to work with. For instance, the Global Model Quality Estimate (GMQE) of 0.85 showed good coverage of the target sequence and good template structure. Moreover, the QMEANDisCo Global of 0.77 ± 0.05 provided a model

with a good local quality score. Both parameters should be taken into account to increase reliability of the quality estimation. It is also important to mention that the RMSD for the alignment process performed in LovoAlign server is 2.15 Å, which can be considered a fair result since AMPK has regions in its subunits that are flexible, and this characteristic can increase the value of the RMSD.[45] The homology model generated by SWISS-Model was validated using TrRosetta, where the model presented TM-Score greater than 0.5, meaning that the confidence of the model is high.[46] In this way, the structure showed to be reliable to be used in the next steps.

Molecular Docking

In order to predict how the protein would interact with the VC, molecular docking was performed with the conditions previously mentioned in the methodology section. Among the 150 poses generated by the analysis performed, the one that showed lower energy (-103.781 kcal/mol) was chosen for the next step (Figure 5a). In this case, this preferred orientation showed to be more stable than others obtained in this investigation. This study also suggested that the vanadium complex interacts with the following residues: Tyr-205, Thr-211, Pro-213, Leu-212, Asp-215 and Tyr-232 which are highlighted in Figure 5b.

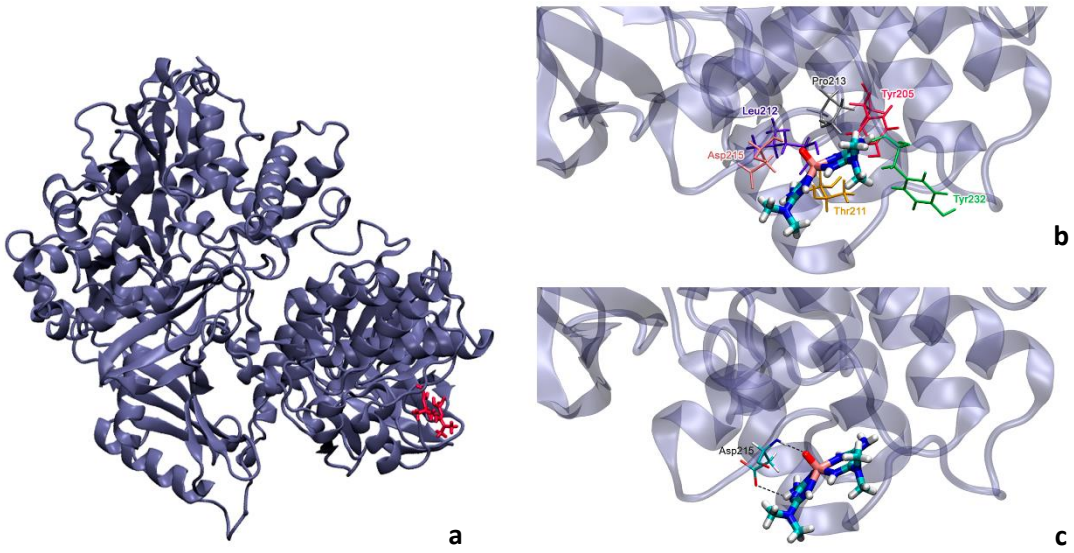

Figure 5. (a) Overview of the system under study. **(b)** Selected pose with lower energy along with residues that interacted with the complex. **(c)** Hydrogen bonds between residue Asp-215 and $VO(metf)_2 \cdot H_2O$.

It is essential to mention that the pose was not elected as a starting point for the simulations solely by its lower energy. As can been seen in Figure 5c, hydrogens bonds between

residue Asp-215 and the complex were successfully reproduced in this investigation (Figure 5c). This information of great value replicated data already reported in literature.[42] Once information about the orientation and hydrogen bonds made by the complex was acquired, MD simulations could be initiated, where the system protein-vanadium complex was investigated in a more in-depth way over a period of time.

Molecular Dynamics: application for Alzheimer's treatment

The behavior of the system comprised by AMPK and $VO(metf)_2 \cdot H_2O$ in explicit solvent was monitored during 800 ns and the RMSD was calculated taking as reference the coordinates of the first frame of the simulation. A first look at Figure 6 allows a better comprehension about the VC fluctuations during the time of simulation, where the average RMSD was equal to 0.2578 Å with a standard deviation of 0.0011 Å. The results obtained for the vanadium complex are a great achievement, showing that the molecule remained stable during 800 ns.

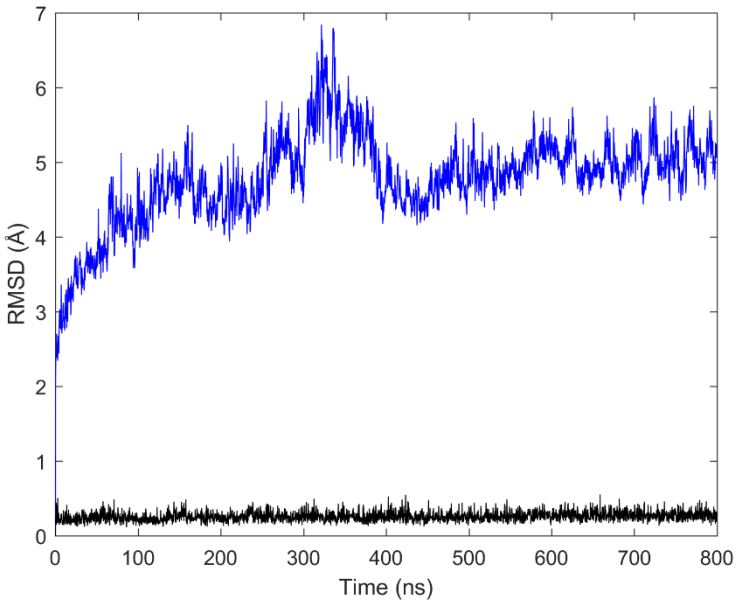

Figure 6. RMSD vs. time graph of the system AMPK-vanadium (IV) complex in explicit solvent. Blue line refers to protein deviation, and black line refers to complex deviation.

The protein, in particular, showed an average RMSD of 4.7774 Å with a standard deviation of 0.0113 Å. These values are quite small considering the reasonable flexibility of its structure.[47]

A sausage representation of the AMPK protein was calculated through software PyMol,[48] where 80 frames were used, 1 frame sampled at every 250 ps of the first 200 ns. As can be seen in Figure 7, the spatial root mean square fluctuation (RMSF) with more displacement are shown in regions with major thickness, i.e., the most mobile regions correspond to major thickness in the sausage representation. Such fluctuations occurred mainly in loop regions, in residues such as Ile-288–Leu-326 (α subunit), Arg-373–Lys-395 (α subunit), Phe-16–Pro-137 (β subunit), Glu-119–Val-130 (γ subunit), Ala-227–Tyr-241 (γ subunit). This information is consistent with the literature, where it is reported that loops connecting helices and sheets are considered to be more flexible.[49]

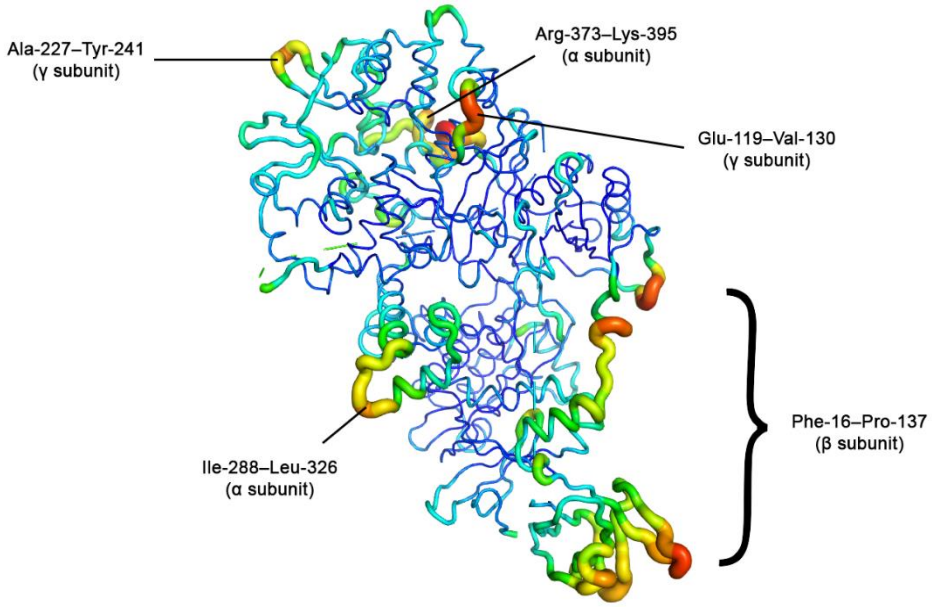

Figure 7. Sausage representation of the superimposed 80 frames of AMPK generated by PyMol v. 2.5.3.

Another aspect of this work that needs to be validated is the hydrogen bonds pointed out during the docking investigation. As stated previously, $VO(metf)_2 \cdot H_2O$ interacted with residues Tyr-205, Thr-211, Pro-213, Leu-212, Asp-215 and Tyr-232. Based on the information obtained from VMD, taking into account the total time of simulation, it was indicated by the hydrogen bond analysis interactions with residues mentioned on the docking study (Tyr-205, Thr-211, Pro-213, Leu-212, Asp-215 and Tyr-232) in addition to six more residues, namely Tyr-205, Cys-209, Gly-210, Phe-214, Thr-233, and Gln-235.

In particular, interactions between residue Leu-212 and $VO(metf)_2 \cdot H_2O$ were reported as most recurring. Although not reported by the literature, interactions between Leu-212@O

and VC@H3, Leu-212@O and VC@I3, and Leu-212@O and VC@I1 were found throughout the simulation, as can be seen in Figure 8.

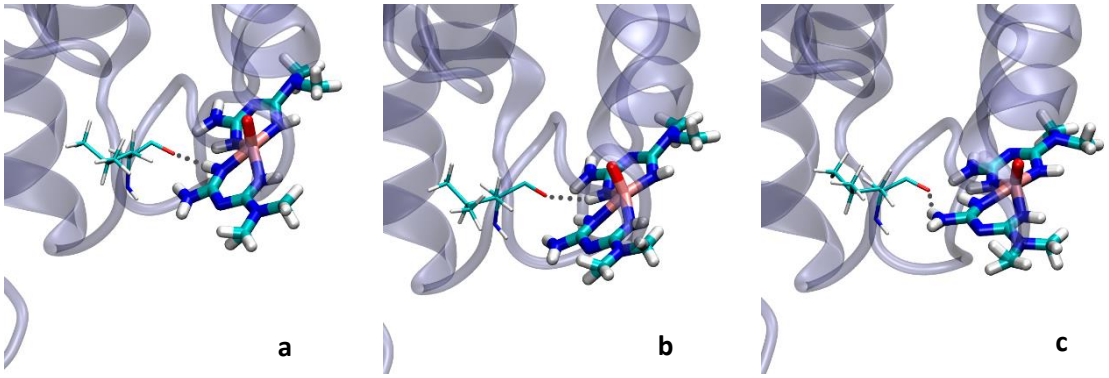

Figure 8. Hydrogen bonds between **(a)** Leu-212@HB2 and VC@N7, **(b)** Leu-212@HB2 and VC@N2 and **(c)** Leu-212@HB2 and VC@N6.

Interestingly, residue Gln-235 participated in the formation of hydrogen bonds as well, and was not pointed out during the docking study, considering the chosen pose. Furthermore, interactions with this residue were the second most recurring. Residue Gln-235@H forms a hydrogen bond with VC@O1. Such interaction was possible due to the displacement of the complex over the last 65 ns of the simulation. This behavior will be addressed next.

Due this displacement, hydrogen bonds between VC and residues Cys-209 and Gly-210 were also reported, where VC@O1 and Cys209@HB3, and VC@H4 interacted Gly210@O were pointed out by the MD. In this case, these interactions were not described by the literature.

Another interaction noteworthy is the hydrogen bonds between Asp-215@H and VC@O1, and between Asp-215@H and VC@N6, that was not described by the literature. In addition, the interaction between nitrogen (N6) from VC and the hydrogen from the same residue were corroborated in this analysis.

Hydrogen bonds formed between residues Tyr-205, Thr-211, Pro-213, Phe-214, Tyr-232, and Thr-233 and the vanadium complex were also confirmed by this analysis, however the occurrence of such bonding was less significant.

Throughout most of the simulation, the protein did not undergo any drastic change. However, it was observed a change in conformation in residues Leu-208 to Asn-238 in the last 615 ns of the simulation, as can be seen in Figure 9.

This conformation change may have affected interactions between VC and residues, such as Asp-215 and Leu-212, in which may have distanced themselves from $VO(metf)_2 \cdot H_2O$.

Presumably, during this conformational change, residues Cys-209, Gly210, and Gln-235 may have approached VC and then a more effective hydrogen bond between those species was formed.

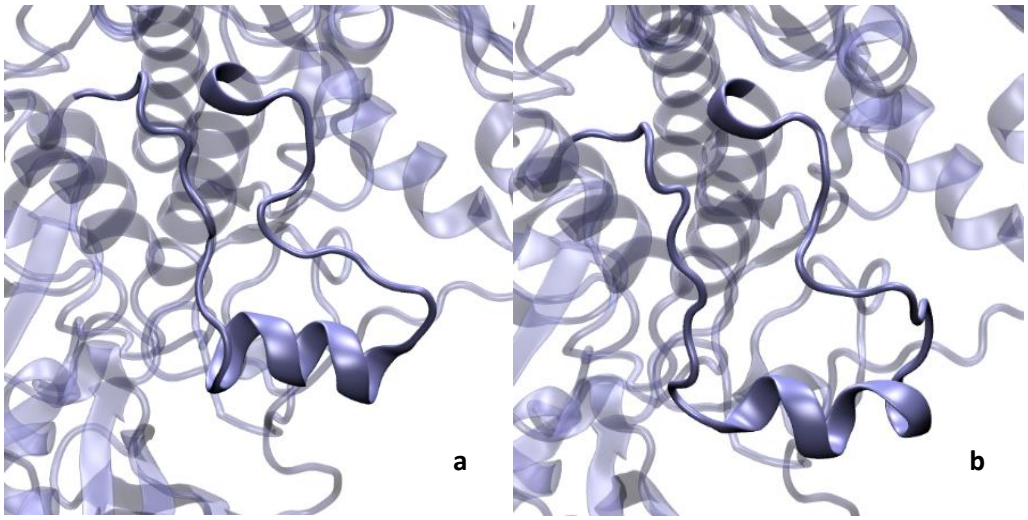

Figure 9. Residues Leu208 to Asn238 undergoing through conformational change. (a) Before the change. (b) After conformational change.

Furthermore, over the 800 ns of simulation, the loops shown in Figure 9 experienced oscillations that might have contributed to the displacement of the complex and formation of the hydrogen bond with the already mentioned residues. Another change that might have contributed is the α-helix, where its length showed considerable variation due to conformation change.

Taking into consideration the fact that AMPK plays key roles in both T2DM and AD,[9] being considered as a bridge between these two diseases, and the promising effects of VC in facing T2DM, turning into a potential agent against the neurodegenerative disease in question, the encouraging results obtained by this work may offer valuable insights in the AD treatment.

4. Conclusion

The present work aimed to understand in a more refined way the interaction of the VC and the AMPK protein (associated with AD and T2DM). To this end, the work consists of two stages which show the relevance and important contribution of the findings to the scientific community.

The first one was motivated by the lack of structural information of the vanadium complex under study in this work. Through computational tools, an AMBER force field was developed and validated using a strategy that showed to be efficient to describe the VC, $VO(metf)_2 \cdot H_2O$.

The mean relative errors for bond lengths and bond angles proved to be considerably small, reinforcing an acquisition of a great geometry. Supported by RMSD analysis, the proposed specific metal-ligand set of parameters lead to an equilibrium condition and stable conformation. Lastly, BLA analysis showed that the new force field was able to reproduce the experimental prediction. Overall, the new parameter set showed better performance that the general and widely used GAFF.

After encouraging results, the second stage for the investigation was carried out, where the biological application, i.e., the interactions and behavior of the system formed by the protein and $VO(metf)_2 \cdot H_2O$ were the focus of the research. Furthermore, the hydrogen bonds pointed out during docking were validated. It is worth mentioning residue Leu-212 as the residue that interacted most with the complex.

Once again, RMSD analysis provided a better understanding of how the system behaved during the simulation time. RMSD values for the VC were considered excellent for this study, where the complex showed stability during the total time of simulation. In turn, the RMSD values of the protein proved to be in line with expectations since the structure has considerable flexibility. Residues Cys-209, Gly210, Phe-214 and Gln-235 that interacted with the molecule after a conformational change of the protein in a specific region near the binding site should be highlighted as well. In general, the results obtained in this step provide a meaningful insight into the behavior of the system under study.

These findings obtained in this work can be considered motivating for future studies that have the purpose of using the vanadium complex for the treatment of AD, since this molecule in question can be considered promising for this specific application, as mentioned before, where improving interactions between residues such as Leu-212 and Asp-215 and the VC may be an excellent approach.

Funding Sources

This work is financially supported by the Brazilian agencies CAPES, CNPq, and FAPEMIG.

Notes

The authors declare no conflict of interest.

Acknowledgements

The authors thank Ander Francisco Pereira for the assistance with the methodology and the comments that greatly improved the manuscript.

References

(1) United Nations, Department of Economic and Social Affairs, Population Division (2022). *World Population Prospects 2022*, Online Edition, available at: https://population.un.org/wpp/Download/Standard/Mortality/ [accessed 1 September 2022].

(2) World Health Organization, Newsroom, Fact Sheets, Detail (2022). *Dementia*, Online Edition, available at: https://www.who.int/news-room/fact-sheets/detail/dementia [accessed 1 September 2022]

(3) Volicer, L. Physiological and pathological functions of beta-amyloid in the brain and Alzheimer's disease: A review. *Chin. J. Physiol.* **2020**, 63, 3, 95, 2020.

(4) Falco, A. D.; Cukierman, D. S.; Hauser-Davis, R. A.; Rey, N. A. Doença de Alzheimer: hipóteses etiológicas e perspectivas de tratamento. *Quim. Nova*. **2016**, 39, 63-80.

(5) Paudel, P.; Park, C. H. Jung, H. A.; Yokozawa, T., Choi, J. S. A systematic review on anti-Alzheimer's disease activity of prescription Kangen-karyu. *Drug Discov. Ther*. **2020**, 14, 61-66.

(6) Nguyen, P. H.; Ramamoorthy, A; Sahoo, B. R.; Zheng, J.; Faller, P.; Straub, J. E.; Dominguez, L.; Shea, J. E.; Dokholyan, N. V.; Simone, A. *et al*. Amyloid oligomers: A joint experimental/computational perspective on Alzheimer's disease, Parkinson's disease, type II diabetes, and amyotrophic lateral sclerosis. *Chem. Rev.* **2021**, 121, 4, 2545-2647.

(7) Doig, A. J.; Castillo-Frias, M. P.; Berthoumieu, O.; Tarus, B.; Nasica-Labouze, J.; Sterpone, F.; Nguyen, P. H.; Hooper, N. M.; Faller, P.; Derreumaux, P. Why is research on amyloid-β failing to give new drugs for Alzheimer's disease? *ACS Chem. Neurosci.* **2017**, 8, 7, 1435-1437, 2017.

(8) Bortoletto, A. S.; Graham, W. V.; Trout, G.; Bonito-Oliva, A.; Kazmi, M. A.; Gong, J.; Weyburne, E.; Houser, B. L.; Sakmar, T. P.; Parchem. R. J. Human Islet Amyloid Polypeptide (hIAPP) Protofibril-Specific Antibodies for Detection and Treatment of Type 2 Diabetes. *Adv. Sci*. **2022**, 9, 34, e2202342.

(9) Chen, M.; Huang, N.; Liu, J.; Huang, J.; Shi, J.; Jin, F. AMPK: A bridge between diabetes mellitus and Alzheimer's disease. *Behav. Brain. Res*. **2021**. 400, 113043.

(10) Kang, P.; Wang, Z.; Qiao, D.; Zhang, B.; Mu, C.; Cui, H.; Li, S. Dissecting genetic links between Alzheimer's disease and type 2 diabetes mellitus in a systems biology way. *Front. Genet*. **2022,** 13.

(11) Peixoto, C. A.; Oliveira, W. H.; Araújo, S. M. R.; Nunes, A. K. S. AMPK activation: Role in the signaling pathways of neuroinflammation and neurodegeneration. *Exp. Neurol*. **2017,** 298, 31-41.

(12) Ge, Y.; Zhou, M.; Chen, C.; Wu, X.; Wang, X. Role of AMPK mediated pathways in autophagy and aging. *Biochimie*. **2022**, 195, 100-113.

(13) Andrade, C. H.; Kummerle, A. E.; Guido, R. V. C. Perspectivas da química medicinal para o século XXI: desafios e oportunidades. *Quim. Nova*. **2018,** 41, 476-483.

(14) Akter, K.; Lanza, E. A.; Martin, S. A.; Myronyuk, N.; Rua, M.; Raffa. R. B. Diabetes mellitus and Alzheimer's disease: shared pathology and treatment? *Br. J. Clin. Pharmacol*. **2011**, 71, 3, 365-76.

(15) Liu, H.; Qu, Y.; Wang, X. Amyloid β-targeted metal complexes for potential applications in Alzheimer's disease. *Future Med. Chem*. **2018**, 10(6), 679-701.

(16) Rusanov, D. A.; Zou, J.; Babak, M. V. Biological Properties of Transition Metal Complexes with Metformin and Its Analogues. *Pharmaceuticals*. **2022**, 15, 4.

(17) Woo, L. C. Y.; Yuen, V. G.; Thompson, K. H.; McNeill, J. H.; Orvig, C. Vanadyl–biguanide complexes as potential synergistic insulin mimics. *J. Inorg. Biochem*. **1999**, 76, 3, 251-257.

(18) Karplus, M.; McCammon, J. A. Molecular dynamics simulations of biomolecules. Nat. Struct. Biol. **2002**, 9, 9, 646-652.

(19) Salo-Ahen, O. M. H.; Alanko, I.; Bhadane, R.; Bonvin, A. M. J. J.; Honorato, R. V.; Hossain, S.; Juffer, A. H.; Kabedev, A.; Lahtela-Kakkonen, M.; Larsen, A. S. *et al*. Molecular dynamics simulations in drug discovery and pharmaceutical development. *Process*. **2020**, 9, 1, 71.

(20) Li, P.; Merz Jr, K. M. Metal Ion Modeling Using Classical Mechanics. *Chem. Rev*. **2017**, 117, 3, 1564-1686.

(21) Pereira, A. F.; Prandi, I. G.; Ramalho, T. C. Parameterization and validation of a new force field for Pt(II) complexes of 2-(4′-amino-2′-hydroxyphenyl)benzothiazole. *Int. J. Quantum Chem*. **2021**, 121, 6, e26525.

(22) Prandi, I. G.; Viani, L.; Andreussi, O.; Mennucci, B. Combining classical molecular dynamics and quantum mechanical methods for the description of electronic excitations: The case of carotenoids. *J. Comput. Chem*. **2016**, 37, 11, 981-991.

(23) Dennington, J. M.; Keith, R. D.; Millam, T. A. *GaussView 5.0.8*, Gaussian. Inc., Wallingford CT. **2008**.

(24) Grimme, S. Semiempirical GGA-type density functional constructed with a long-range dispersion correction. *J. Comput. Chem*. **2006**, 27, 15, 1787-1799.

(25) Frisch, M. J; Trucks, G. W.; Schlegel, H. B.; Scuseria, G. E.; Robb, M. A.; Cheeseman, J. R; Scalmani, G.; Barone, V.; Petersson,G. A.; Nakatsuji, H. *et al*. *Gaussian 16, Revision C.01*, Gaussian. Inc., Wallingford CT, **2016**.

(26) Kaur, N.; Kumari, I.; Gupta, S; Goel, N. Spin Inversion Phenomenon and Two-State Reactivity Mechanism for Direct Benzene Hydroxylation by V4O10 Cluster. *J. Phys. Chem A*. **2016**, 120, 48, 9588-9597.

(27) *HyperChem Professional 7.0*, Hypercube, Inc., Gainesville FL, **2002**.

(28) Neese, F., Software update: the ORCA program system, version 4.0. WIREs Comput. Mol. Sci. **2018**, 8, 1, e1327.

(29) Cárdenas, G.; Marquetand, P.; Mai, S.; González, L. A Force Field for a Manganese-Vanadium Water Oxidation Catalyst: Redox Potentials in Solution as Showcase. *Catalysts*. **2021**, 11, 4.

(30) Santos, L. A.; Prandi, I. G.; Ramalho, T. C. Could Quantum Mechanical Properties Be Reflected on Classical Molecular Dynamics? The Case of Halogenated Organic Compounds of Biological Interest. Front. Chem. **2019**, 7.

(31) Humphrey, W.; Dalke, A.; Schulten, K. VMD: Visual molecular dynamics. *J. Mol. Graph*. **1996**, 14, 1, 33-38.

(32) Cornell, W. D.; Cieplak, P.; Bayly, C. I.; Gould, I. R.; Merz Jr, K. M.; Ferguson, D. M.; Spellmeyer, D. C.; Fox, T.; Caldwell, J. W.; Kollman, P. A. A Second Generation Force Field for the Simulation of Proteins, Nucleic Acids, and Organic Molecules. *J. Am. Chem. Soc*. **1995**, 117, 19, 5179-5197.

(33) Monticelli, L.; Tieleman, D.P. Force Fields for Classical Molecular Dynamics. In *Biomolecular Simulations: Methods and Protocols,* Humana Press, **2013**; pp. 197-213.

(34) Zheng, S.; Tang, Q.; He, J.; Du, S.; Xu, S.; Wang, C.; Xu, Y.; Lin, F. VFFDT: A New Software for Preparing AMBER Force Field Parameters for Metal-Containing Molecular Systems. *J. Chem. Inf. Model*. **2016**, 56, 4, 811-818.

(35) Šebesta, F., Sláma, V.; Melcr, J.; Futera, Z.; Burda, J. V. Estimation of Transition-Metal Empirical Parameters for Molecular Mechanical Force Fields. *J. Chem. Theory Comput.* **2016**, 12, 8, 3681-3688.

(36) Case, D. A.; Darden, T. A.; Cheatham, T. E.; III, Simmerling, C. L.; Wang, J.; Duke, R. E.; Luo, R.; Walker, R. C.; Zhang, W.; Merz, K. M. *et al*. *AMBER 11*, University of California, San Francisco CA, **2010**.

(37) Yan, Y.; Zhou, E.; Novick, S. J.; Shaw, S. J.; Li, Y.; Brunzelle, J. S.; Hitosh, Y.; Griffin, P. R.; Xu, H. E. Melcher, K. Structures of AMP-activated protein kinase bound to novel pharmacological activators in phosphorylated, non-phosphorylated, and nucleotide-free states. J. Biol. Chem. **2019**, 294, 3, 953-967.

(38) Waterhouse, A.; Bertoni, M.; Bienert, S.; Studer, G.; Tauriello, G.; Gumienny, R.; Heer, F. T.; Beer, T. A. P.; Rempfer, C.; Bordoli, L. *et al*. SWISS-MODEL: homology modelling of protein structures and complexes. *Nucleic Acids Res*. **2018**, 46, W1, W296-W303.

(39) Martínez, L.; Andreani, R.; Martínez, J.M. Convergent algorithms for protein structural alignment. *BMC Bioinform*. **2007**, 8, 1, 306.

(40) *BIOVIA Discovery Studio Visualizer*. Dassault Systèmes, San Diego CA, **2021**.

(41) *Molegro Virtual Docker*. Molexus, Rørth Denmark, **2011**.

(42) Thabah, D.; Syiem, D.; Pakyntein, C.; Banerjee, S.; Kharshiing, C. E.; Bhattacharjee, A. Potentilla fulgens upregulate GLUT4, AMPK, AKT and insulin in alloxan-induced diabetic mice: an in vivo and in silico study. Arch. Physiol. Biochem. **2021**, 1-13.

(43) Thomsen, R.; Christensen, M.H. MolDock: A New Technique for High-Accuracy Molecular Docking. *J. Med. Chem*. **2006**, 49, 11, 3315-3321.

(44) Aledavoo, E.; Forte, A.; Estarellas, C.; Luque, J. Structural basis of the selective activation of enzyme isoforms: Allosteric response to activators of β1- and β2-containing AMPK complexes. *Comput. Struc. Biotechnol. J*. **2021**, 19, 3394-3406.

(45) Martínez, L. Automatic Identification of Mobile and Rigid Substructures in Molecular Dynamics Simulations and Fractional Structural Fluctuation Analysis. PLoS ONE. **2015**, 10, 3, e0119264.

(46) Du, Z.; Su, H.; Wang, W.; Ye, L.; Wei, H.; Peng, Z.; Anishchenko, I.; Baker, D.; Yang, J. The trRosetta server for fast and accurate protein structure prediction. *Nat. Protoc*. **2021**, 16, 12, 5634-5651.

(47) Kurumbail, R.G. and M.F. Calabrese, Structure and Regulation of AMPK. In *AMP-activated Protein Kinase*, Springer, **2016**; pp. 3-22.

(48) *The PyMOL Molecular Graphics System*. Schrödinger, LLC, **2015**.

(49) Subramani, A. Floudas, C.A. Structure prediction of loops with fixed and flexible stems. *J. Phys. Chem. B.* **2012**, 116, 23, 6670-6682.

CHAPTER THREE – SECOND PAPER

Parameterization and validation of a new AMBER force field for an oxovanadium (IV) complex with therapeutic potential implications in Alzheimer's Disease

Article submitted to Journal of Molecular Graphics and Modelling

Abstract

The scarcity of efficient force fields to describe metal complexes may be a problem for new advances in medicinal chemistry. Thus, the development of force fields for these compounds can be valuable for the scientific community, especially when it comes to molecules that show interesting outputs regarding potential treating of diseases. Vanadium complexes, for instance, have shown promising results towards therapeutics of Alzheimer's Disease, most notably the bis(maltolato)oxovanadium (IV). Therefore, the mainly goal of this work is to develop and validate a new set of parameters for this vanadium complex from a minimum energy structure, obtained by DFT calculations, where great results of the new force field are found when confronted with experimental and quantum reference values. Moreover, the new force field showed to be quite effective to describe the molecule of under study whilst GAFF could not describe it effectively. In addition, a case study points out hydrogen bonds in the vanadium complex-PTP1B system.

Keywords: Vanadium Complex. AMBER Force Field. Molecular Dynamics. Docking. Alzheimer's Disease.

1. Introduction

Approximately 50 million people worldwide have been affected by dementia. The consequence of this syndrome is a decline in cognitive function beyond what is normally expected during aging.[1] The estimated global cost of dementia exceeds $1.3 trillion annually and is expected to increase to $2.8 trillion by 2030.[2] Besides the economic impact, this neurodegenerative condition can aggressively affect the patient and their family from a physical and psychological point of view.[3]

One of the most recurrent conditions associated with dementia is the so-called Alzheimer's disease (AD), an extremely complex disease that has been studied very closely by the scientific community in the search of further clarification of its pathogenesis.[4] AD is known for having three stages, where in the first stage, the patient can experience memory lapses but

may function independently. For stage two, communicative and cognitive skills are affected. The symptoms become progressively more intense throughout the third stage, the nerve cells in the brain are damaged and the individual loses their ability to respond to the environment.[5]

Different hypotheses have attempted to explain what causes such severe condition. The amyloid cascade hypothesis is considered one of the main premises that has been the subject of study for more than 25 years.[3,6] However, recently evidence suggests that the inhibition of protein tyrosine phosphatase 1B (PTP1B) may potentially modulate several processes in the central nervous system, affecting the development of AD.[7]

Tyrosine-protein phosphatase non-receptor type 1, also known as protein-tyrosine phosphatase 1B (PTP1B), is a negative regulator of the insulin signaling pathway, inducing insulin resistance.[8] PTP1B is also associated with conditions such as inflammation and obesity.[9]

Moreover, PTP1B has been indicated as a modulator of the brain-derived neurotrophic factor (BDNF), a regulator of synaptic plasticity. Since brains affected by AD presents decreasing levels of BDNF, PTP1B is, in fact, considered a promising approach for potential treatment of AD.[7] Thus, it is possible to infer, based on such findings, that PTP1B can be considered a bridge between AD and T2DM.

Accordingly, antidiabetic drugs have been explored as promising treatment strategies to approach AD, based on their neuroprotective mechanisms, showing improvement of cognitive ability and spatial memory.[10,11] Furthermore, preclinical, and clinical trials show encouraging results towards neurodegeneration and need further clarification.[12]

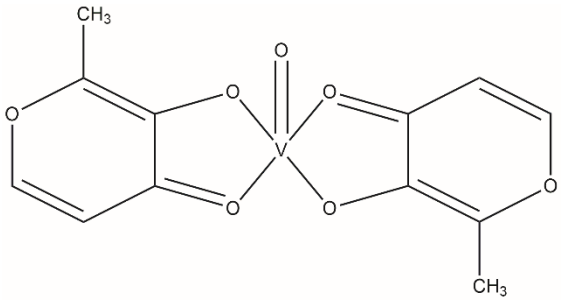

Figure 1. Structure of BMOV.

Among the potential candidates, insulin, metformin, and a variety of metal complexes, such as platinum, copper, cobalt, and vanadium, have been under investigation.[12,13] Particularly, among the vanadium complexes under study, bis(maltolato)oxovanadium (IV) (BMOV) (Figure 1) is considered a benchmark for antidiabetic agents, having the best effect on inhibiting PTP1B activity, and enhancing insulin receptor activation *in vivo*.[14]

Although experimental techniques, such as X-ray crystallography, are essential to precisely describe the structure of a complex, a theoretical approach may contribute

significantly by seeking to understand the structural, and chemical behavior of such complex, making possible the study of this potential agent against this neurodegenerative disease, based on therapeutic effects of BMOV.[15]

Molecular Dynamics (MD) is an effective theoretical method that provides accurate description of systems in general, its results are highly dependent on a reliable parameterization of the force field (FF) and the attempt to model a chemical system described by force field can be very challenging. In addition, the choice of force fields is an essential step for the correct description of the system under study. [16,17,18,**19**]

Another important point to be addressed is the scarcity of parameters for metal centers, making this situation even more complex.[17] General force fields cannot be applicable or transferable to other systems due to different atom types that are not considered during the force field development.[18] Moreover, for metal-containing molecules, most of the general force fields predict the structure of complexes in an unreliable way.[20] Thus, a new Assisted Model Building with Energy Refinement (AMBER) force field for the vanadium complex BMOV is considered necessary. A recent work has explored the development of new parameters for a vanadium complex, $VO(metf)_2 \cdot H_2O$, where the results are excellent and encourage such investigation.[21]

With that being said, the purpose of this work is to effectively obtain a set of parameters for this relevant BMOV (Figure 1) allowing further studies to provide a deeper understanding of the behavior of the system associated with AD and T2DM. The methodology used in this work involves developing and validating the new AMBER force field through classical MD simulations and comparison with experimental data and quantum reference.

Furthermore, in a second step, a case study was proposed to investigate the interactions between BMOV and PTP1B, where hydrogen bonds (HBonds) in the BMOV-PTP1B system were pointed out during the docking investigation and validated based on MD simulation (200 ns) in explicit solvent.

2. Computational Details

This step was divided into three important parts. The first one was the acquaintance of an accurate starting point with a global minimum energy for the parameterization of BMOV. After building the initial structure through GaussView 5.0.8, the geometry optimization with level theory B3LYP and basis set def2-TZVP plus LANL2DZ ECP for the vanadium atom was performed using Gaussian 09.[22,23] Such functional and basis set are suitable for describing

systems that have vanadium in their structure since results found in literature showed consistency when compared to experimental data.[24]

The second moment relied on using a relativistic method to evaluate the performance of the Quantum Mechanical (QM) calculation in describing the system under study. The software ORCA was used, B3LYP functional and def2-TZVP basis set with relativistic method ZORA were adopted for the calculation even though the central metal atom of the structure does not present prominent relativistic effects due to vanadium being an atom that is relatively lighter than other metals.[25] However, this calculation is still relevant in view of the robustness of such method. Moreover, this basis set was chosen for this step due to its efficiency in describing systems containing vanadium in their structures.[26]

Finally, to test its effectiveness in describing the complex, the AMBER96 force field available on software HyperChem 7.0 was used for the BMOV structural optimization for comparison purposes.[27]

Parameterization of a new AMBER force field

The process of identification and labeling the structure, i.e., assigning atom types to better describe the system considers structural and vibrational characteristics, distinguishing the atoms and making possible to develop an accurate set of parameters.[17]

Based on requirements from the AMBER simulation package, the atom types were assigned using one letter and one number through VMD 1.9.1 software.[28] For the vanadium complex under study, carbon atoms were represented by letters C and D, oxygen atoms by O, hydrogen atoms, H, and I, and vanadium atom by letter V as shown in Figure 2. It is important to mention that the symmetry of the molecule was taken into consideration. More information about equivalent atom types, bonds, angles and dihedrals can be found in table S4.1.

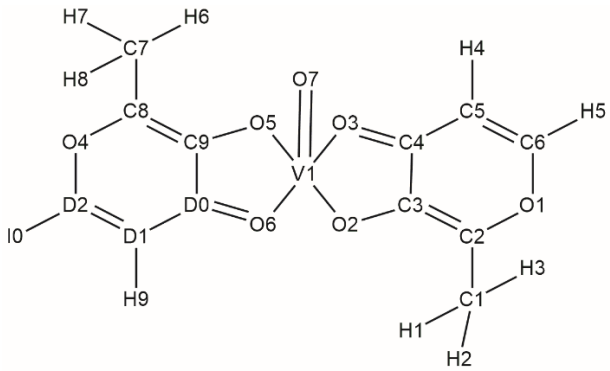

Figure 2. Atom types assigned to the vanadium complex BMOV.

The structure with global minimum energy derived from the Density Functional Theory (DFT) calculations was adopted as a starting point for the development of the parameters of

BMOV. Equation 1 gives the total energy of the system being equal to the sum of all terms, bonded and non-bonded, involved in describing the molecule. Bonds, angles, and dihedrals represent the bonded terms while Coulomb and Lennard-Jones terms represent the non-bonded contribution.

$$V_{total} = \sum_{bonds} K_b(b - b_0)^2 + \sum_{angles} K_\theta(\theta - \theta_0)^2 + \sum_{dihedrals} K_\phi\,[cos(n\phi\ -\ \delta) + 1] + \sum_{\text{Coulomb}} \left[\frac{q_i q_j}{4\pi\varepsilon_0 r_{ij}}\right] + \sum_{\text{Lennard-Jones}} 4\epsilon_{ij}\left[\frac{\sigma^{12}}{r_{ij}^{12}} - \frac{\sigma^6}{r_{ij}^6}\right] \quad (1)$$

In this equation, K_b, K_θ, and K_ϕ are the force constants, b and θ correspond to bond length and angle respectively, b_0 and θ_0 are the equilibrium values, n is the periodicity, ϕ represents the dihedral angle, δ is the phase angle, r_{ij} is the distance between atoms i and j, ϵ is the depth of the potential well, σ is the distance at which the Lennard-Jones Potential is zero, q_i and q_j are the partial atomic charges of each atom, and ε_0 corresponds to vacuum permittivity.[29]

To obtain the Hessian matrix, a calculation using B3LYP/def2-TZVP plus ECP for the vanadium atom level of theory was performed based on the global minimum geometry. After that, the force constants for the bonded terms were obtained through the diagonalization of the Hessian matrix. The Coulomb interaction parameters were acquired from the calculation of the Restrained Electrostatic Potential (RESP) atomic charges. The QM method used to calculate the ESP charges and to generate the coordinates of ESP points was DFT, at B3LYP/ def2-TZVP + LANL2DZ ECP and a van der Waals radius equals to 2.05 Å was used for the vanadium atom[30,31]. Finally, the Lennard-Jones parameters for all atoms, except vanadium, were assigned based on General Amber Force Field (GAFF) values. Based on values found in literature, the non-bonded Lennard-Jones parameters ϵ and σ for vanadium atom were assigned.[32]

After gathering all the information from previous steps, an MD simulation in vacuum was performed using AMBER20 simulation package using the *sander* program, at room temperature (T=300 K) and total simulation time of 20 ns, with a time step of 0.001 ps.[33] Langevin thermostat and Berendsen barostat were used in the simulation. Then, the results obtained through the new force field were compared to experimental data and the quantum reference, using the last 10 ns of the simulation to assure that the molecule reached an equilibrium condition.

3. Results and Discussion

Optimization analysis

The performance of the level of theory chosen to describe BMOV (B3LYP/def2-TZVP LANL2DZ ECP) was evaluated through comparison to the structure obtained from DFT calculation using ORCA and to the experimental data, obtained by X-ray crystallography.[23] Furthermore, a comparison between B3LYP/def2-TZVP LANL2DZ ECP (Gaussian) and AMBER96 force field available on HyperChem was made as well.

Table 1 shows the mean of relative error for bond lengths and bond angles of BMOV from different methods and levels of theory. In total, 23 bonds and 38 angles were taken into account for this analysis.

Table 1. Mean of relative error (%) of different methods and levels of theory.

	AMBER96 vs. Exp.[a]	ECP[b] vs. Exp.	ZORA[c] vs. Exp	ECP vs. ZORA
Bond Lengths	6.499	1.955	1.903	0.174
Bond Angles	4.531	2.261	2.276	0.130

[a] Exp: Experimental data. [b] ECP: Effective core potential [c] ZORA: Zeroth Order Regular Approximation.

Based on the mean of relative error, optimization using AMBER96 force field available on HyperChem was not able to accurately describe the system under study, in which both bond lengths and bond angles showed mean of relative error greater than other methods. This result demonstrates the importance of developing a specific force field to describe the molecule BMOV, since the general AMBER96 force field available did not showed good performance.

Furthermore, B3LYP/def2-TZVP LANL2DZ ECP level of theory showed good reproduction of bond lengths and bond angles in general, with mean of relative errors smaller than the AMBER96 force field. The good performance of the DFT calculation performed on Gaussian is also noticeable when compared to the mean of relative error associated to the more robust relativistic method ZORA. The slight difference between the two methods suggests that the level of theory chosen for the optimization of BMOV is quite effective.

In addition, the complete tables associated to this analysis are available in the Section S1 of the Supporting Information (SI). According to information exhibited in such tables, it is important to highlight that the coordination sphere of the vanadium complex is well described by the DFT calculation using B3LYP level of theory and basis set /def2-TZVP LANL2DZ ECP. On the other hand, the values obtained by the AMBER96 force field, available on HyperChem, differ drastically from the experimental data.

Validation Calculations of the New Amber Force Field

To attest to the validity of the new force field, bond lengths and bond angles were compared as well. The experimental values were considered as a reference, where the mean of relative error for lengths and angles were calculated, according to Equation 2. The comparison included results obtained by DFT calculation, GAFF and the new force field, taking into account the last 10 ns of the MD simulation.

$$Relative\ error = \left|\frac{Calculated\ value - Experimental\ data}{Experimental\ data}\right| \times 100\% \qquad (2)$$

Based on Table 2, the mean relative error for both bond lengths and angles from the new model showed to be in accordance as well. Although particularly for bond lengths, the new force field showed an average relative error slightly greater than the one from GAFF, the results proved to be consistent overall. The complete tables for the validation can be found in the Section 2 of SI.

Table 2. Mean of relative error (%) of GAFF and New Force Field simulations.

	ECP vs. Exp.	GAFF vs. Exp.	New FF vs. Exp.
Bond Lengths	1.955	1.835	1.944
Bond Angles	2.261	5.646	3.946

Additionally, based on experimental data, the structure of BMOV is a square pyramidal with the two maltolato ligands in a *trans* arrangement. The geometry achieved over the entire MD simulation using GAFF (Figure 3) does not represent the physical structure since the base of the square pyramid presented some distortions.

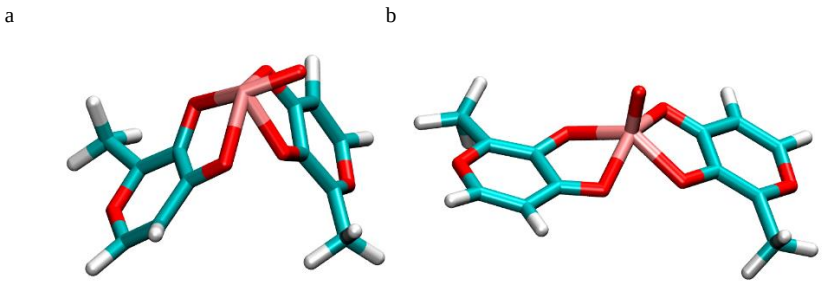

Figure 3. BMOV geometry obtained by (a) GAFF simulation and (b) new force field simulation.

It is evident that the mean of relative error with respect to the data obtained by GAFF showed considerable results, especially for bond lengths. However, it is important to mention that the geometry acquired by GAFF presented distortions, thus this general force field is not adequate to describe BMOV. The simulation carried out using the new AMBER force field showed small mean of relative error, stressing the reliable geometry obtained.

The New Amber Force Field Analysis

The performance of the new force field was analyzed through a time-dependent calculation of the root mean square deviation (RMSD), where the last 10 ns of the simulation were considered, and the structure derived from the DFT calculation was taken as a reference. Such calculation was performed in vacuum with the absence of any other molecule that could restrict the flexibility of the complex. According to Figure 4, the structure of BMOV had an amplitude of oscillation of 1.5 Å, with average of RMSD equal to 0.547±0.005. Furthermore, it was possible to achieve the equilibrium condition for this system, in which the conformation acquired by the vanadium complex was stable.

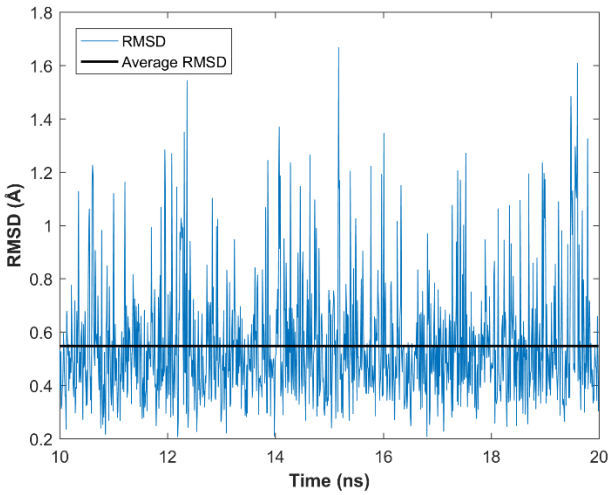

Figure 4. RMSD plot over 10 ns for vanadium (IV) complex in vacuum using the new parameters.

Regarding to the performance of GAFF, an MD simulation was carried out with the same conditions as the previous simulation. For the time-dependent calculation of the root mean square deviation (RMSD), the last 10 ns of the simulation were considered as well, and the structure derived from the DFT calculation was taken as a reference. As can be seen in Figure 5, amplitude of oscillation of the structure of the vanadium complex was equal to 0.3 Å, with average of RMSD equal to 2.331E06± 0.001 Å. The magnitude of the values found by GAFF

in this analysis are far from the real-life context. Based on that, it is considered that GAFF did not have a great performance in this simulation.

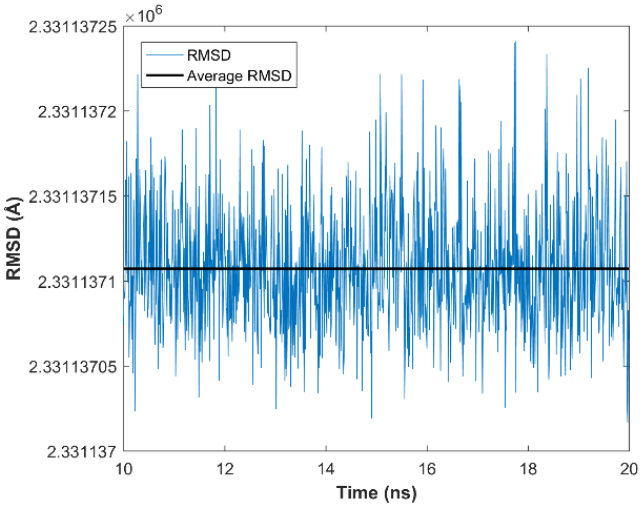

Figure 5. RMSD plot over 10 ns for vanadium (IV) complex in vacuum using GAFF.

A case study of BMOV-PTP1B

Given the relevance of the PTP1B protein in biological processes in addition to the fact that it is considered a bridge between T2DM and AD, a case study focused on the system composed of PTP1B and BMOV was carried out, aiming to provide relevant information towards the therapeutics of AD.

The crystal structure of PTP1B was downloaded from Protein Data Bank (PDB code: 1NWL) and prepared using BIOVIA Discovery Studio Visualizer v. 21, where hydrogens were added and the charge was calculated.[34,35] For the molecular docking simulation, the radius of the binding site was set to 6 Å and the radius of the flexible residues, to 7 Å. MolDock Score [GRID] was the score algorithm used, the grid resolution was set to 0.30 Å, and the MolDock Optimizer was used as the search algorithm. Moreover, the potential binding site of PTP1B for the vanadium complex was comprised of residues Tyr46, Phe182, Ser216, Ala217, Gly218, Ile219, Gly220, and Arg221.[36] The residues mentioned were pointed out to interact with cis-BMOV and were considered a good insight regarding to the binding site of the system under study in this work.

The molecular docking was carried out to provide information about the interactions between BMOV and PTP1B, involved in the developing of AD, both from the energy and the structural point of view. A total of 150 poses were generated and the pose that presented lower energy (-104.811 kcal mol^{-1}) was selected as the best and most stable orientation. The analysis

pointed out seven residues from the protein that had interacted with BMOV: Gly183, Cys215, Ala217, Gly218, Ile219, Gly220, and Arg221 (Figure 6).

Another important information that was taken into consideration for the selection of the pose was the occurrence of hydrogen bonds between BMOV-Gly183 and BMOV-Arg221. This hydrogen bonds were already pointed out in the literature and the docking study performed in this work was able to effectively reproduce this behavior in similar conditions.[37] Thus, using the orientation of the complex in the already mentioned binding site, an MD simulation was carried out to analyze the system in a thorough manner.

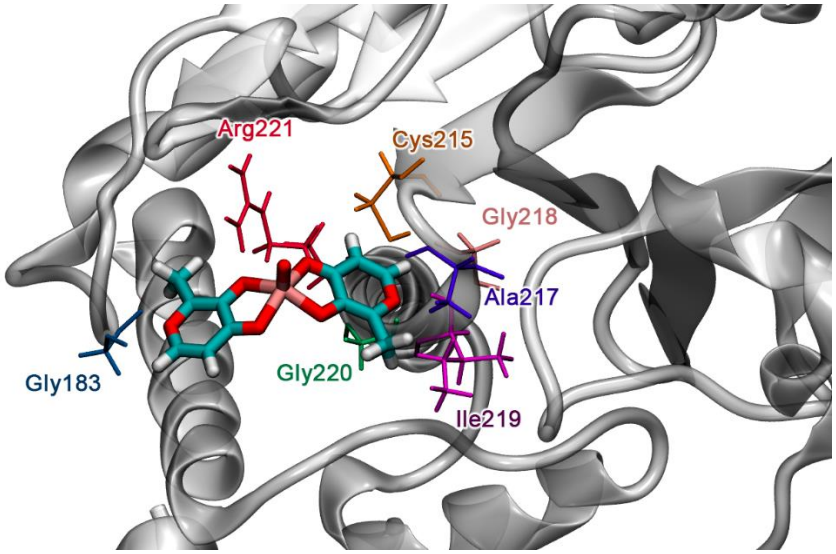

Figure 6. Complete view of the selected pose of BMOV-PTP1B system and the interacting residues pointed out by the docking study.

After that, a classical MD was carried out, with the following details: the force field developed in this work was used to describe the BMOV, whereas the Amber ff99SB force field was used to simulate the PTP1B protein.[38] Using the AMBER20 program package, the four simulation steps were performed for the BMOV-PTP1B system.

Firstly, the system was minimized using the 1000 steps of steepest descent and the 1000 steps of the conjugate gradient, under a harmonic constraint of 10.0 kcal mol^{-1} $Å^{-2}$). Then, the system was relaxed by 5000 steps of steepest descent and 15 000 steps of the conjugate gradient. Next, the system was gradually heated in 5 steps from 0 K to 300 K by a 50 ps NVT simulation and equilibrated by a 500 ps NPT simulation at 1 atm and 300 K, where the restriction was gradually decreased. Lastly, for the production step, the 200 ns NPT simulation of the vanadium complex-PTP1B system was carried out without any restraint, using the TIP3P model and in presence of three Na^+ counterions.[37]

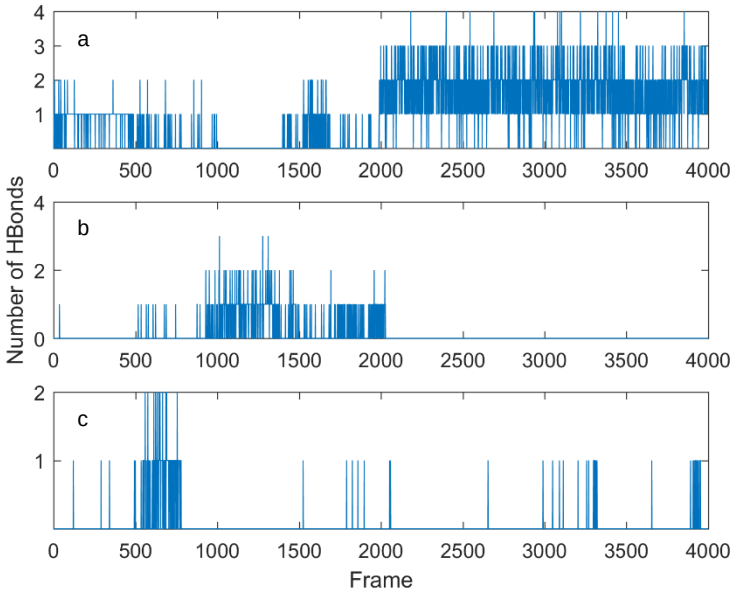

Figure 7. Number of hydrogen bonds found per frame between BMOV and residues (a) Arg221, (b) Gly183, and (c) Gln262.

The hydrogen bonds pointed out in the docking investigation were validated. As mentioned earlier in this paper, it was suggested by the docking study that BMOV interacted with residues Gly183, Cys215, Ala217, Gly218, Ile219, Gly220, and Arg221.

Interactions between Arg221-BMOV were pointed out as the most recurring interactions in the system under study by the MD simulation (Figure 7.a). Gly183-BMOV (Figure 7.b) and Gln262-BMOV (Figure 7.c) were also pointed out. However, residue Gln262 was not identified in the docking study and was suggested as the least occurring interaction among the three mentioned above. Residues Arg221 and Gly183 were stated as possible interactions in the system.

Broadly speaking, it is known that PTP1B is considered a promising biological target to prevent the development of this neurodegenerative disease since this protein is a regulator of different processes within the central nervous system.[7] Thus, the advantageous findings exposed in this work regarding the interactions between the vanadium complex, especially the hydrogen bond between residue Arg221 and BMOV, may provide a better understanding of the system, contributing to strategies to tackle AD.

4. Conclusions

The purpose of this work was to develop an efficient set of parameters to describe the vanadium complex considered a potential agent against T2DM and, as a case study, investigate the behavior of such complex in interaction with PTP1B, a protein associated with AD, in order to obtain more information and encourage future studies targeting the treatment of this disease.

This study was initially developed to fulfill the need for specific force field for BMOV, a metallic complex, since such information is scarce in the literature. Thus, the new AMBER force field was validated, and excellent results were obtained, where the results suggested that the parameterization was efficient to describe BMOV, i.e., the new AMBER force field successfully describe the bond lengths and bond angles. The mean of the relative errors corroborates the good performance of the new force field. On the other hand, the results obtained by GAFF were not adequate, i.e., the geometry acquired of the complex did not correspond to a real representation of BMOV. RMSD analysis of the complex in vacuum pointed out that the conformation assumed by BMOV was stable and the equilibrium condition was reached.

Relevant results were also obtained for the second part of the work, in which interactions between the biological target and the BMOV were investigated. Firstly, docking studies indicate relevant hydrogen bonds, between BMOV and residues Arg221 and Gly183, that were then validated after the MD simulation. Arg221-BMOV was characterized as the most frequent in this system and were closely explored.

Overall, the data gathered in this work stimulates future studies that intend to explore the use of BMOV as a potential agent against one of the most complex neurodegenerative disorders. The interactions found in the case study can be a great approach for further investigations.

Declaration of competing interest

The authors declare no conflict of interest.

Acknowledgments

This work is financially supported by the Brazilian agencies CAPES, CNPq, and FAPEMIG. The authors thank M.Sc. Ander Francisco Pereira for the assistance with the methodology and the comments that greatly improved the manuscript.

References

1. World Health Organization, Newsroom, Fact Sheets, Detail (2022). Dementia, Online Edition, available at: https://population.un.org/wpp/Download/Standard/Mortality/ (accessed September 1, 2022).
2. Alzheimer's Disease International (2021). Dementia Statistics, Online Edition, available at: https://www.alzint.org/about/dementia-facts-figures/dementia-statistics/ (September 1, 2022).
3. Paudel, P., Park, C. H., Jung, H. A., Yokozawa, T., and Choi, J. S. *Drug Discov Ther.* **2020**, 14(2), 61-66.
4. Chen, M., Huang, N., Liu, J., Huang, J., Shi, J., and Jin, F. *Behav. Brain Res*. **2021**, 400, 113043-113053.
5. Bondi, M. W., Edmonds, E. C., and Salmon, D. P. *J. Int. Neuropsychol. Soc.* **2017**, 23(9-10), 818-831.
6. Falco, A. D., Cukierman, D. S., Hauser-Davis, R. A., and Rey, N. A. *Quim. Nova*. **2016**, 39(1), 63-80.
7. Vieira, M. N., Lyra e Silva, N. M., Ferreira, S. T., and De Felice, F. G. *Front. Aging Neurosci.* **2017**, 9, 1-9.
8. Koren, S., and Fantus, I. G. *Best Pract. Res. Clin. Endocrinol. Metab*. **2007**, 21(4), 621-640.
9. Nair, P. C. *Anticancer Agents Med Chem*. **2011**, 11(1), 151-163.
10. Akter, K., Lanza, E. A., Martin, S. A., Myronyuk, N., Rua, M., and Raffa, R. B. *Br. J. Clin. Pharmacol*. **2011**, 71(3), 365-376.
11. Stanciu, G. D., Bild, V., Ababei, D. C., Rusu, R. N., Cobzaru, A., Paduraru, L., and Bulea, D. *J. Clin. Med*. **2020**, 9, 1-27.
12. Femminella, G. D., Bencivenga, L., Petraglia, L., Visaggi, L., Gioia, L., Grieco, F. V., Lucia, C., Komici, K., Corbi, G., Edison, P., Rengo, G. and Ferrara, N. *J. Diabetes Res.* **2017**, 1-7.
13. Liu, H., Qu, Y., and Wang, X. *Future Med. Chem*. **2018,** 10(6), 679-701.
14. Peters, K. G., Davis, M. G., Howard, B. W., Pokross, M., Rastogi, V., Diven, C., Greis, K. D., Eby-Wilkens, E., Maier, M., Evdokimov, A., Soper, S. and Genbauffe, F. *J. Inorg. Biochem.* **2003**, 96, 321-330.
15. Salo-Ahen, O. M., Alanko, I., Bhadane, R., Bonvin, A. M., Honorato, R. V., Hossain, S., Juffer, A. H., Kabedev, A., Lahtela-Kakkonen, M., Larsen, A. S., Lescrinier, E.,

Marimuthu, P., Mirza, M. U., Mustafa, G., Nunes-Alves, A., Pantsar, T., Saadabadi, A., Singaravelu, K., and Vanmeert, M. *Processes*. **2021**, 9(1), 1-60.

16. Martínez, L., Borin, I. A., and Skaf, M. S. In Fundamentos de simulação por dinâmica molecular. Editora Livraria da Física: São Paulo, pp 413-452.
17. Pereira, A. F., Prandi, I. G., and Ramalho, T. C. *Int. J. Quantum Chem*. **2021**, 121(6), 1-10.
18. Vanommeslaeghe, K., and Guvench, O. *Curr. Pharm. Des*. **2014**, 20(20), 3281-3292.
19. Zhao, S., Schaub, A. J., Tsai, S., and Luo, R. *J. Chem. Inf. Model.*, **2021**, 61(2), 856-868.
20. Prandi, I. G., Viani, L., Andreussi, O., and Mennucci, B. *J. Comput. Chem*. **2016**, 37(11), 981-991.
21. Tavares, C. A., Santos, T. M. R., da Cunha, E . F. F., Ramalho, T. C. J. Phys. Chem. B. **2023**, 127(2), 495-504.
22. Dennington, R. D., Keith, T. A., and Millam, J. M. GaussView 5.0, Gaussian. Inc., Wallingford CT, 2008.
23. Frisch, M. J., Trucks, G. W., Schlegel, H. B., Scuseria, G. E., Robb, M. A., Cheeseman, J. R., Scalmani, G., Barone, V., Petersson, G. A., Nakatsuji, H., Li, X., Caricato, M., Marenich, A. V., Bloino, J., Janesko, B. G., Gomperts, R., Mennucci, B., Hratchian, H. P., Ortiz, J. V., Izmaylov, A. F., Sonnenberg, J. L., Williams-Young, D., Ding, F., Lipparini, F., Egidi, F., Goings, J., Peng, B., Petrone, A., Henderson, T., Ranasinghe, D., Zakrzewski, V. G., Gao, J., Rega, N., Zheng, G., Liang, W., Hada, M., Ehara, M., Toyota, K., Fukuda, R., Hasegawa, J., Ishida, M., Nakajima, T., Honda, Y., Kitao, O., Nakai, H., Vreven, T., Throssell, K., Montgomery, J. A., Jr., Peralta, J. E., Ogliaro, F., Bearpark, M. J., Heyd, J. J., Brothers, E. N., Kudin, K. N., Staroverov, V. N., Keith, T. A., Kobayashi, R., Normand, J., Raghavachari, K., Rendell, A. P., Burant, J. C., Iyengar, S. S., Tomasi, J., Cossi, M., Millam, J. M., Klene, M., Adamo, C., Cammi, R., Ochterski, J. W., Martin, R. L., Morokuma, K., Farkas, O., Foresman, J. B., and Fox, D. J. Gaussian 16, Revision C.01, Gaussian, Inc., Wallingford CT, 2016.
24. Caravan, P., Gelmini, L., Glover, N., Herring, F. G., Li, H., McNeill, J. H., Rettig, S. J., Setyawati, I. A., Shuter, E., Sun, Y., Tracey, A. S., Yuen, V. G., Orvig, C. *J. Am. Chem. Soc*. **1995**, 117(51), 12759-12770.
25. Neese, F. *Wiley Interdiscip. Rev. Comput. Mol. Sci*. **2018**, 8(1), 1-6.
26. Cárdenas, G., Marquetand, P., Mai, S., and González, L. *Catalysts*. **2021**, 11(4), 1-16.

27. Froimowitz, M. *Biotechniques*. **1993**, 1 4(6), 1010-1013.
28. Humphrey, W., Dalke, A., and Schulten, K. *J. Mol. Graph*. **1996**, 14(1), 33-38.
29. Cornell, W. D., Cieplak, P., Bayly, C. I., Gould, I. R., Merz, K. M., Ferguson, D. M., Spellmeyer, D. C., Fox, T., Caldwell, J. W. and Kollman, P. A. *J. Am. Chem. Soc*. **1995**, 117(19), 5179-5197.
30. Bayly, C. I., Cieplak, P., Cornell, W. D., Kollman, P. A. *J. Phys. Chem.* **1993**, 97(40), 10269-10280.
31. Anderson, G., Behera, R. N., Gomatam, R. A Theoretical Approach to Engineering a New Enzyme. In: Journal of Physics: Conference Series, E. C. Vagenas and D. S. Vlachos, Eds., IOP Publishing, Athens, **2016**, Vol. 738, pp. 1-7.
32. Šebesta, F., Sláma, V., Melcr, J., Futera, Z., and Burda, J. V. *J. Chem. Theory Comput.* **2016**, 12(8), 3681-3688.
33. Case, D. A., Darden, T. A., Cheatham III, T. E., Simmerling, C. L., Wang, J., Duke, R. E., Luo, R., Walker, R. C., Zhang, W., Merz, K., Wang, B., Hayik, S. A., Roitberg, A., Seabra, G. M., Kolossváry, I., Wong, K. F., Paesani, F., Vanicek, J., Liu, J., Wu, X., Brozell, S. R., Steinbrecher, T., Gohlke, H., Cai, Q., Ye, X., Hsieh, M., Hornak, V., Cui, G., Roe, D. R., Mathews, D. H., Seetin, M. G., Sagui, C., Babin, V., Luchko, T., Gusarov, S., Kovalenko, A., Kollman, P. A and Roberts, B. P. AMBER 20, University of California, San Francisco CA, 2010.
34. Erlanson, D. A., McDowell, R. S., He, M. M., Randal, M., Simmons, R. L., Kung, J., Waight, A. and Hansen, S. K. *J. Am. Chem. Soc*. **2003**, 125(19), 5602-5603.
35. Dassault Systèmes. BIOVIA Discovery Studio Visualizer. San Diego CA, 2021.
36. Scior, T., Mack, H. G., García, J. A. G., Koch, W. *Drug. Des. Devel. Ther.*, **2009**, , 221-231.
37. Han, W., Cai, J., Zhong, W., Xu, G., Wang, F., Tian, X., Zhou, X., Liu, Q., Liu, Y. and Wang, J. *Bioorg. Chem*. **2020**, 96.
38. Hornak, V., Abel, R., Okur, A., Strockbine, B., Roitberg, A. Simmerling, C. *Proteins: Structure, Function, and Bioinformatics*, **2006**, 65(3), 712-725.

ATTACHMENTS

List of Publications

1. **Value of Contrast-enhanced Magnetic Resonance Imaging (MRI) in the Diagnosis of Breast Cancer**

Mateus A. Gonçalves, Bruna T. L. Pereira, Camila A. Tavares, Taináh M. R. Santos, Elaine F. F. da Cunha and Teodorico C. Ramalho

Scientific article published in *Mini-Reviews in Medicinal Chemistry*

DOI: 10.2174/1389557521666210521113155

2. **Molecular Dynamics-Assisted Interaction of Vanadium Complex-AMPK: from the force field development to biological application for Alzheimer's treatment**

Camila A. Tavares, Taináh M. R. Santos, Elaine F. F. da Cunha and Teodorico C. Ramalho

Scientific article published in *Journal of Physical Chemistry B*

DOI: 10.1021/acs.jpcb.2c07147

3. **Parameterization and validation of a new AMBER force field for an oxovanadium (IV) complex with therapeutic potential implications in Alzheimer's Disease**

Camila A. Tavares, Taináh M. R. Santos, Elaine F. F. da Cunha and Teodorico C. Ramalho

Scientific article submitted to *Journal of Molecular Graphics and Modelling*

4. **Enhanced Sampling in Molecular Dynamics simulations: how many MD snapshots can be needed to reproduce the biological behavior?**

Camila A. Tavares, Taináh M. R. Santos, Mateus A. Gonçalves, Elaine F. F. Cunha and Teodorico C. Ramalho

Scientific article submitted in *Mini-Reviews in Medicinal Chemistry*

5. **Evaluation of autophagy inhibition to combat cancer: (vanadium complex)–protein interactions, parameterization, and validation of a new force field**

Taináh M. R. Santos, Camila A. Tavares, Ander F. Pereira, Elaine F. F. Cunha and Teodorico C. Ramalho

Scientific article submitted in *Journal of Molecular Modeling*

6. **Vanadium complex as a possible modulator of autophagy through proteins at the beginning (PI3K) and at the end (ULK1) of its signaling pathway: development and validation of a specific force field for [$VO(bpy)_2Cl$]**

Taináh M. R. Santos, Camila A. Tavares, Elaine F. F. Cunha and Teodorico C. Ramalho

Scientific article submitted in *Journal of Computer-Aided Molecular Design*

7. **Improving the path to obtain spectroscopic parameters for the PI3K–(platinum complex) system: implications for the diagnosis and treatment of breast cancer**

Taináh M. R. Santos, Gustavo A. Andolpho, Camila A. Tavares, Mateus A. Gonçalves, and Teodorico C. Ramalho

Scientific article submitted in *Magnetochemistry*

8. **Smoothing and differentiation of data by Tikhonov and fractional derivative tools, applied to surface-enhanced Raman scattering (SERS) spectra of crystal violet dye**

Nelson H. T. Lemes, Taináh M. R. Santos, Camila A. Tavares, Luciano S. Virtuoso, Kelly A. S. Souza and Teodorico C. Ramalho

Scientific article submitted in *Computational and Applied Mathematics*

Supporting Information – First Paper

Section S1

Table S1.1. Equivalence of the residues from the original structure and the residues from the model generated by SWISS-MODEL.

α Subunit		**β Subunit**		**γ Subunit**	
Original Strcuture	**Model**	**Original Structure**	**Model**	**Original Structure**	**Model**
G11	G9	P74	-	-	S24
S12	S10	A75	-	-	N25
V13	V11	Q76	-	N25	N26
K14	K12	A77	-	S26	S27
I15	I13	R78	R12	V27	V28
G16	G14	P79	P13	Y28	Y29
H17	H15	T80	T14	T29	T30
Y18	Y16	V81	V15	S30	S31
I19	I17	F82	F16	F31	F32
L20	L18	R83	R17	M32	M33
G21	G19	W84	W18	K33	K34
D22	D20	T85	T19	S34	S35
T23	T21	G86	G20	H35	H36
L24	L22	G87	G21	R36	R37
G25	G23	G88	G22	C37	C38
V26	V24	K89	K23	Y38	Y39
G27	G25	E90	E24	D39	D40

T28	T26	V91	V25	L40	L41
F29	F27	Y92	Y26	I41	I42
G30	G28	L93	L27	P42	P43
K31	K29	S94	S28	T43	T44
V32	V30	G95	G29	S44	S45
K33	K31	S96	S30	S45	S46
V34	V32	F97	F31	K46	K47
G35	G33	N98	N32	L47	L48
K36	K34	N99	N33	V48	V49
H37	H35	W100	W34	V49	V50
E38	E36	S101	S35	F50	F51
L39	L37	K102	K36	D51	D52
T40	T38	L103	L37	T52	T53
G41	G39	P104	P38	S53	S54
H42	H40	L105	L39	L54	L55
K43	K41	T106	T40	Q55	Q56
V44	V42	R107	R41	V56	V57
A45	A43	D108	D42	K57	K58
V46	V44	H109	H43	K58	K59
K47	K45	N110	N44	A59	A60
I48	I46	N111	N45	F60	F61
L49	L47	F112	F46	F61	F62
N50	N48	V113	V47	A62	A63

R51	R49	A114	A48	L63	L64
Q52	Q50	I115	I49	V64	V65
K53	K51	L116	L50	T65	T66
I54	I52	D117	D51	N66	N67
R55	R53	L118	L52	G67	G68
S56	S54	P119	P53	V68	V69
L57	L55	E120	E54	R69	R70
D58	D56	G121	G55	A70	A71
V59	V57	E122	E56	A71	A72
V60	V58	H123	H57	P72	P73
G61	G59	Q124	Q58	L73	L74
K62	K60	Y125	Y59	W74	W75
I63	I61	K126	K60	D75	D76
R64	R62	F127	F61	S76	S77
R65	R63	F128	F62	K77	K78
E66	E64	V129	V63	K78	K79
I67	I65	D130	D64	Q79	Q80
Q68	Q66	G131	G65	S80	S81
N69	N67	Q132	Q66	F81	F82
L70	L68	W133	W67	V82	V83
K71	K69	T134	T68	G83	G84
L72	L70	H135	H69	M84	M85
F73	F71	D136	D70	L85	L86

R74	R72	P137	P71	T86	T87
H75	H73	S138	S72	I87	I88
P76	P74	E139	E73	T88	T89
H77	H75	P140	P74	D89	D90
I78	I76	I141	I75	F90	F91
I79	I77	V142	V76	I91	I92
K80	K78	T143	T77	N92	N93
L81	L79	S144	S78	I93	I94
Y82	Y80	Q145	Q79	L94	L95
Q83	Q81	L146	L80	H95	H96
V84	V82	G147	G81	R96	R97
I85	I83	T148	T82	Y97	Y98
S86	S84	V149	V83	Y98	Y99
T87	T85	N150	N84	K99	K100
P88	P86	N151	N85	S100	S101
S89	S87	I152	I86	A101	A102
D90	D88	I153	I87	L102	L103
I91	I89	Q154	Q88	V103	V104
F92	F90	V155	V89	Q104	Q105
M93	M91	K156	K90	I105	I106
V94	V92	K157	K91	Y106	Y107
M95	M93	T158	T92	E107	E108
E96	E94	D159	D93	L108	L109

Y97	Y95	F160	F94	E109	E110
V98	V96	E161	E95	E110	E111
S99	S97	V162	V96	H111	H112
G100	G98	F163	F97	K112	K113
G101	G99	D164	D98	I113	I114
E102	E100	A165	A99	E114	E115
L103	L101	L166	L100	T115	T116
F104	F102	M167	M101	W116	W117
D105	D103	V168	V102	R117	R118
Y106	Y104	D169	D103	E118	E119
I107	I105	S170	S104	V119	V120
C108	C106	Q171	Q105	Y120	Y121
K109	K107	K172	K106	L121	L122
N110	N108	-	C107	Q122	Q123
G111	G109	-	S108	D123	D124
R112	R110	-	D109	S124	S125
L113	L111	-	V110	F125	F126
D114	D112	-	S111	K126	K127
E115	E113	-	E112	P127	P128
K116	K114	-	L113	L128	L129
E117	E115	-	S114	V129	V130
S118	S116	-	S115	C130	C131
R119	R117	-	S116	I131	I132

R120	R118	-	P117	S132	S133
L121	L119	-	P118	P133	P134
F122	F120	H188	G119	N134	N135
Q123	Q121	Q189	P120	A135	A136
Q124	Q122	E190	Y121	S136	S137
I125	I123	P91	H122	L137	L138
L126	L124	Y192	Q123	F138	F139
S127	S125	V193	E124	D139	D140
G128	G126	C194	P125	A140	A141
V129	V127	K195	Y126	V141	V142
D130	D128	-	V127	S142	S143
Y131	Y129	-	C128	S143	S144
C132	C130	-	K129	L144	L145
H133	H131	-	P130	I145	I146
R134	R132	-	E131	R146	R147
H135	H133	-	E132	N147	N148
M136	M134	-	R133	K148	K149
V137	V135	-	F134	I149	I150
V138	V136	R201	R135	H150	H151
H139	H137	A202	A136	R151	R152
R140	R138	P203	P137	L152	L153
D141	D139	P204	P138	P153	P154
L142	L140	I205	I139	V154	V155

K143	K141	L206	L140	I155	I156
P144	P142	P207	P141	D156	D157
E145	E143	P208	P142	P157	P158
N146	N144	H209	H143	E158	E159
V147	V145	L210	L144	S159	S160
L148	L146	L211	L145	G160	G161
L149	L147	Q212	Q146	N161	N162
D150	D148	V213	V147	T162	T163
A151	A149	I214	I148	L163	L164
H152	H150	L215	L149	Y164	Y165
M153	M151	N216	N150	I165	I166
N154	N152	K217	K151	L166	L167
A155	A153	D218	D152	T167	T168
K156	K154	T219	T153	H168	H169
I157	I155	G220	G154	K169	K170
A158	A156	I221	I155	R170	R171
D159	D157	S222	S156	I171	I172
F160	F158	C223	C157	L172	L173
G161	G159	D224	D158	K173	K174
L162	L160	P225	P159	F174	F175
S163	S161	A226	A160	L175	L176
N164	N162	L227	L161	K176	K177
M165	M163	L228	L162	L177	L178

M166	M164	P229	P163	F178	F179
S167	S165	E230	E164	I179	I180
D168	D166	P231	P165	T180	T181
G169	G167	N232	N166	E181	E182
E170	E168	H233	H167	F182	F183
F171	F169	V234	V168	P183	P184
L172	L170	M235	M169	K184	K185
R173	R171	L236	L170	P185	P186
-	T172	N237	N171	E186	E187
S175	S173	H238	H172	F187	F188
C176	C174	L239	L173	M188	M189
G177	G175	Y240	Y174	S189	S190
S178	S176	A241	A175	K190	K191
P179	P177	L242	L176	S191	S192
N180	N178	S243	S177	L192	L193
Y181	Y179	I244	I178	E193	E194
A182	A180	K245	K179	E194	E195
A183	A181	D246	D180	L195	L196
P184	P182	G247	G181	Q196	Q197
E185	E183	V248	V182	I197	I198
V186	V184	M249	M183	G198	G199
I187	I185	V250	V184	T199	T200
S188	S186	L251	L185	Y200	Y201

G189	G187	S252	S186	A201	A202
R190	R188	A253	A187	N202	N203
L191	L189	T254	T188	I203	I204
Y192	Y190	H255	H189	A204	A205
A193	A191	R256	R190	M205	M206
G194	G192	Y257	Y191	V206	V207
P195	P193	K258	K192	R207	R208
E196	E194	K259	K193	T208	T209
V197	V195	K260	K194	T209	T210
D198	D196	Y261	Y195	T210	T211
I199	I197	V262	V196	P211	P212
W200	W198	T263	T197	V212	V213
S201	S199	T264	T198	Y213	Y214
S202	S200	L265	L199	V214	V215
G203	G201	L266	L200	A215	A216
V204	V202	Y267	Y201	L216	L217
I205	I203	K268	K202	G217	G218
L206	L204	P269	P203	I218	I219
Y207	Y205	I270	I204	F219	F220
A208	A206			V220	V221
L209	L207			Q221	Q222
L210	L208			H222	H223
C211	C209			R223	R224

G212	G210
T213	T211
L214	L212
P215	P213
F216	F214
D217	D215
D218	D216
D219	D217
H220	H218
V221	V219
P222	P220
T223	T221
L224	L222
F225	F223
K226	K224
K227	K225
I228	I226
C229	C227
D230	D228
G231	G229
I232	I230
F233	F231
Y234	Y232

V224	V225
S225	S226
A226	A227
L227	L228
P228	P229
V229	V230
V230	V231
D231	D232
E232	E233
K233	K234
G234	G235
R235	R236
V236	V237
V237	V238
D238	D239
I239	I240
Y240	Y241
S241	S242
K242	K243
F243	F244
D244	D245
V245	V246
I246	I247

T235	T233
P236	P234
Q237	Q235
Y238	Y236
L239	L237
N240	N238
P241	P239
S242	S240
V243	V241
I244	I242
S245	S243
L246	L244
L247	L245
K248	K246
H249	H247
M250	M248
L251	L249
Q252	Q250
V253	V251
D254	D252
P255	P253
M256	M254
K257	K255

N247	N248
L248	L249
A249	A250
A250	A251
E251	E252
K252	K253
T253	T254
Y254	Y255
N255	N256
N256	N257
L257	L258
D258	D259
V259	V260
S260	S261
V261	V262
T262	T263
K263	K264
A264	A265
L265	L266
Q266	Q267
H267	H268
R268	R269
S269	S270

R258	R256
A259	A257
T260	T258
I261	I259
K262	K260
D263	D261
I264	I262
R265	R263
E266	E264
H267	H265
E268	E266
W269	W267
F270	F268
K271	K269
Q272	Q270
D273	D271
L274	L272
P275	P273
K276	K274
Y277	Y275
L278	L276
F279	F277
P280	P278

H270	H271
Y271	Y272
F272	F273
E273	E274
G274	G275
V275	V276
L276	L277
K277	K278
C278	C279
Y279	Y280
L280	L281
H281	H282
E282	E283
T283	T284
L284	L285
E285	E286
T286	T287
I287	I288
I288	I289
N289	N290
R290	R291
L291	L292
V292	V293

-	E279
E281	D280
-	P281
-	S282
-	Y283
-	S284
-	S285
-	T286
-	M287
-	I288
-	D289
-	D290
-	E291
-	A292
-	L293
-	K294
-	E295
-	V296
-	C297
-	E298
-	K299
-	F300
-	E301

E293	E294
A294	A295
E295	E296
V296	V297
H297	H298
R298	R299
L299	L300
V300	V301
V301	V302
V302	V303
D303	D304
E304	E305
N305	N306
D306	D307
V307	V308
V308	V309
K309	K310
G310	G311
I311	I312
V312	V313
S313	S314
L314	L315
S315	S316

-	C302
-	S303
-	E304
-	E305
-	E306
-	V307
-	L308
-	S309
-	C310
-	L311
-	Y312
-	N313
-	R314
-	N315
-	H316
-	Q317
-	D318
-	P319
-	L320
-	A321
-	V322
-	A323
-	Y324

D316	D317
I317	I318
L318	L319
Q319	Q320
A320	A321
L321	L322
V322	V323
L323	L324
-	T325
T324	G326

-	H325
-	L326
-	I327
I330	I328
D331	D329
N332	N330
R333	R331
R334	R332
I335	I333
M336	M334
N337	N335
E338	E336
A339	A337
K340	K338
D341	D339
F342	F340
-	Y341
-	L342
-	A343
-	T344
-	S345
-	P346
-	P347

-	D348
-	S349
-	F350
-	L351
-	D352
-	D353
-	H354
-	H355
-	L356
-	T357
-	R358
-	P359
-	H360
-	P361
-	E362
-	R363
-	V364
-	P365
-	F366
-	L367
-	V368
-	A369
-	E370

-	T371
-	P372
-	R373
-	A374
-	R375
-	H376
-	T377
-	L378
-	D379
-	E380
-	L381
-	N382
-	P383
-	Q384
-	K385
-	S386
-	K387
R394	H388
-	Q389
-	G390
-	V391
-	R392
K395	K393

A396	A394
K397	K395
W398	W396
H399	H397
L400	L398
G401	G399
I402	I400
R403	R401
S404	S402
Q405	Q403
S406	S404
R407	R405
P408	P406
N409	N407
D410	D408
I411	I409
M412	M410
A413	A411
E414	E412
V415	V413
C416	C414
R417	R415
A418	A416

I419	I417
K420	K418
Q421	Q419
L422	L420
D423	D421
Y424	Y422
E425	E423
W426	W424
K427	K425
V428	V426
V429	V427
N430	N428
P431	P429
Y432	Y430
Y433	Y431
L434	L432
R435	R433
V436	V434
R437	R435
R438	R436
K439	K437
N440	N438
P441	P439

V442	V440
T443	T441
S444	S442
T445	T443
Y446	Y444
S447	S445
K448	K446
M449	M447
S450	S448
L451	L449
Q452	Q450
L453	L451
Y454	Y452
Q455	Q453
V456	V454
D457	D455
S458	S456
R459	R457
T460	T458
Y461	Y459
L462	L460
L463	L461
D464	D462

F465	F463
R466	R464
S467	S465
I468	I466
D469	D467
D470	D468
E471	E469
L526	L470
T527	T471
P528	P472
R529	R473
P530	P474
G531	G475
S532	S476
H533	H477
T534	T478
I535	I479
E536	E480
F537	F481
F538	F482
E539	E483
M540	M484
C541	C485

A542	A486
N543	N487
L544	L488
I545	I489
K546	K490
I547	I491
L548	L492
A549	A493

Section S2

Table S2.1. Bond lengths in Angstroms (Å) for different methods and levels of theory.

	AMBER *(HyperChem)*	**B3LYP/def2-TVZP+LANL2DZ ECP** *(Gaussian 09)*	**B3LYP/def2-TVZP with ZORA** *(ORCA)*
H1-N1	0.936	1.007	1.007
H2-N1	0.936	1.007	1.008
N1-C1	1.290	1.384	1.386
C1-N4	1.290	1.329	1.330
C1-N2	1.291	1.324	1.325
N4-C2	1.293	1.342	1.342
N2-H3	0.936	1.012	1.014
C2-N5	1.302	1.377	1.378
C2-N3	1.298	1.326	1.330
N2-V1	1.839	2.037	2.042
N3-V1	1.843	2.055	2.051
N3-H4	0.936	1.009	1.010
N5-C3	1.396	1.454	1.457
N5-C4	1.395	1.448	1.452
C3-H5	1.090	1.083	1.084
C3-H6	1.091	1.093	1.097
C3-H7	1.090	1.096	1.093
C4-H8	1.091	1.088	1.088
C4-H9	1.090	1.093	1.097

C4-I0	1.089	1.098	1.095
V1-O1	1.880	1.579	1.595
N7-V1	1.848	2.046	2.043
N9-V1	1.846	2.045	2.050
N7-I3	0.936	1.013	1.014
N9-I4	0.935	1.009	1.010
N7-C5	1.294	1.322	1.325
C5-N6	1.290	1.384	1.386
N6-I1	0.936	1.007	1.007
N6-I2	0.936	1.007	1.008
C5-N8	1.292	1.331	1.331
N8-C6	1.295	1.340	1.342
C6-N9	1.294	1.328	1.330
C6-M0	1.305	1.376	1.378
M0-C8	1.397	1.447	1.452
M0-C7	1.397	1.453	1.457
C7-I5	1.091	1.083	1.084
C7-I6	1.091	1.094	1.097
C7-I7	1.090	1.096	1.093
C8-I8	1.089	1.098	1.096
C8-I9	1.090	1.092	1.096
C8-J0	1.089	1.090	1.088

Table S2.2. Relative error (%) of bond lengths of different methods and levels of theory.

	AMBER *vs.* ZORA	**ECP *vs.* ZORA**
H1-N1	7.037	0.097
H2-N1	7.072	0.086
N1-C1	6.752	0.139
C1-N4	2.921	0.109
C1-N2	2.457	0.078
N4-C2	3.603	0.014
N2-H3	7.577	0.107
C2-N5	5.418	0.067
C2-N3	2.162	0.271
N2-V1	9.710	0.249
N3-V1	10.305	0.176
N3-H4	7.299	0.100
N5-C3	3.961	0.209
N5-C4	3.623	0.267
C3-H5	0.679	0.062
C3-H6	0.270	0.308
C3-H7	0.544	0.315
C4-H8	0.188	0.014
C4-H9	0.215	0.352
C4-I0	0.836	0.256
V1-O1	19.043	0.998

N7-V1	9.701	0.157
N9-V1	9.728	0.258
N7-I3	7.631	0.069
N9-I4	7.332	0.140
N7-C5	2.111	0.213
C5-N6	6.793	0.110
N6-I1	7.041	0.082
N6-I2	7.081	0.074
C5-N8	2.918	0.018
N8-C6	3.345	0.136
C6-N9	2.629	0.118
C6-M0	5.162	0.101
M0-C8	3.454	0.290
M0-C7	3.831	0.238
C7-I5	0.714	0.054
C7-I6	0.303	0.262
C7-I7	0.506	0.278
C8-I8	0.838	0.254
C8-I9	0.146	0.393
C8-J0	0.118	0.064

Table S2.3. Bond angles in degrees (°) of different methods and levels of theory.

	AMBER *(HyperChem)*	**B3LYP/def2-TVZP+LANL2DZ ECP** *(Gaussian 09)*	**B3LYP/def2-TVZP with ZORA** *(ORCA)*
H1-N1-H2	119.423	114.956	114.825
H1-N1-C1	120.448	117.385	117.390
H2-N1-C1	120.105	113.916	113.790
N1-C1-N4	118.652	113.632	113.602
N1-C1-N2	120.006	118.701	118.806
C1-N4-C2	124.971	122.291	122.409
C1-N2-V1	120.728	129.800	129.012
C1-N2-H3	119.125	111.915	111.940
H3-N2-V1	117.994	118.268	118.773
N4-C2-N5	118.745	115.131	115.112
N4-C2-N3	120.988	125.129	125.232
C2-N3-H4	119.04	112.845	112.800
N3-C2-N5	120.202	119.740	119.653
H4-N3-V1	117.746	115.690	116.191
C2-N5-C4	121.392	120.954	120.593
C2-N5-C3	121.121	122.209	121.815
N5-C3-H5	111.328	109.047	109.013
N5-C3-H6	109.344	110.126	111.524
N5-C3-H7	109.378	111.018	109.602
N5-C4-H8	109.464	108.644	108.651

N5-C4-H9	109.307	111.464	112.392
N5-C4-I0	111.174	112.851	111.872
N2-V1-O1	117.754	110.114	108.146
N3-V1-O1	115.619	106.161	107.364
N2-V1-N7	80.736	87.063	86.898
N3-V1-N9	77.6168	86.725	87.06
N3-V1-N7	130.033	147.690	144.919
N2-V1-N9	128.385	139.820	144.056
N2-V1-N3	84.4669	82.159	82.377
H5-C3-H6	108.66	109.291	108.568
H6-C3-H7	109.062	108.279	108.602
H5-C3-H7	109.033	109.052	109.505
H8-C4-H9	109.138	107.325	107.876
H9-C4-I0	108.687	108.693	108.691
H8-C4-I0	109.038	107.646	107.149
V1-N3-C2	123.096	130.690	130.317
I1-N6-I2	119.488	114.824	114.799
I1-N6-C5	120.386	117.252	117.365
I2-N6-C5	120.112	113.792	113.761
N6-C5-N8	119.396	113.545	113.607
N6-C5-N7	120.728	118.938	118.84
C5-N8-C6	122.13	122.191	122.343
C5-N7-V1	118.6	128.866	128.8
C5-N7-I3	118.038	111.945	111.955

I3-N7-V1	119.538	118.532	118.859
N8-C6-M0	120.775	115.236	115.147
N8-C6-N9	117.426	125.244	125.229
C6-N9-I4	119.243	112.847	112.807
N9-C6-M0	121.426	119.516	119.623
I4-N9-V1	121.158	116.458	116.495
C6-M0-C8	118.855	121.175	120.575
C6-M0-C7	119.062	122.260	121.811
M0-C7-I5	110.005	109.045	109.019
M0-C7-I6	109.576	110.391	111.539
M0-C7-I7	109.344	110.741	109.602
M0-C8-I8	110.28	112.974	111.949
M0-C8-I9	109.462	111.230	112.304
M0-C8-J0	110.542	108.652	108.661
N7-V1-O1	113.527	106.148	107.716
N9-V1-O1	113.66	110.066	107.798
N7-V1-N9	75.2329	82.096	82.304
V1-N9-C6	119.258	130.667	130.206
I5-C7-I6	109.329	109.156	108.535
I6-C7-I7	109.075	108.259	108.61
I5-C7-I7	108.357	109.221	109.51
I8-C8-I9	109.319	108.733	108.686
I9-C8-J0	109.001	107.462	107.899
I8-C8-J0	108.206	107.581	107.133

N2-C1-N4	121.273	127.639	127.555
N7-C5-N8	119.695	127.481	127.514
C4-N5-C3	117.468	116.123	116.662
C8-M0-C7	117.475	116.082	116.722

Table S2.4. Relative error (%) of bond angles of different methods and levels of theory.

	AMBER *vs.* ZORA	**ECP *vs.* ZORA**
H1-N1-H2	3.886	0.114
H1-N1-C1	2.609	0.004
H2-N1-C1	5.433	0.111
N1-C1-N4	4.418	0.026
N1-C1-N2	1.099	0.088
C1-N4-C2	2.191	0.096
C1-N2-V1	6.989	0.607
C1-N2-H3	6.442	0.022
H3-N2-V1	0.232	0.427
N4-C2-N5	3.139	0.017
N4-C2-N3	3.309	0.082
C2-N3-H4	5.490	0.040
N3-C2-N5	0.386	0.073
H4-N3-V1	1.777	0.433
C2-N5-C4	0.362	0.298
C2-N5-C3	0.890	0.322
N5-C3-H5	2.092	0.031

N5-C3-H6	0.710	1.269
N5-C3-H7	1.477	1.275
N5-C4-H8	0.755	0.006
N5-C4-H9	1.935	0.833
N5-C4-I0	1.486	0.868
N2-V1-O1	6.938	1.787
N3-V1-O1	8.909	1.133
N2-V1-N7	7.267	0.190
N3-V1-N9	10.502	0.386
N3-V1-N7	11.955	1.876
N2-V1-N9	8.178	3.030
N2-V1-N3	2.809	0.265
H5-C3-H6	0.577	0.662
H6-C3-H7	0.723	0.298
H5-C3-H7	0.017	0.415
H8-C4-H9	1.689	0.513
H9-C4-I0	0.006	0.002
H8-C4-I0	1.293	0.462
V1-N3-C2	5.811	0.285
I1-N6-I2	4.062	0.022
I1-N6-C5	2.673	0.096
I2-N6-C5	5.554	0.027
N6-C5-N8	5.153	0.055
N6-C5-N7	1.505	0.082

C5-N8-C6	0.050	0.124
C5-N7-V1	7.966	0.051
C5-N7-I3	5.443	0.009
I3-N7-V1	0.849	0.276
N8-C6-M0	4.807	0.077
N8-C6-N9	6.242	0.012
C6-N9-I4	5.668	0.035
N9-C6-M0	1.598	0.090
I4-N9-V1	4.036	0.032
C6-M0-C8	1.915	0.495
C6-M0-C7	2.616	0.367
M0-C7-I5	0.880	0.024
M0-C7-I6	0.738	1.040
M0-C7-I7	1.262	1.029
M0-C8-I8	2.385	0.907
M0-C8-I9	1.589	0.966
M0-C8-J0	1.739	0.008
N7-V1-O1	6.952	1.477
N9-V1-O1	3.265	2.061
N7-V1-N9	8.360	0.253
V1-N9-C6	8.731	0.353
I5-C7-I6	0.158	0.569
I6-C7-I7	0.754	0.324
I5-C7-I7	0.791	0.265

I8-C8-I9	0.539	0.043
I9-C8-J0	1.432	0.407
I8-C8-J0	0.581	0.416
N2-C1-N4	4.988	0.066
N7-C5-N8	6.107	0.027
C4-N5-C3	1.158	0.464
C8-M0-C7	1.200	0.552

Table S2.5. Comparison of the mean of the relative error (%) for different levels of theory.

	Mean of relative error AMBER *vs*. ZORA	**Mean of relative error ECP *vs*. ZORA**
Bond Lengths	4.465	0.185
Bond Angles	3.299	0.437

Section S3

Table S3.1. Bond lengths in Angstroms (Å) obtained by different calculations for validation purposes.

	B3LYP/def2-TVZP+LANL2DZ ECP *(Gaussian 09)*	**MD with GAFF** *(average and standard deviation)*	**MD with New FF** *(average and standard deviation)*
H1-N1	1.007	1.001±0.001	1.001±0.001
H2-N1	1.007	1.002±0.001	1.004±0.001
N1-C1	1.384	1.342±0.001	1.363±0.001
C1-N4	1.329	1.312±0.001	1.322±0.001
C1-N2	1.324	1.310±0.001	1.318±0.001
N4-C2	1.342	1.348±0.001	1.353±0.001
N2-H3	1.012	1.005±0.001	1.001±0.001
C2-N5	1.377	1.086±0.001	1.403±0.001
C2-N3	1.326	1.337±0.001	1.338±0.001
N2-V1	2.037	2.012±0.002	2.046±0.002
N3-V1	2.055	2.072±0.002	2.037±0.002
N3-H4	1.009	1.003±0.001	1.004±0.001
N5-C3	1.454	1.466±0.001	1.471±0.001
N5-C4	1.448	1.461±0.001	1.465±0.001
C3-H5	1.083	1.086±0.001	1.086±0.001
C3-H6	1.093	1.098±0.001	1.095±0.001
C3-H7	1.096	1.095±0.001	1.099±0.001
C4-H8	1.088	1.090±0.001	1.090±0.001
C4-H9	1.093	1.100±0.001	1.100±0.001

C4-I0	1.098	1.095±0.001	1.095±0.001
V1-O1	1.579	1.569±0.001	1.570±0.001
N7-V1	2.046	1.999±0.002	2.050±0.002
N9-V1	2.045	2.050±0.002	2.037±0.002
N7-I3	1.013	1.006±0.001	1.001±0.001
N9-I4	1.009	1.004±0.001	1.004±0.001
N7-C5	1.322	1.310±0.001	1.317±0.001
C5-N6	1.384	1.341±0.001	1.362±0.001
N6-I1	1.007	1.000±0.001	1.001±0.001
N6-I2	1.007	1.002±0.001	1.005±0.001
C5-N8	1.331	1.315±0.001	1.323±0.001
N8-C6	1.340	1.346±0.001	1.353±0.001
C6-N9	1.328	1.336±0.001	1.338±0.001
C6-M0	1.376	1.391±0.001	1.405±0.001
M0-C8	1.447	1.461±0.001	1.465±0.001
M0-C7	1.453	1.466±0.001	1.473±0.001
C7-I5	1.083	1.097±0.001	1.085±0.001
C7-I6	1.094	1.096±0.001	1.097±0.001
C7-I7	1.096	1.085±0.001	1.097±0.001
C8-I8	1.098	1.085±0.001	1.097±0.001
C8-I9	1.092	1.092±0.001	1.095±0.001
C8-J0	1.089	1.100±0.001	1.092±0.001

Table S3.2. Comparison of the relative error (%) of bond lengths of different methods and levels of theory for validation purposes.

	ECP *vs.* New Force Field	**ECP *vs.* GAFF**
H1-N1	0.517	0.521
H2-N1	0.255	0.464
N1-C1	1.516	3.043
C1-N4	0.523	1.290
C1-N2	0.452	1.079
N4-C2	0.855	0.493
N2-H3	1.091	0.765
C2-N5	1.857	21.155
C2-N3	0.922	0.845
N2-V1	0.450	1.224
N3-V1	0.845	0.821
N3-H4	0.524	0.610
N5-C3	1.176	0.829
N5-C4	1.194	0.927
C3-H5	0.239	0.247
C3-H6	0.117	0.379
C3-H7	0.224	0.133
C4-H8	0.115	0.158
C4-H9	0.700	0.636
C4-I0	0.307	0.252

V1-O1	0.551	0.621
N7-V1	0.208	2.320
N9-V1	0.373	0.246
N7-I3	1.180	0.659
N9-I4	0.426	0.459
N7-C5	0.336	0.889
C5-N6	1.573	3.093
N6-I1	0.550	0.669
N6-I2	0.205	0.484
C5-N8	0.564	1.178
N8-C6	1.013	0.496
C6-N9	0.741	0.583
C6-M0	2.100	1.040
M0-C8	1.241	0.954
M0-C7	1.342	0.911
C7-I5	0.185	1.318
C7-I6	0.267	0.145
C7-I7	0.121	0.968
C8-I8	0.108	1.195
C8-I9	0.237	0.037
C8-J0	0.297	1.028

Table S3.3. Bond angles in degrees (°)) obtained by different calculations for validation purposes.

	B3LYP/def2-TVZP+LANL2DZ ECP *(Gaussian 09)*	**MD with GAFF** *(average and standard deviation)*	**MD with New FF** *(average and standard deviation)*
H1-N1-H2	114.956	108.917±0.239	124.336±0.169
H1-N1-C1	117.385	104.800±0.209	123.562±0.160
H2-N1-C1	113.916	99.389±0.207	111.231±0.155
N1-C1-N4	113.632	104.972±0.144	109.568±0.119
N1-C1-N2	118.701	116.207±0.143	118.725±0.115
C1-N4-C2	122.291	110.968±0.100	114.918±0.094
C1-N2-V1	129.800	126.850±0.159	126.757±0.117
C1-N2-H3	111.915	103.934±0.199	99.484±0.156
H3-N2-V1	118.268	112.781±0.226	120.764±0.192
N4-C2-N5	115.131	115.648±0.097	116.555±0.085
N4-C2-N3	125.129	123.640±0.101	122.754±0.088
C2-N3-H4	112.845	100.715±0.184	103.411±0.159
N3-C2-N5	119.740	119.079±0.099	119.961±0.086
H4-N3-V1	115.690	116.107±0.184	111.528±0.168
C2-N5-C4	120.954	118.223±0.114	120.622±0.085
C2-N5-C3	122.209	121.441±0.109	125.063±0.081
N5-C3-H5	109.047	109.454±0.148	110.149±0.198
N5-C3-H6	110.126	110.827±0.149	113.954±0.195
N5-C3-H7	111.018	112.184±0.152	116.342±0.190
N5-C4-H8	108.644	113.315±0.152	111.675±0.135

N5-C4-H9	111.464	109.497±0.152	112.588±0.143
N5-C4-I0	112.851	111.974±0.151	111.150±0.146
N2-V1-O1	110.114	113.600±0.272	106.256±0.346
N3-V1-O1	106.161	48.671±0.178	98.213±0.338
N2-V1-N7	87.063	47.201±0.107	60.949±0.098
N3-V1-N9	86.725	53.313±0.176	128.946±0.109
N3-V1-N7	147.690	73.493±0.172	127.501±0.161
N2-V1-N9	139.820	100.064±0.167	130.776±0.146
N2-V1-N3	82.159	66.947±0.094	74.303±0.079
H5-C3-H6	109.291	107.938±0.222	95.566±0.810
H6-C3-H7	108.279	107.210±0.208	98.084±0.791
H5-C3-H7	109.052	108.176±0.211	111.094±0.524
H8-C4-H9	107.325	106.529±0.214	106.556±0.114
H9-C4-I0	108.693	107.603±0.211	107.120±0.115
H8-C4-I0	107.646	106.686±0.216	107.216±0.119
V1-N3-C2	130.690	131.880±0.136	131.775±0.116
I1-N6-I2	114.824	115.401±0.233	124.019±0.179
I1-N6-C5	117.252	105.806±0.207	123.242±0.158
I2-N6-C5	113.792	101.003±0.200	111.817±0.167
N6-C5-N8	113.545	105.430±0.142	109.480±0.117
N6-C5-N7	118.938	115.605±0.144	118.664±0.115
C5-N8-C6	122.191	111.623±0.105	115.252±0.093
C5-N7-V1	128.866	124.994±0.154	126.351±0.113
C5-N7-I3	111.945	99.752±0.190	100.505±0.173

I3-N7-V1	118.532	93.556±0.228	121.764±0.183
N8-C6-M0	115.236	115.930±0.102	116.610±0.084
N8-C6-N9	125.244	122.788±0.101	121.816±0.086
C6-N9-I4	112.847	101.466±1.190	104.305±0.159
N9-C6-M0	119.516	119.635±0.099	120.751±0.085
I4-N9-V1	116.458	109.144±0.221	110.347±0.176
C6-M0-C8	121.175	118.349±0.111	121.803±0.089
C6-M0-C7	122.260	121.668±0.106	124.689±0.084
M0-C7-I5	109.045	110.932±0.145	110.029±0.191
M0-C7-I6	110.391	111.692±0.148	113.785±0.197
M0-C7-I7	110.741	109.703±0.152	115.895±0.185
M0-C8-I8	112.974	111.948±0.158	119.671±0.175
M0-C8-I9	111.230	109.464±0.149	114.855±0.192
M0-C8-J0	108.652	113.633±0.150	108.427±0.175
N7-V1-O1	106.148	109.867±0.302	117.403±0.366
N9-V1-O1	110.066	49.801±0.191	109.849±0.310
N7-V1-N9	82.096	67.844±0.092	73.962±0.077
V1-N9-C6	130.667	131.015±0.138	131.365±0.112
I5-C7-I6	109.156	107.454±0.198	91.700±0.807
I6-C7-I7	108.259	107.977±0.209	113.500±0.442
I5-C7-I7	109.221	108.110±0.211	100.568±0.781
I8-C8-I9	108.733	106.704±0.217	115.090±0.273
I9-C8-J0	107.462	106.410±0.210	82.453±0.735
I8-C8-J0	107.581	107.471±0.197	103.310±0.686

N2-C1-N4	127.639	125.316±0.138	130.416±0.105
N7-C5-N8	127.481	124.862±0.137	130.564±0.104
C4-N5-C3	116.123	114.227±0.118	114.275±0.086
C8-M0-C7	116.082	114.230±0.114	113.300±0.092

Table S3.4. Comparison of the relative error (%) of bond angles of different methods and levels of theory for validation purposes.

	ECP *vs*. New Force Field	**ECP *vs*. GAFF**
H1-N1-H2	8.160	5.254
H1-N1-C1	5.262	10.721
H2-N1-C1	2.357	12.752
N1-C1-N4	3.577	7.621
N1-C1-N2	0.020	2.101
C1-N4-C2	6.029	9.259
C1-N2-V1	2.345	2.273
C1-N2-H3	11.108	7.131
H3-N2-V1	2.110	4.639
N4-C2-N5	1.237	0.449
N4-C2-N3	1.898	1.190
C2-N3-H4	8.361	10.749
N3-C2-N5	0.184	0.552
H4-N3-V1	3.598	0.361
C2-N5-C4	0.274	2.258
C2-N5-C3	2.335	0.628

N5-C3-H5	1.010	0.373
N5-C3-H6	3.476	0.636
N5-C3-H7	4.796	1.051
N5-C4-H8	2.790	4.299
N5-C4-H9	1.009	1.765
N5-C4-I0	1.507	0.777
N2-V1-O1	3.503	3.166
N3-V1-O1	7.487	54.154
N2-V1-N7	29.995	45.785
N3-V1-N9	48.684	38.527
N3-V1-N7	13.670	50.238
N2-V1-N9	6.468	28.434
N2-V1-N3	9.562	18.516
H5-C3-H6	12.559	1.238
H6-C3-H7	9.415	0.987
H5-C3-H7	1.873	0.803
H8-C4-H9	0.716	0.742
H9-C4-I0	1.447	1.003
H8-C4-I0	0.399	0.892
V1-N3-C2	0.830	0.911
I1-N6-I2	8.008	0.503
I1-N6-C5	5.109	9.762
I2-N6-C5	1.735	11.239
N6-C5-N8	3.580	7.147

N6-C5-N7	0.230	2.802
C5-N8-C6	5.679	8.648
C5-N7-V1	1.952	3.004
C5-N7-I3	10.219	10.892
I3-N7-V1	2.726	21.071
N8-C6-M0	1.193	0.603
N8-C6-N9	2.737	1.961
C6-N9-I4	7.569	10.085
N9-C6-M0	1.034	0.100
I4-N9-V1	5.247	6.281
C6-M0-C8	0.518	2.332
C6-M0-C7	1.987	0.485
M0-C7-I5	0.902	1.731
M0-C7-I6	3.074	1.179
M0-C7-I7	4.654	0.938
M0-C8-I8	5.928	0.908
M0-C8-I9	3.259	1.588
M0-C8-J0	0.207	4.585
N7-V1-O1	10.603	3.504
N9-V1-O1	0.197	54.754
N7-V1-N9	9.908	17.360
V1-N9-C6	0.534	0.266
I5-C7-I6	15.992	1.559
I6-C7-I7	4.841	0.261

I5-C7-I7	7.923	1.017
I8-C8-I9	5.847	1.866
I9-C8-J0	23.273	0.979
I8-C8-J0	3.970	0.102
N2-C1-N4	2.175	1.820
N7-C5-N8	2.419	2.054
C4-N5-C3	1.592	1.633
C8-M0-C7	2.396	1.595

Table S3.5. Comparison of the mean of the relative error (%) for different levels of theory for validation purposes.

	Mean of relative error ECP *vs*. New Force Field	**Mean of relative error ECP *vs*. GAFF**
Bond Lengths	0.671	1.345
Bond Angles	5.407	7.345

Section S4

```
MASS
V1     50.94  0.0
O1     16.00  0.0
C1     12.01  0.0
C2     12.01  0.0
C3     12.01  0.0
C4     12.01  0.0
C5     12.01  0.0
C6     12.01  0.0
C7     12.01  0.0
C8     12.01  0.0
N1     14.01  0.0
N2     14.01  0.0
N3     14.01  0.0
N4     14.01  0.0
N5     14.01  0.0
N6     14.01  0.0
N7     14.01  0.0
N8     14.01  0.0
N9     14.01  0.0
M0     14.01  0.0
H1     1.008  0.0
H2     1.008  0.0
H3     1.008  0.0
H4     1.008  0.0
H5     1.008  0.0
H6     1.008  0.0
H7     1.008  0.0
H8     1.008  0.0
H9     1.008  0.0
I0     1.008  0.0
I1     1.008  0.0
I2     1.008  0.0
```

```
I3    1.008  0.0
I4    1.008  0.0
I5    1.008  0.0
I6    1.008  0.0
I7    1.008  0.0
I8    1.008  0.0
I9    1.008  0.0
J0    1.008  0.0

BONDS
V1   N7      112.105    2.0414
V1   N9      108.659    2.0499
V1   N3      108.659    2.0499
V1   N2      112.105    2.0414
V1   O1      547.961    1.5791
N7   C5      495.282    1.3229
N7   I3      458.715    1.0127
N9   C6      480.984    1.3274
N9   I4      472.996    1.0091
N3   C2      480.984    1.3274
N3   H4      472.996    1.0091
N2   C1      495.282    1.3229
N2   H3      458.715    1.0127
C5   N8      455.535    1.3300
C5   N6      425.467    1.3839
C1   N4      455.535    1.3300
C1   N1      425.467    1.3839
C2   N4      425.002    1.3407
C2   N5      455.828    1.3766
C6   N8      425.002    1.3407
C6   M0      455.828    1.3766
N1   H2      487.610    1.0068
N1   H1      486.324    1.0066
N5   C4      354.905    1.4476
```

N5	C3	346.889	1.4533
N6	I1	486.324	1.0066
N6	I2	487.610	1.0068
M0	C7	346.889	1.4533
M0	C8	354.905	1.4476
C7	I5	371.204	1.0831
C7	I7	333.923	1.0961
C7	I6	340.150	1.0938
C8	I9	344.032	1.0925
C8	J0	355.108	1.0888
C8	I8	328.687	1.0983
C4	H9	344.032	1.0925
C4	I0	328.687	1.0983
C4	H8	355.108	1.0888
C3	H6	340.150	1.0938
C3	H7	333.923	1.0961
C3	H5	371.204	1.0831

ANGLES

N7	V1	N9	5.795	82.13
N7	V1	N3	1.914	143.76
N7	V1	N2	5.415	87.06
N7	V1	O1	2.819	143.76
N9	V1	N3	5.412	86.73
N9	V1	N2	1.914	143.76
N9	V1	O1	2.814	108.12
N3	V1	N2	5.795	82.13
N3	V1	O1	2.814	108.12
N2	V1	O1	2.819	108.13
V1	N7	C5	15.903	129.34
V1	N7	I3	16.048	118.40
C5	N7	I3	23.980	111.93
V1	N9	C6	16.530	130.68
V1	N9	I4	16.587	116.08

C6	N9	I4	23.983	112.85
V1	N3	C2	16.530	130.68
V1	N3	H4	16.587	116.08
C2	N3	H4	23.983	112.85
V1	N2	C1	15.903	129.34
V1	N2	H3	16.048	118.40
C1	N2	H3	23.980	111.93
N7	C5	N8	29.149	127.56
N7	C5	N6	51.404	118.82
N8	C5	N6	53.247	113.59
N2	C1	N4	29.149	127.56
N2	C1	N1	51.404	118.82
N4	C1	N1	53.247	113.59
N3	C2	N4	30.959	125.19
N3	C2	N5	67.913	119.63
N4	C2	N5	69.887	115.19
N9	C6	N8	30.959	125.19
N9	C6	M0	67.913	119.63
N8	C6	M0	69.887	115.19
C1	N4	C2	30.714	122.24
C5	N8	C6	30.714	122.24
C1	N1	H2	29.874	113.86
C1	N1	H1	30.487	117.32
H2	N1	H1	19.761	114.89
C2	N5	C4	54.034	118.52
C2	N5	C3	61.139	122.24
C4	N5	C3	48.929	116.10
C5	N6	I1	30.487	117.32
C5	N6	I2	29.874	113.86
I1	N6	I2	19.761	114.89
C6	M0	C7	61.139	122.24
C6	M0	C8	54.034	118.52
C7	M0	C8	48.929	116.10
M0	C7	I5	34.399	109.05

```
M0   C7   I7       37.409    110.88
M0   C7   I6       37.430    110.26
I5   C7   I7       16.473    109.14
I5   C7   I6       16.308    109.23
I7   C7   I6       18.571    108.27
M0   C8   I9       34.765    111.35
M0   C8   J0       36.564    108.65
M0   C8   I8       35.361    112.91
I9   C8   J0       16.485    107.40
I9   C8   I8       17.840    108.71
J0   C8   I8       17.104    107.62
N5   C4   H9       34.765    111.35
N5   C4   I0       35.361    112.91
N5   C4   H8       36.564    108.65
H9   C4   I0       17.840    108.71
H9   C4   H8       16.485    107.40
I0   C4   H8       17.104    107.62
N5   C3   H6       37.430    110.26
N5   C3   H7       37.409    111.88
N5   C3   H5       34.399    109.05
H6   C3   H7       18.571    108.27
H6   C3   H5       16.308    109.23
H7   C3   H5       16.473    109.14

DIHEDRALS
N9-V1-N7-C5   1    3.3000     0.00  3.000
N9-V1-N7-I3   1    3.3000     0.00  3.000
N3-V1-N7-C5   1    3.3000     0.00  3.000
N3-V1-N7-I3   1    3.3000     0.00  3.000
N2-V1-N7-C5   1    3.3000     0.00  3.000
N2-V1-N7-I3   1    3.3000     0.00  3.000
O1-V1-N7-C5   1    1.7500     0.00  2.000
O1-V1-N7-I3   1    1.7500     0.00  2.000
N7-V1-N9-C6   1    3.3000     0.00  3.000
```

N7-V1-N9-I4	1	3.3000	0.00	3.000
N3-V1-N9-C6	1	3.3000	0.00	3.000
N3-V1-N9-I4	1	3.3000	0.00	3.000
N2-V1-N9-C6	1	3.3000	0.00	3.000
N2-V1-N9-I4	1	3.3000	0.00	3.000
O1-V1-N9-C6	1	1.7500	0.00	2.000
O1-V1-N9-I4	1	1.7500	0.00	2.000
N7-V1-N3-C2	1	3.3000	0.00	3.000
N7-V1-N3-H4	1	3.3000	0.00	3.000
N9-V1-N3-C2	1	3.3000	0.00	3.000
N9-V1-N3-H4	1	3.3000	0.00	3.000
N2-V1-N3-C2	1	3.3000	0.00	3.000
N2-V1-N3-H4	1	3.3000	0.00	3.000
O1-V1-N3-C2	1	1.7500	0.00	2.000
O1-V1-N3-H4	1	1.7500	0.00	2.000
N7-V1-N2-C1	1	3.3000	0.00	3.000
N7-V1-N2-H3	1	3.3000	0.00	3.000
N9-V1-N2-C1	1	3.3000	0.00	3.000
N9-V1-N2-H3	1	3.3000	0.00	3.000
N3-V1-N2-C1	1	3.3000	0.00	3.000
N3-V1-N2-H3	1	3.3000	0.00	3.000
O1-V1-N2-C1	1	1.7500	0.00	2.000
O1-V1-N2-H3	1	1.7500	0.00	2.000
V1-N7-C5-N8	1	3.3000	0.00	3.000
V1-N7-C5-N6	1	3.3000	0.00	3.000
I3-N7-C5-N8	3	20.0000	180.00	2.000
I3-N7-C5-N6	3	20.0000	180.00	2.000
V1-N9-C6-N8	1	3.3000	0.00	3.000
V1-N9-C6-M0	1	3.3000	0.00	3.000
I4-N9-C6-N8	3	20.0000	180.00	2.000
I4-N9-C6-M0	3	20.0000	180.00	2.000
V1-N3-C2-N4	1	3.3000	0.00	3.000
V1-N3-C2-N5	1	3.3000	0.00	3.000
H4-N3-C2-N4	3	20.0000	180.00	2.000

```
H4-N3-C2-N5   3   20.0000   180.00  2.000
V1-N2-C1-N4   1    3.3000     0.00  3.000
V1-N2-C1-N1   1    3.3000     0.00  3.000
H3-N2-C1-N4   3   20.0000   180.00  2.000
H3-N2-C1-N1   3   20.0000   180.00  2.000
N7-C5-N8-C6   3   20.0000   180.00  2.000
N6-C5-N8-C6   3   20.0000   180.00  2.000
N7-C5-N6-I1   3   20.0000   180.00  2.000
N7-C5-N6-I2   3   20.0000   180.00  2.000
N8-C5-N6-I1   3   20.0000   180.00  2.000
N8-C5-N6-I2   3   20.0000   180.00  2.000
N2-C1-N4-C2   3   20.0000   180.00  2.000
N1-C1-N4-C2   3   20.0000   180.00  2.000
N2-C1-N1-H2   3   20.0000   180.00  2.000
N2-C1-N1-H1   3   20.0000   180.00  2.000
N4-C1-N1-H2   3   20.0000   180.00  2.000
N4-C1-N1-H1   3   20.0000   180.00  2.000
N3-C2-N4-C1   3   20.0000   180.00  2.000
N5-C2-N4-C1   3   20.0000   180.00  2.000
N3-C2-N5-C4   3   20.0000   180.00  2.000
N3-C2-N5-C3   3   20.0000   180.00  2.000
N4-C2-N5-C4   3   20.0000   180.00  2.000
N4-C2-N5-C3   3   20.0000   180.00  2.000
N9-C6-N8-C5   3   20.0000   180.00  2.000
M0-C6-N8-C5   3   20.0000   180.00  2.000
N9-C6-M0-C7   3   20.0000   180.00  2.000
N9-C6-M0-C8   3   20.0000   180.00  2.000
N8-C6-M0-C7   3   20.0000   180.00  2.000
N8-C6-M0-C8   3   20.0000   180.00  2.000
C2-N5-C4-H9   3   20.0000   180.00  6.000
C2-N5-C4-I0   3   20.0000   180.00  6.000
C2-N5-C4-H8   3   20.0000   180.00  6.000
C3-N5-C4-H9   3   20.0000   180.00  6.000
C3-N5-C4-I0   3   20.0000   180.00  6.000
```

```
C3-N5-C4-H8   3   20.0000   180.00  6.000
C2-N5-C3-H6   3   20.0000   180.00  2.000
C2-N5-C3-H7   3   20.0000   180.00  2.000
C2-N5-C3-H5   3   20.0000   180.00  2.000
C4-N5-C3-H6   3   20.0000   180.00  2.000
C4-N5-C3-H7   3   20.0000   180.00  2.000
C4-N5-C3-H5   3   20.0000   180.00  2.000
C6-M0-C7-I5   3   20.0000   180.00  2.000
C6-M0-C7-I7   3   20.0000   180.00  2.000
C6-M0-C7-I6   3   20.0000   180.00  2.000
C8-M0-C7-I5   3   20.0000   180.00  2.000
C8-M0-C7-I7   3   20.0000   180.00  2.000
C8-M0-C7-I6   3   20.0000   180.00  2.000
C6-M0-C8-I9   3   20.0000   180.00  2.000
C6-M0-C8-J0   3   20.0000   180.00  2.000
C6-M0-C8-I8   3   20.0000   180.00  2.000
C7-M0-C8-I9   3   20.0000   180.00  2.000
C7-M0-C8-J0   3   20.0000   180.00  2.000
C7-M0-C8-I8   3   20.0000   180.00  2.000

NONBONDED
V1             2.7670     1.9040    !
N7             1.8240     0.1700    !
N9             1.8240     0.1700    !
N3             1.8240     0.1700    !
N2             1.8240     0.1700    !
C5             1.9080     0.0860    !
C1             1.9080     0.0860    !
C2             1.9080     0.0860    !
C6             1.9080     0.0860    !
N4             1.8240     0.1700    !
N8             1.8240     0.1700    !
O1             1.6621     0.2100    !
N1             1.8240     0.1700    !
```

```
N5              1.8240     0.1700    !
N6              1.8240     0.1700    !
M0              1.8240     0.1700    !
I1              0.6000     0.0157    !
I2              0.6000     0.0157    !
H2              0.6000     0.0157    !
H1              0.6000     0.0157    !
I3              0.6000     0.0157    !
H3              0.6000     0.0157    !
C7              1.9080     0.1094    !
C8              1.9080     0.1094    !
C4              1.9080     0.1094    !
C3              1.9080     0.1094    !
I5              1.3870     0.0157    !
I7              1.3870     0.0157    !
I6              1.3870     0.0157    !
I9              1.3870     0.0157    !
J0              1.3870     0.0157    !
I8              1.3870     0.0157    !
H9              1.3870     0.0157    !
I0              1.3870     0.0157    !
H8              1.3870     0.0157    !
H6              1.3870     0.0157    !
H7              1.3870     0.0157    !
H5              1.3870     0.0157    !
I4              0.6000     0.0157    !
H4              0.6000     0.0157    !
END
```

Table S4.1 Atomic charges (RESP) for the vanadium complex.

Atom Types	q (e^-)
V1	0.401938
N7	-0.455306
N9	-0.482159
N3	-0.482159
N2	-0.455306
C5	0.543038
C1	0.543038
C2	0.429041
C6	0.429041
N4	-0.486021
N8	-0.486021
O1	-0.397267
N1	-0.803079
N5	-0.068518
N6	-0.803079
M0	-0.068518
I1	0.345923
I2	0.345923
H2	0.345923
H1	0.345923
I3	0.260138
H3	0.260138

C7	-0.223140
C8	-0.223140
C4	-0.223140
C3	-0.223140
I5	0.093831
I7	0.093831
I6	0.093831
I9	0.093831
J0	0.093831
I8	0.093831
H9	0.093831
I0	0.093831
H8	0.093831
H6	0.093831
H7	0.093831
H5	0.093831
I4	0.251977
H4	0.251977

Figure S4.1 Potential energy surface (PES) of dihedrals N11-C9-N16-C24 and N10-C8-N14-C25 for different methods.

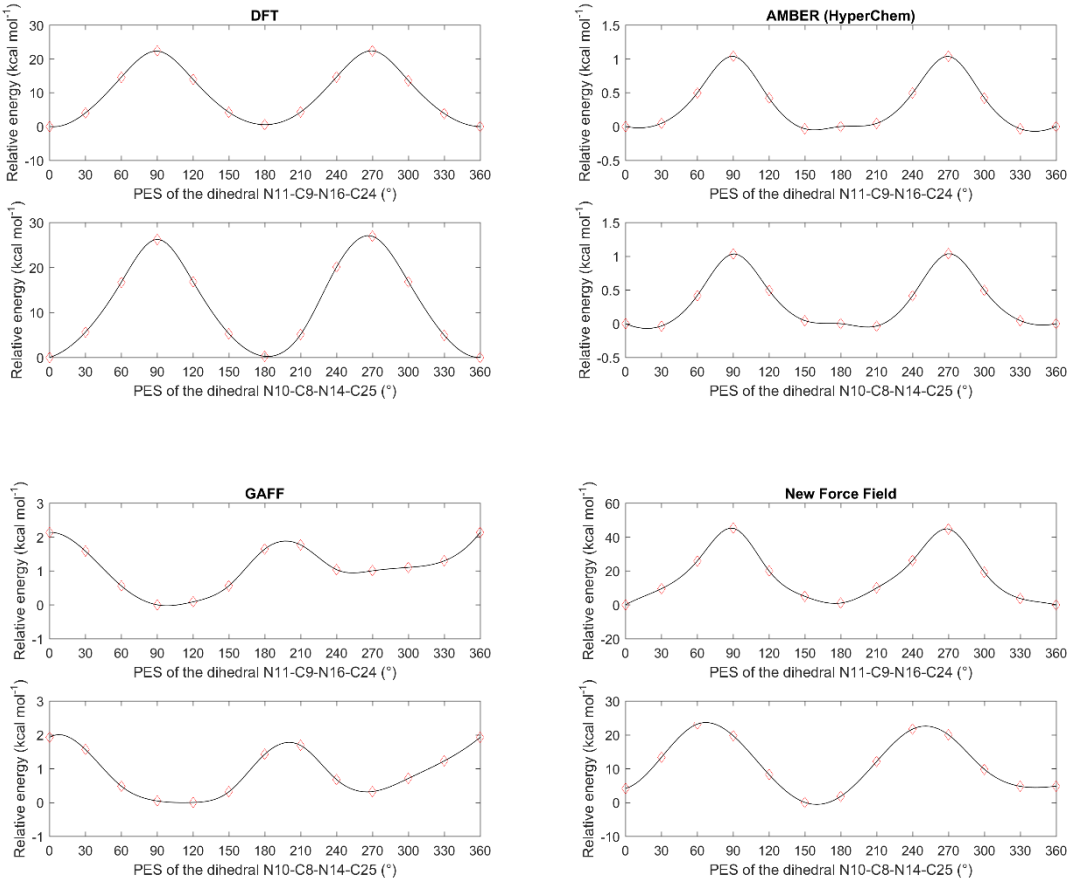

Figure S4.2. RMSD analysis of VC in aqueous solution.

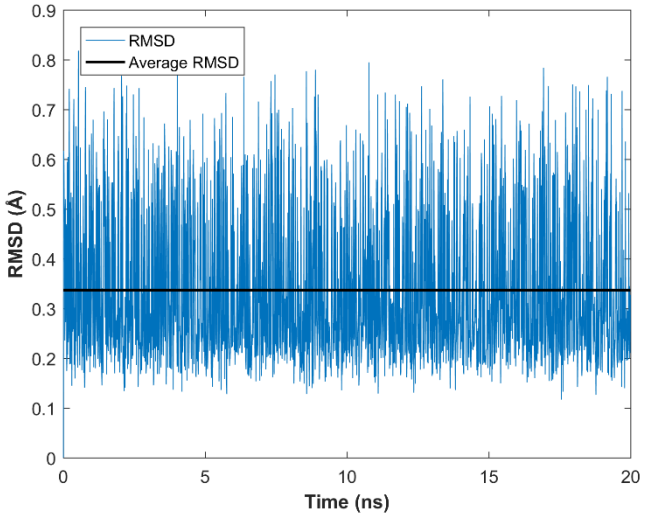

Supporting Information – Second Paper

Section S1

Table S1.1. Bond lengths in Angstroms (Å) for different methods and levels of theory.

	Experimental Data	**AMBER** (HyperChem)	**B3LYP/def2-TVZP+LANL2DZ ECP** (Gaussian 09)	**B3LYP/def2-TVZP with ZORA** (ORCA)
V1-O2	1.971	1.794	1.973	1.976
V1-O3	1.998	1.793	2.054	2.056
O3-C4	1.290	1.223	1.268	1.271
O2-C3	1.360	1.222	1.311	1.314
C4-C3	1.390	1.381	1.445	1.447
C4-C5	1.460	1.400	1.420	1.421
C3-C2	1.410	1.408	1.372	1.372
C5-C6	1.310	1.411	1.354	1.355
C2-O1	1.370	1.256	1.365	1.369
C2-C1	1.440	1.513	1.483	1.483
O1-C6	1.350	1.257	1.332	1.336
V1-O7	1.596	1.880	1.571	1.586
V1-O5	1.958	1.793	1.973	1.977
V1-O6	2.024	1.793	2.054	2.056
O6-D0	1.270	1.223	1.268	1.270
O5-C9	1.360	1.222	1.311	1.314
C9-D0	1.420	1.382	1.444	1.447
D0-D1	1.410	1.398	1.420	1.421

C9-C8	1.340	1.356	1.372	1.372
D1-D2	1.290	1.408	1.354	1.355
C8-O4	1.360	1.258	1.365	1.369
C8-C7	1.480	1.446	1.483	1.483
D2-O4	1.350	1.255	1.332	1.336

Table S1.2. Relative error (%) of bond lengths of different methods and levels of theory.

	Comparison (%) AMBER *vs.* Experimental	**Comparison (%) ECP *vs.* Experimental**	**Comparison (%) ZORA *vs.* Experimental**	**Comparison (%) ECP *vs.* ZORA**
V1-O2	8.982	0.083	0.266	0.182
V1-O3	10.263	2.809	2.915	0.103
O3-C4	5.186	1.688	1.504	0.187
O2-C3	10.128	3.615	3.416	0.206
C4-C3	0.624	3.922	4.070	0.142
C4-C5	4.142	2.747	2.702	0.046
C3-C2	0.127	2.722	2.713	0.009
C5-C6	7.695	3.379	3.434	0.054
C2-O1	8.307	0.387	0.083	0.304
C2-C1	5.083	3.003	3.013	0.009
O1-C6	6.903	1.350	1.064	0.288
V1-O7	17.772	1.563	0.642	0.928
V1-O5	8.404	0.761	0.954	0.191
V1-O6	11.389	1.501	1.596	0.093

O6-D0	3.672	0.141	0.020	0.161
O5-C9	10.115	3.619	3.395	0.232
C9-D0	2.679	1.724	1.880	0.153
D0-D1	0.826	0.704	0.759	0.055
C9-C8	1.167	2.357	2.354	0.002
D1-D2	9.155	4.984	5.043	0.056
C8-O4	7.501	0.346	0.656	0.308
C8-C7	2.307	0.220	0.226	0.006
D2-O4	7.047	1.348	1.069	0.282

Table S1.3. Bond angles in degrees (°) of different methods and levels of theory.

	Experimental Data	**AMBER** (HyperChem)	**B3LYP/def2-TVZP+LANL2DZ ECP** (Gaussian 09)	**B3LYP/def2-TVZP with ZORA** (ORCA)
O3-V1-O2	82.500	82.183	80.152	79.892
O3-V1-O6	146.800	127.741	150.410	150.351
O3-V1-O5	86.300	79.599	88.419	88.870
O3-V1-O7	107.000	117.309	104.806	104.805
O2-V1-O7	108.700	114.822	112.857	112.558
V1-O3-C4	112.900	115.252	112.379	112.598
V1-O2-C3	108.100	115.488	113.957	114.095
O3-C4-C3	114.000	113.729	116.943	116.747
O3-C4-C5	123.000	128.029	125.022	125.160
C3-C4-C5	121.000	118.236	118.035	118.093

O2-C3-C4	120.000	113.328	115.948	115.764
O2-C3-C2	120.000	127.856	124.965	125.075
C4-C3-C2	119.000	118.808	119.083	119.160
C4-C5-C6	113.000	116.788	118.473	118.467
C3-C2-O1	118.000	119.527	120.080	119.998
C3-C2-C1	125.000	120.395	126.000	125.997
O1-C2-C1	116.000	120.077	113.920	114.005
C5-C6-O1	128.000	121.058	122.965	122.979
C8-O4-D2	120.000	125.638	121.361	121.312
O6-V1-O5	81.500	82.086	80.130	79.864
O2-V1-O5	140.600	127.487	134.255	134.813
O2-V1-O6	87.600	71.415	88.454	88.740
O6-V1-O7	106.100	114.627	104.784	104.844
O5-V1-O7	110.600	117.348	112.888	112.629
V1-O6-D0	112.300	115.270	112.391	112.665
V1-O5-C9	119.900	115.732	113.965	114.114
O6-D0-C9	117.000	115.270	116.933	116.728
O6-D0-D1	128.000	127.979	125.035	125.164
C9-D0-D1	113.000	118.192	118.032	118.107
O5-C9-D0	115.000	113.091	115.948	115.755
O5-C9-C8	122.000	127.775	124.961	125.080
D0-C9-C8	121.000	119.104	119.088	119.165
D0-D1-D2	123.000	116.486	118.471	118.436
C9-C8-O4	119.000	120.410	120.080	119.983

C9-C8-C7	126.000	120.263	125.999	126.050
O4-C8-C7	113.000	119.316	113.921	113.967
D1-D2-O4	120.000	120.164	122.967	122.991
C2-O1-C6	118.000	125.584	121.364	121.299

Table S1.4. Relative error (%) of bond angles of different methods and levels of theory.

	Comparison (%) AMBER *vs.* Experimental	**Comparison (%) ECP *vs.* Experimental**	**Comparison (%) ZORA *vs.* Experimental**	**Comparison (%) ECP *vs.* ZORA**
O3-V1-O2	0.385	2.846	3.161	0.325
O3-V1-O6	12.983	2.459	2.419	0.039
O3-V1-O5	7.764	2.456	2.978	0.507
O3-V1-O7	9.635	2.051	2.052	0.001
O2-V1-O7	5.632	3.824	3.549	0.266
V1-O3-C4	2.083	0.461	0.268	0.194
V1-O2-C3	6.834	5.418	5.546	0.121
O3-C4-C3	0.238	2.581	2.409	0.168
O3-C4-C5	4.089	1.644	1.756	0.110
C3-C4-C5	2.284	2.451	2.402	0.050
O2-C3-C4	5.560	3.376	3.530	0.159
O2-C3-C2	6.547	4.138	4.229	0.088
C4-C3-C2	0.161	0.070	0.135	0.065
C4-C5-C6	3.352	4.843	4.838	0.005
C3-C2-O1	1.294	1.762	1.693	0.068

C3-C2-C1	3.684	0.800	0.797	0.003
O1-C2-C1	3.515	1.793	1.720	0.074
C5-C6-O1	5.423	3.933	3.923	0.011
C8-O4-D2	4.698	1.134	1.093	0.040
O6-V1-O5	0.719	1.681	2.007	0.333
O2-V1-O5	9.326	4.513	4.116	0.414
O2-V1-O6	18.476	0.975	1.302	0.322
O6-V1-O7	8.037	1.240	1.183	0.057
O5-V1-O7	6.101	2.069	1.835	0.230
V1-O6-D0	2.645	0.081	0.325	0.244
V1-O5-C9	3.476	4.950	4.826	0.131
O6-D0-C9	1.479	0.057	0.232	0.175
O6-D0-D1	0.016	2.317	2.215	0.104
C9-D0-D1	4.595	4.453	4.519	0.064
O5-C9-D0	1.660	0.825	0.657	0.167
O5-C9-C8	4.734	2.427	2.524	0.095
D0-C9-C8	1.567	1.580	1.517	0.065
D0-D1-D2	5.296	3.682	3.711	0.030
C9-C8-O4	1.185	0.908	0.826	0.081
C9-C8-C7	4.553	0.001	0.040	0.041
O4-C8-C7	5.589	0.815	0.855	0.040
D1-D2-O4	0.137	2.473	2.493	0.020
C2-O1-C6	6.427	2.851	2.796	0.054

Section S2

Table S2.1. Bond lengths in Angstroms (Å) of different methods and levels of theory for validation purposes.

	Experimental Data (values with standard deviation)	**B3LYP/def2-TVZP+LANL2DZ ECP** (Gaussian 09)	**MD with GAFF** (average and standard deviation)	**MD with New FF** (average and standard deviation)
V1-O2	1.971±0.008	1.973	1.966±0.002	1.951±0.002
V1-O3	1.998±0.008	2.054	2.011±0.002	2.014±0.002
O3-C4	1.290±0.010	1.268	1.262±0.001	1.262±0.001
O2-C3	1.360±0.010	1.311	1.317±0.001	1.315±0.001
C4-C3	1.390±0.020	1.445	1.452±0.001	1.457±0.001
C4-C5	1.460±0.020	1.420	1.428±0.001	1.429±0.001
C3-C2	1.410±0.020	1.372	1.378±0.001	1.384±0.001
C5-C6	1.310±0.020	1.354	1.360±0.001	1.362±0.001
C2-O1	1.370±0.010	1.365	1.376±0.001	1.376±0.001
C2-C1	1.440±0.020	1.483	1.428±0.001	1.486±0.001
O1-C6	1.350±0.020	1.332	1.339±0.001	1.339±0.001
V1-O7	1.596±0.007	1.571	1.566±0.001	1.565±0.001
V1-O5	1.958±0.008	1.973	1.964±0.002	1.953±0.002
V1-O6	2.024±0.008	2.054	2.013±0.002	2.012±0.002
O6-D0	1.270±0.010	1.268	1.261±0.001	1.264±0.001
O5-C9	1.360±0.010	1.311	1.316±0.001	1.316±0.001
C9-D0	1.420±0.020	1.444	1.453±0.001	1.457±0.001
D0-D1	1.410±0.020	1.420	1.427±0.001	1.429±0.001
C9-C8	1.340±0.020	1.372	1.381±0.001	1.380±0.001

D1-D2	1.290±0.020	1.354	1.360±0.001	1.360±0.001
C8-O4	1.360±0.010	1.365	1.378±0.001	1.376±0.001
C8-C7	1.480±0.020	1.483	1.484±0.001	1.487±0.001
D2-O4	1.350±0.020	1.332	1.338±0.001	1.338±0.001

Table S2.2. Relative error (%) of bond lengths of different methods and levels of theory for validation purposes

	Comparison (%) ECP *vs.* Experimental	**Comparison (%) GAFF *vs.* Experimental**	**Comparison (%) New Force Field *vs.* Experimental**
V1-O2	0.083	0.231	1.003
V1-O3	2.809	0.653	0.811
O3-C4	1.688	2.133	2.191
O2-C3	3.615	3.126	3.277
C4-C3	3.922	4.463	4.789
C4-C5	2.747	2.210	2.102
C3-C2	2.722	2.254	1.859
C5-C6	3.379	3.831	3.958
C2-O1	0.387	0.469	0.470
C2-C1	3.003	0.852	3.208
O1-C6	1.350	0.799	0.791
V1-O7	1.563	1.883	1.926
V1-O5	0.761	0.311	0.253
V1-O6	1.501	0.538	0.578

O6-D0	0.141	0.738	0.447
O5-C9	3.619	3.228	3.251
C9-D0	1.724	2.302	2.615
D0-D1	0.704	1.231	1.343
C9-C8	2.357	3.097	3.016
D1-D2	4.984	5.395	5.446
C8-O4	0.346	1.341	1.164
C8-C7	0.220	0.259	0.456
D2-O4	1.348	0.864	0.901

Table S2.3. Bond angles in degrees (º) of different methods and levels of theory for validation purposes.

	Experimental Data (values with standard deviation)	**B3LYP/def2-TVZP+LANL2DZ ECP** (Gaussian 09)	**MD with GAFF** (average and standard deviation)	**MD with New FF** (average and standard deviation)
O3-V1-O2	82.500±0.400	80.152	81.933±0.118	82.260±0.126
O3-V1-O6	146.800±0.300	150.410	119.930±0.393	130.060±0.507
O3-V1-O5	86.300±0.040	88.419	57.434±0.249	75.354±0.547
O3-V1-O7	107.000±0.500	104.806	101.060±0.753	109.953±0.504
O2-V1-O7	108.700±0.400	112.857	105.696±0.934	116.468±0.483
V1-O3-C4	112.900±0.800	112.379	109.957±0.138	107.620±0.145
V1-O2-C3	108.100±0.700	113.957	111.446±0.137	109.049±0.137
O3-C4-C3	114.000±1.000	116.943	117.898±0.131	117.584±0.128
O3-C4-C5	123.000±1.000	125.022	120.407±0.134	122.641±0.127

C3-C4-C5	121.000±1.000	118.035	119.379±0.107	119.441±0.107
O2-C3-C4	120.000±1.000	115.948	114.747±0.118	115.189±0.118
O2-C3-C2	120.000±1.000	124.965	126.794±0.123	126.951±0.121
C4-C3-C2	119.000±2.000	119.083	116.590±0.100	117.281±0.102
C4-C5-C6	113.000±1.000	118.473	117.662±0.110	118.392±0.104
C3-C2-O1	118.000±1.000	120.080	119.721±0.099	120.160±0.098
C3-C2-C1	125.000±1.000	126.000	125.628±0.123	125.918±0.120
O1-C2-C1	116.000±1.000	113.920	112.903±0.125	113.481±0.119
C5-C6-O1	128.000±1.000	122.965	120.640±0.110	121.603±0.106
C8-O4-D2	120.000±1.000	121.361	122.532±0.104	122.813±0.107
O6-V1-O5	81.500±0.300	80.130	82.010±0.125	82.217±0.132
O2-V1-O5	140.600±0.300	134.255	91.873±0.337	119.624±0.540
O2-V1-O6	87.600±0.400	88.454	57.560±0.230	77.319±0.568
O6-V1-O7	106.100±0.500	104.784	103.911±0.768	109.933±0.490
O5-V1-O7	110.600±0.400	112.888	110.097±0.948	116.369±0.509
V1-O6-D0	112.300±0.800	112.391	109.948±0146	107.599±0.141
V1-O5-C9	119.900±0.700	113.965	111.607±0142	109.088±0.145
O6-D0-C9	117.000±1.000	116.933	118.098±0134	117.562±0.128
O6-D0-D1	128.000±1.000	125.035	120.210±0.129	122.655±0.0.127
C9-D0-D1	113.000±1.000	118.032	119.609±0.107	119.445±0.106
O5-C9-D0	115.000±1.000	115.948	114.713±0.123	115.039±0.122
O5-C9-C8	122.000±1.000	124.961	126.965±0.129	127.218±0.120
D0-C9-C8	121.000±1.000	119.088	116.272±0.106	117.153±0.104
D0-D1-D2	123.000±1.000	118.471	117.605±0.109	118.560±0.105

C9-C8-O4	119.000±1.000	120.080	119.882±0.099	120.196±0.101
C9-C8-C7	126.000±1.000	125.999	125.394±0.119	126.074±0.119
O4-C8-C7	113.000±1.000	113.921	113.074±0.119	113.298±0.114
D1-D2-O4	120.000±1.000	122.967	120.879±0.111	121.257±0.106
C2-O1-C6	118.000±1.000	121.364	122.645±0.109	122.570±0.107

Table S2.4. Relative error (%) of bond angles of different methods and levels of theory for validation purposes.

	Comparison (%) ECP *vs.* Experimental	**Comparison (%) ZORA *vs.* Experimental**	**Comparison (%) ECP *vs.* ZORA**
O3-V1-O2	2.846	0.291	0.687
O3-V1-O6	2.459	11.403	18.304
O3-V1-O5	2.456	12.684	33.448
O3-V1-O7	2.051	2.760	5.552
O2-V1-O7	3.824	7.146	2.763
V1-O3-C4	0.461	4.677	2.607
V1-O2-C3	5.418	0.878	3.095
O3-C4-C3	2.581	3.144	3.419
O3-C4-C5	1.644	0.292	2.108
C3-C4-C5	2.451	1.289	1.340
O2-C3-C4	3.376	4.009	4.377
O2-C3-C2	4.138	5.793	5.661
C4-C3-C2	0.070	1.444	2.025
C4-C5-C6	4.843	4.771	4.126

C3-C2-O1	1.762	1.830	1.458
C3-C2-C1	0.800	0.735	0.502
O1-C2-C1	1.793	2.171	2.670
C5-C6-O1	3.933	4.998	5.750
C8-O4-D2	1.134	2.344	2.110
O6-V1-O5	1.681	0.880	0.625
O2-V1-O5	4.513	14.919	34.656
O2-V1-O6	0.975	11.736	34.293
O6-V1-O7	1.240	3.612	2.063
O5-V1-O7	2.069	5.216	0.455
V1-O6-D0	0.081	4.186	2.094
V1-O5-C9	4.950	9.018	6.916
O6-D0-C9	0.057	0.480	0.938
O6-D0-D1	2.317	4.176	6.086
C9-D0-D1	4.453	5.703	5.849
O5-C9-D0	0.825	0.034	0.250
O5-C9-C8	2.427	4.277	4.070
D0-C9-C8	1.580	3.180	3.907
D0-D1-D2	3.682	3.610	4.386
C9-C8-O4	0.908	1.005	0.741
C9-C8-C7	0.001	0.059	0.481
O4-C8-C7	0.815	0.263	0.065
D1-D2-O4	2.473	1.047	0.733
C2-O1-C6	2.851	3.873	3.936

Section S3

```
MASS
V1     50.94   0.0
O1     16.00   0.0
O2     16.00   0.0
O3     16.00   0.0
O4     16.00   0.0
O5     16.00   0.0
O6     16.00   0.0
O7     16.00   0.0
C1     12.01   0.0
C2     12.01   0.0
C3     12.01   0.0
C4     12.01   0.0
C5     12.01   0.0
C6     12.01   0.0
C7     12.01   0.0
C8     12.01   0.0
C9     12.01   0.0
D0     12.01   0.0
D1     12.01   0.0
D2     12.01   0.0
H1     1.008   0.0
H2     1.008   0.0
H3     1.008   0.0
H4     1.008   0.0
H5     1.008   0.0
H6     1.008   0.0
H7     1.008   0.0
H8     1.008   0.0
H9     1.008   0.0
I0     1.008   0.0
```

BONDS

V1	O3	81.720	2.0543
V1	O2	112.512	1.9728
V1	O6	81.720	2.0543
V1	O5	112.512	1.9728
V1	O7	567.153	1.5710
O3	C4	540.762	1.2682
O2	C3	435.669	1.3108
O6	D0	540.762	1.2682
O5	C9	435.669	1.3108
C4	C3	240.660	1.4445
C4	C5	359.709	1.4199
C3	C2	448.080	1.3716
C9	D0	240.660	1.4445
C9	C8	448.080	1.3716
D0	D1	359.709	1.4199
C5	C6	483.448	1.3543
C5	H4	378.559	1.0804
C2	O1	334.128	1.3647
C2	C1	329.193	1.4833
C6	O1	400.134	1.3318
C6	H5	380.385	1.0800
C8	O4	334.128	1.3647
C8	C7	329.193	1.4833
D2	D1	483.448	1.3543
D2	O4	400.134	1.3318
D2	I0	380.385	1.0800
D1	H9	378.559	1.0804
C7	H6	361.554	1.0875
C7	H7	344.950	1.0932
C7	H8	344.782	1.0932
C1	H2	344.950	1.0932
C1	H1	361.554	1.0875

C1 H3 344.782 1.0932

ANGLES

O2	V1	O5	2.646	142.34
O2	V1	O6	5.481	88.44
O2	V1	O7	4.741	112.88
O3	V1	O2	7.411	80.14
O3	V1	O6	2.646	142.34
O3	V1	O5	5.481	88.44
O3	V1	O7	4.616	104.80
O5	V1	O7	4.741	112.88
O6	V1	O5	7.411	80.14
O6	V1	O7	4.616	104.80
V1	O2	C3	18.598	113.96
V1	O3	C4	18.622	112.39
V1	O5	C9	18.598	113.96
V1	O6	D0	18.622	112.39
O1	C2	C1	37.394	113.92
O1	C6	H5	29.183	112.03
O2	C3	C4	22.767	115.95
O2	C3	C2	29.922	124.97
O3	C4	C3	23.628	116.94
O3	C4	C5	29.381	125.03
O4	C8	C7	37.394	113.92
O4	D2	I0	29.183	112.03
O5	C9	D0	22.767	115.95
O5	C9	C8	29.922	124.97
O6	D0	C9	23.628	116.94
O6	D0	D1	29.381	125.03
C2	C1	H2	30.354	111.02
C2	C1	H1	30.628	109.09
C2	C1	H3	30.360	111.03
C2	O1	C6	32.760	121.36
C3	C4	C5	22.230	118.03

C3	C2	O1	28.496	120.08	
C3	C2	C1	32.533	126.00	
C4	C3	C2	23.817	119.09	
D0	C9	C8	23.817	119.09	
C4	C5	C6	23.739	118.47	
C4	C5	H4	21.709	120.79	
C5	C6	O1	28.505	122.97	
C5	C6	H5	24.441	125.00	
C6	C5	H4	21.739	120.74	
C8	C7	H6	30.628	109.09	
C8	C7	H7	30.354	111.02	
C8	C7	H8	30.360	111.03	
C8	O4	D2	32.760	121.36	
C9	D0	D1	22.230	118.03	
C9	C8	O4	28.496	120.08	
C9	C8	C7	32.533	126.00	
D0	D1	D2	23.739	118.47	
D0	D1	H9	21.709	120.79	
D1	D2	O4	28.505	122.97	
D1	D2	I0	24.441	125.00	
D2	D1	H9	21.739	120.74	
H1	C1	H3	15.743	109.00	
H2	C1	H1	15.742	109.02	
H2	C1	H3	16.121	107.64	
H6	C7	H7	15.742	109.02	
H6	C7	H8	15.743	109.00	
H7	C7	H8	16.121	107.64	

DIHEDRALS

O2-V1-O3-C4	1	0.0601	173.44	4.000
O6-V1-O3-C4	1	0.2060	104.67	4.000
O5-V1-O3-C4	1	0.1116	37.93	4.000
O7-V1-O3-C4	1	1.1750	0.00	2.000
O3-V1-O2-C3	1	0.0555	186.93	4.000

O6-V1-O2-C3	1	0.1192	339.52	4.000
O5-V1-O2-C3	1	0.3267	180.00	4.000
O7-V1-O2-C3	1	1.1750	0.00	2.000
O3-V1-O6-D0	1	0.2060	104.67	4.000
O2-V1-O6-D0	1	0.1116	37.93	4.000
O5-V1-O6-D0	1	0.0601	173.44	4.000
O7-V1-O6-D0	1	1.1750	0.00	2.000
O3-V1-O5-C9	1	0.1192	339.52	4.000
O2-V1-O5-C9	1	0.3267	180.00	4.000
O6-V1-O5-C9	1	0.0555	186.93	4.000
O7-V1-O5-C9	1	1.1750	0.00	2.000
V1-O3-C4-C3	1	0.0000	180.00	2.000
V1-O3-C4-C5	2	0.0000	180.00	2.000
V1-O2-C3-C4	2	0.0000	180.00	2.000
V1-O2-C3-C2	2	0.0000	180.00	2.000
V1-O6-D0-C9	2	0.0000	180.00	2.000
V1-O6-D0-D1	2	0.0000	180.00	2.000
V1-O5-C9-D0	2	0.0000	180.00	2.000
V1-O5-C9-C8	1	0.0000	180.00	2.000
O3-C4-C3-O2	1	1.1750	0.00	2.000
O3-C4-C3-C2	4	26.6000	180.00	2.000
C5-C4-C3-O2	4	26.6000	180.00	2.000
C5-C4-C3-C2	4	26.6000	180.00	2.000
O3-C4-C5-C6	4	26.6000	180.00	2.000
O3-C4-C5-H4	4	26.6000	180.00	2.000
C3-C4-C5-C6	4	26.6000	180.00	2.000
C3-C4-C5-H4	4	26.6000	180.00	2.000
O2-C3-C2-O1	1	1.1750	0.00	2.000
O2-C3-C2-C1	4	26.6000	180.00	2.000
C4-C3-C2-O1	4	26.6000	180.00	2.000
C4-C3-C2-C1	4	26.6000	180.00	2.000
O5-C9-D0-O6	1	1.1750	0.00	2.000
O5-C9-D0-D1	4	26.6000	180.00	2.000
C8-C9-D0-O6	4	26.6000	180.00	2.000

C8-C9-D0-D1	4	26.6000	180.00	2.000
O5-C9-C8-O4	1	1.1750	0.00	2.000
O5-C9-C8-C7	4	26.6000	180.00	2.000
D0-C9-C8-O4	4	26.6000	180.00	2.000
D0-C9-C8-C7	4	26.6000	180.00	2.000
O6-D0-D1-D2	4	26.6000	180.00	2.000
O6-D0-D1-H9	4	26.6000	180.00	2.000
C9-D0-D1-D2	4	26.6000	180.00	2.000
C9-D0-D1-H9	4	26.6000	180.00	2.000
C4-C5-C6-O1	4	26.6000	180.00	2.000
C4-C5-C6-H5	4	26.6000	180.00	2.000
H4-C5-C6-O1	4	26.6000	180.00	2.000
H4-C5-C6-H5	4	26.6000	180.00	2.000
C3-C2-O1-C6	4	26.6000	180.00	2.000
C1-C2-O1-C6	2	5.4000	180.00	2.000
C3-C2-C1-H2	6	0.0000	180.00	2.000
C3-C2-C1-H1	6	0.0000	180.00	2.000
C3-C2-C1-H3	6	0.0000	180.00	2.000
O1-C2-C1-H2	6	0.0000	180.00	2.000
O1-C2-C1-H1	6	0.0000	180.00	2.000
O1-C2-C1-H3	6	0.0000	180.00	2.000
C5-C6-O1-C2	4	26.6000	180.00	2.000
H5-C6-O1-C2	2	2.1000	180.00	2.000
C9-C8-O4-D2	4	26.6000	180.00	2.000
C7-C8-O4-D2	2	5.4000	180.00	2.000
C9-C8-C7-H6	6	0.0000	180.00	2.000
C9-C8-C7-H7	6	0.0000	180.00	2.000
C9-C8-C7-H8	6	0.0000	180.00	2.000
O4-C8-C7-H6	6	0.0000	180.00	2.000
O4-C8-C7-H7	6	0.0000	180.00	2.000
O4-C8-C7-H8	6	0.0000	180.00	2.000
O4-D2-D1-D0	4	26.6000	180.00	2.000
O4-D2-D1-H9	4	26.6000	180.00	2.000
I0-D2-D1-D0	4	26.6000	180.00	2.000

```
I0-D2-D1-H9   4   26.6000   180.00  2.000
D1-D2-O4-C8   2   26.6000   180.00  2.000
I0-D2-O4-C8   2    2.1000   180.00  2.000

NONBONDED
V1             2.7670     1.9040    !
O3             1.6837     0.1700    !
O2             1.6837     0.1700    !
O6             1.6837     0.1700    !
O5             1.6837     0.1700    !
C4             1.9080     0.0860    !
C3             1.9080     0.0860    !
C9             1.9080     0.0860    !
D0             1.9080     0.0860    !
C5             1.9080     0.0860    !
C2             1.9080     0.0860    !
C6             1.9080     0.0860    !
C8             1.9080     0.0860    !
D2             1.9080     0.0860    !
D1             1.9080     0.0860    !
O4             1.6837     0.1700    !
O1             1.6837     0.1700    !
O7             1.6612     0.2100    !
C7             1.9080     0.1094    !
C1             1.9080     0.1094    !
H6             1.3870     0.0157    !
H7             1.3870     0.0157    !
H8             1.3870     0.0157    !
H2             1.3870     0.0157    !
H1             1.3870     0.0157    !
H3             1.3870     0.0157    !
H4             1.3870     0.0157    !
H5             1.3870     0.0157    !
H9             1.3870     0.0157    !
```

```
I0              1.3870      0.0157     !
END
```

Table S3.1 Atomic charges (RESP) for BMOV.

Atom Types	q (e^-)
V1	0.871302
O3	-0.439100
O2	-0.435549
O6	-0.439100
O5	-0.435549
C4	0.461864
C3	0.081161
C9	0.081161
D0	0.461864
C5	-0.335553
C2	0.226995
C6	0.020388
C8	0.226995
D2	0.020388
D1	-0.335553
O4	-0.180713
O1	-0.180713
O7	-0.426260
C7	-0.212930
C1	-0.212930

H6	0.083644
H7	0.083644
H8	0.083644
H2	0.083644
H1	0.083644
H3	0.083644
H4	0.180564
H5	0.159419
H9	0.180564
I0	0.159419

Section S4

Table S4.1 Equivalence among atom types, bonds, angles and dihedrals.

Atoms	
O1	O4
O2	O5
O3	O6
C1	C7
C2	C8
C3	C9
C4	D0
C5	D1
C6	D2
H1	H6
H2	H7
H3	H8
H4	H9

H5	I0
Bonds	
V1-O2	V1-O5
V1-O3	V1-O6
O3-C4	O6-D0
O2-C3	O5-C9
C4-C3	C9-D0
C4-C5	D0-D1
C3-C2	C9-C8
C5-C6	D1-D2
C5-H4	D1-H9
C2-O1	C8-O4
C2-C1	C8-C7
C6-H5	I0-D2
O1-C6	D2-O4
C1-H1	C7-H6
C1-H2	C7-H7
C1-H3	C7-H8
Angles	
O3-V1-O2	O6-V1-O5
O3-V1-O6	O2-V1-O5
O3-V1-O5	O2-V1-O6
O3-V1-O7	O6-V1-O7
O2-V1-O7	O5-V1-O7
V1-O3-C4	V1-O6-D0
V1-O2-C3	V1-O5-C9
O3-C4-C3	O6-D0-C9
O3-C4-C5	O6-D0-D1
C3-C4-C5	C9-D0-D1
O2-C3-C4	O5-C9-D0

O2-C3-C2	O5-C9-C8
C4-C3-C2	D0-C9-C8
C4-C5-C6	D0-D1-D2
C4-C5-H4	D0-D1-H9
C6-C5-H4	D2-D1-H9
C3-C2-O1	C9-C8-O4
C3-C2-C1	C9-C8-C7
O1-C2-C1	O4-C8-C7
C5-C6-O1	D1-D2-O4
C5-C6-H5	D1-D2-I0
O1-C6-H5	O4-D2-I0
C8-O4-D2	C2-O1-C6
C8-C7-H6	C2-C1-H1
C8-C7-H7	C2-C1-H2
C8-C7-H8	C2-C1-H3
H6-C7-H7	H2-C1-H1
H6-C7-H8	H1-C1-H3
H7-C7-H8	H2-C1-H3

Dihedrals

O2-V1-O3-C4	O5-V1-O6-D0
O6-V1-O3-C4	O3-V1-O6-D0
O5-V1-O3-C4	O2-V1-O6-D0
O7-V1-O3-C4	O7-V1-O6-D0
O3-V1-O2-C3	O6-V1-O5-C9
O6-V1-O2-C3	O3-V1-O5-C9
O5-V1-O2-C3	O2-V1-O5-C9
O7-V1-O2-C3	O7-V1-O5-C9
V1-O3-C4-C3	V1-O6-D0-C9
V1-O3-C4-C5	V1-O6-D0-D1
V1-O2-C3-C4	V1-O5-C9-D0

V1-O2-C3-C2	V1-O5-C9-C8
O3-C4-C3-O2	O5-C9-D0-O6
O3-C4-C3-C2	C8-C9-D0-O6
C5-C4-C3-O2	O5-C9-D0-D1
C5-C4-C3-C2	C8-C9-D0-D1
O3-C4-C5-C6	O6-D0-D1-D2
O3-C4-C5-H4	O6-D0-D1-H9
C3-C4-C5-C6	C9-D0-D1-D2
C3-C4-C5-H4	C9-D0-D1-H9
O2-C3-C2-O1	O5-C9-C8-O4
O2-C3-C2-C1	O5-C9-C8-C7
C4-C3-C2-O1	D0-C9-C8-O4
C4-C3-C2-C1	D0-C9-C8-C7
C4-C5-C6-O1	O4-D2-D1-D0
C4-C5-C6-H5	I0-D2-D1-D0
H4-C5-C6-O1	O4-D2-D1-H9
H4-C5-C6-H5	I0-D2-D1-H9
C3-C2-O1-C6	C9-C8-O4-D2
C1-C2-O1-C6	C7-C8-O4-D2
C3-C2-C1-H2	C9-C8-C7-H7
C3-C2-C1-H1	C9-C8-C7-H6
C3-C2-C1-H3	C9-C8-C7-H8
O1-C2-C1-H2	O4-C8-C7-H7
O1-C2-C1-H1	O4-C8-C7-H6
O1-C2-C1-H3	O4-C8-C7-H8
C5-C6-O1-C2	D1-D2-O4-C8
H5-C6-O1-C2	I0-D2-O4-C8

AKTER, K.; LANZA, E. A.; MARTIN, S. A.; MYRONYUK, N. *et al.* Diabetes mellitus and Alzheimer's disease: shared pathology and treatment? **Br J Clin Pharmacol**, 71, n. 3, p. 365-376, Mar 2011.

ALAVI, S. **Molecular simulations: fundamentals and practice**. John Wiley & Sons, 2020. 3527341056.

ALCÁCER, L. Introdução à química quântica computacional. **energia**, 265, n. 268, p. 273, 2007.

BICKELHAUPT, F. M.; BAERENDS, E. J. Kohn-Sham density functional theory: predicting and understanding chemistry. **Reviews in computational chemistry**, p. 1-86, 2000.

BOCCARDI, V.; MURASECCO, I.; MECOCCI, P. Diabetes drugs in the fight against Alzheimer's disease. **Ageing research reviews**, 54, p. 100936, 2019.

BONDI, M. W.; EDMONDS, E. C.; SALMON, D. P. Alzheimer's Disease: Past, Present, and Future. **Journal of the International Neuropsychological Society**, 23, n. 9-10, p. 818-831, 2017.

BORTOLUZZI, E. C.; MASCARELO, A.; DELLANI, M. P.; ALVES, A. L. S. A. *et al.* Expectativa de vida de idosos e doenças crônicas. **Brazilian Journal of Health Review**, 4, n. 1, p. 3057-3071, 2021.

BREIJYEH, Z.; KARAMAN, R. Comprehensive review on Alzheimer's disease: causes and treatment. **Molecules**, 25, n. 24, p. 5789, 2020.

BROOIJMANS, N.; KUNTZ, I. D. Molecular recognition and docking algorithms. **Annual review of biophysics and biomolecular structure**, 32, n. 1, p. 335-373, 2003.

CAPELLE, K. A bird's-eye view of density-functional theory. **Brazilian journal of physics**, 36, p. 1318-1343, 2006.

CHEN, M.; HUANG, N.; LIU, J.; HUANG, J. *et al.* AMPK: A bridge between diabetes mellitus and Alzheimer's disease. **Behav Brain Res**, 400, p. 113043, 02 26 2021.

COSTA, M. A. D. S. **Investigação Teórica do Processo de Inclusão do Fluconazol com Ciclodextrinas e Calixarenos**. 2014. - Departamento de Química, Universidade Federal de São João del-Rei, São João del-Rei.

DEL CARPIO, E.; HERNÁNDEZ, L.; CIANGHEROTTI, C.; COA, V. V. *et al.* Vanadium: History, chemistry, interactions with α-amino acids and potential therapeutic applications. **Coordination chemistry reviews**, 372, p. 117-140, 2018.

DOIG, A. J.; DEL CASTILLO-FRIAS, M. P.; BERTHOUMIEU, O.; TARUS, B. *et al.* Why Is Research on Amyloid-β Failing to Give New Drugs for Alzheimer's Disease? **ACS Chem Neurosci**, 8, n. 7, p. 1435-1437, Jul 19 2017.

DUARTE, H. A. Índices de reatividade química a partir da teoria do funcional de densidade: formalismo e perspectivas. **Química Nova**, 24, p. 501-508, 2001.

FALCO, A. D.; CUKIERMAN, D. S.; HAUSER-DAVIS, R. A.; REY, N. A. Doença de Alzheimer: hipóteses etiológicas e perspectivas de tratamento. **Química Nova**, 39, n. 1, p. 63-80, 2016.

FOGARTY, S.; HARDIE, D. G. Development of protein kinase activators: AMPK as a target in metabolic disorders and cancer. **Biochim Biophys Acta**, 1804, n. 3, p. 581-591, Mar 2010.

GE, Y.; ZHOU, M.; CHEN, C.; WU, X. *et al.* Role of AMPK mediated pathways in autophagy and aging. **Biochimie**, 195, p. 100-113, Apr 2022.

GRIFFITHS, D. J.; FREITAS, L. **Mecânica quântica**. Pearson Prentice Hall, 2011. 8576059274.

HONIG, L.; MAYEUX, R. Natural history of Alzheimer's disease. **Aging Clinical and Experimental Research**, 13, n. 3, p. 171-182, 2001.

JACOBS, M. R. **Parametrização de campo de força derivado de cálculos mecânico-quânticos para o cristal líquido 4-Ciano-4'-Pentilbifenila**. 2017. - Instituto de Química, Universidade Federal do Rio Grande do Sul, Porto Alegre.

JENSEN, F. Computational chemistry: The exciting opportunities and the boring details. **Israel Journal of Chemistry**, 62, n. 1-2, p. e202100027, 2022.

KAMETANI, F.; HASEGAWA, M. Reconsideration of amyloid hypothesis and tau hypothesis in Alzheimer's disease. **Frontiers in neuroscience**, p. 25, 2018.

KANG, P.; WANG, Z.; QIAO, D.; ZHANG, B. *et al.* Dissecting genetic links between Alzheimer's disease and type 2 diabetes mellitus in a systems biology way. **Front Genet**, 13, p. 1019860, 2022.

KIOSEOGLOU, E.; PETANIDIS, S.; GABRIEL, C.; SALIFOGLOU, A. The chemistry and biology of vanadium compounds in cancer therapeutics. **Coordination Chemistry Reviews**, 301, p. 87-105, 2015.

KIRCHMAIR, J.; GÖLLER, A. H.; LANG, D.; KUNZE, J. *et al.* Predicting drug metabolism: experiment and/or computation? **Nature reviews Drug discovery**, 14, n. 6, p. 387-404, 2015.

KOSTAL, J. Computational Chemistry in Predictive Toxicology: status quo et quo vadis? *In*: **Advances in molecular toxicology**: Elsevier, 2016. v. 10, p. 139-186.

LAPOINTE, S. M.; WEAVER, D. F. A review of density functional theory quantum mechanics as applied to pharmaceutically relevant systems. **Current Computer-Aided Drug Design**, 3, n. 4, p. 290-296, 2007.

LESZCZYNSKI, J. **Handbook of computational chemistry**. Springer Science & Business Media, 2012. 940070710X.

LI, P.; MERZ, K. M. Metal Ion Modeling Using Classical Mechanics. **Chemical Reviews**, 117, n. 3, p. 1564-1686, 2017/02/08 2017.

LIU, H.; QU, Y.; WANG, X. Amyloid β-targeted metal complexes for potential applications in Alzheimer's disease. **Future Med Chem**, 10, n. 6, p. 679-701, 03 01 2018.

LIU, R.; MATHIEU, C.; BERTHELET, J.; ZHANG, W. *et al.* Human Protein Tyrosine Phosphatase 1B (PTP1B): From Structure to Clinical Inhibitor Perspectives. **International Journal of Molecular Sciences**, 23, n. 13, p. 7027, 2022.

LIVINGSTON, G.; HUNTLEY, J.; SOMMERLAD, A.; AMES, D. *et al.* Dementia prevention, intervention, and care: 2020 report of the Lancet Commission. **Lancet**, 396, n. 10248, p. 413-446, Aug 08 2020.

MAGALHÃES, C. D.; BARBOSA, H.; DARDENNE, L. Métodos de docking receptor-ligante para o desenho racional de compostos bioativos. **Métodos de Química Teórica e Modelagem Molecular**, 654, 2007.

MARTÍNEZ, L.; BORIN, I.; SKAF, M. S. Fundamentos de simulação por dinâmica molecular. **Métodos de Química Teórica e Modelagem Molecular**, p. 413-452, 2007.

MENG, X.-Y.; ZHANG, H.-X.; MEZEI, M.; CUI, M. Molecular docking: a powerful approach for structure-based drug discovery. **Current computer-aided drug design**, 7, n. 2, p. 146-157, 2011.

MURALEEDHARAN, R.; DASGUPTA, B. AMPK in the brain: its roles in glucose and neural metabolism. **FEBS J**, 289, n. 8, p. 2247-2262, Apr 2022.

ORGANIZATION, W. H. **Dementia**. 2022. Disponível em: https://www.who.int/news-room/fact-sheets/detail/dementia. Acesso em: 07/08/2022.

PAUDEL, P.; PARK, C. H.; JUNG, H. A.; YOKOZAWA, T. *et al.* A systematic review on anti-Alzheimer's disease activity of prescription Kangen-karyu. **Drug Discov Ther**, 14, n. 2, p. 61-66, May 06 2020.

PEREIRA, A. F. **Development and biological application of a quantum mechanically derived force field: the case of a platinum (II) complex**. 2020. - Departamento de Química, Universidade Federal de Lavras, Lavras.

PEREIRA, A. F.; PRANDI, I. G.; RAMALHO, T. C. Parameterization and validation of a new force field for Pt(II) complexes of 2-(4’-amino-2’-hydroxyphenyl)benzothiazole. **International Journal of Quantum Chemistry**, 121, n. 6, p. e26525, 2021/03/15 2021. https://doi.org/10.1002/qua.26525.

PEREIRA, R. A. **Estudo teórico de compostos de inclusão dos herbicidas 2,4-D e Dicamba em b-Ciclodextrina.** 2016. - Departamento de Química, Universidade Federal de Lavras, Lavras.

PETERS, K. G.; DAVIS, M. G.; HOWARD, B. W.; POKROSS, M. *et al.* Mechanism of insulin sensitization by BMOV (bis maltolato oxo vanadium); unliganded vanadium (VO4) as the active component. **Journal of Inorganic Biochemistry**, 96, n. 2, p. 321-330, 2003/08/01/ 2003.

PLIEGO JR, J. R. Modelos contínuos do solvente: fundamentos. **Química Nova**, 29, p. 535-542, 2006.

RAIMUNDO, A. F.; FERREIRA, S.; MARTINS, I. C.; MENEZES, R. Islet Amyloid Polypeptide: A Partner in Crime With Aβ in the Pathology of Alzheimer's Disease. **Frontiers in Molecular Neuroscience**, 13, p. 35, 2020.

REHDER, D. The potentiality of vanadium in medicinal applications. **Future medicinal chemistry**, 4, n. 14, p. 1823-1837, 2012.

RUSANOV, D. A.; ZOU, J.; BABAK, M. V. Biological Properties of Transition Metal Complexes with Metformin and Its Analogues. **Pharmaceuticals (Basel)**, 15, n. 4, Apr 06 2022.

SALO-AHEN, O. M. H.; ALANKO, I.; BHADANE, R.; BONVIN, A. M. J. J. *et al.* Molecular Dynamics Simulations in Drug Discovery and Pharmaceutical Development. **Processes**, 9, n. 1, 2021.

SEMIZ, S. Vanadium as potential therapeutic agent for COVID-19: A focus on its antiviral, antiinflamatory, and antihyperglycemic effects. **Journal of Trace Elements in Medicine and Biology**, 69, p. 126887, 2022.

SHOICHET, B. K.; MCGOVERN, S. L.; WEI, B.; IRWIN, J. J. Lead discovery using molecular docking. **Current opinion in chemical biology**, 6, n. 4, p. 439-446, 2002.

SMITH, D. Artificial intelligence can detect Alzheimer's disease in brain scans six years before a diagnosis. **University of California San Fransisco**, p. 01-02, 2019.

STANCIU, G. D.; BILD, V.; ABABEI, D. C.; RUSU, R. N. *et al.* Link between Diabetes and Alzheimer's Disease Due to the Shared Amyloid Aggregation and Deposition Involving Both Neurodegenerative Changes and Neurovascular Damages. **Journal of Clinical Medicine**, v.9, n. 6, DOI: 10.3390/jcm9061713.

SUN, Y.; MA, C.; SUN, H.; WANG, H. *et al.* Metabolism: A Novel Shared Link between Diabetes Mellitus and Alzheimer's Disease. **J Diabetes Res**, 2020, p. 4981814, 2020.

THOMSEN, R.; CHRISTENSEN, M. H. MolDock: a new technique for high-accuracy molecular docking. **Journal of medicinal chemistry**, 49, n. 11, p. 3315-3321, 2006.

TORRES, P. H.; SODERO, A. C.; JOFILY, P.; SILVA-JR, F. P. Key topics in molecular docking for drug design. **International journal of molecular sciences**, 20, n. 18, p. 4574, 2019.

TREVIÑO, S.; DIAZ, A. Vanadium and insulin: Partners in metabolic regulation. **Journal of Inorganic Biochemistry**, 208, p. 111094, 2020.

VANOMMESLAEGHE, K.; GUVENCH, O. Molecular mechanics. **Current pharmaceutical design**, 20, n. 20, p. 3281-3292, 2014.

VIEIRA, M. N.; LYRA E SILVA, N. M.; FERREIRA, S. T.; DE FELICE, F. G. Protein Tyrosine Phosphatase 1B (PTP1B): A Potential Target for Alzheimer's Therapy? **Front Aging Neurosci**, 9, p. 7, 2017.

VOLICER, L. Physiological and pathological functions of beta-amyloid in the brain and alzheimer's disease: A review. **Chinese Journal of Physiology**, 63, n. 3, p. 95-100, May 1, 2020 2020. Review Article.

WOLOHAN, P.; YOO, J.; WELCH, M. J.; REICHERT, D. E. QSAR studies of copper azamacrocycles and thiosemicarbazones: MM3 parameter development and prediction of biological properties. **Journal of medicinal chemistry**, 48, n. 17, p. 5561-5569, 2005.

WOO, L. C. Y.; YUEN, V. G.; THOMPSON, K. H.; MCNEILL, J. H. *et al.* Vanadyl–biguanide complexes as potential synergistic insulin mimics. **Journal of Inorganic Biochemistry**, 76, n. 3, p. 251-257, 1999/09/15/ 1999.

ZHOU, T.; HUANG, D.; CAFLISCH, A. Quantum mechanical methods for drug design. **Current topics in medicinal chemistry**, 10, n. 1, p. 33-45, 2010.